Theory Manual

Mefisto 2.8

Contents

1 Introduction....4
2 Methods in Solid Mechanics....5
2.1 Notation....5
2.2 Static Response....6
2.3 Normal Modes....7
2.4 Frequency Response....10
2.4.1 Direct Frequency Response Analysis....11
2.4.2 Modal Frequency Response Analysis....11
2.4.3 Enhanced Modal Reduction....13
2.5 Transient Response....14
2.5.1 Direct Transient Response Analysis....14
2.5.2 Modal Transient Response Analysis....16
2.5.3 Enhanced Modal Reduction....17
2.6 Estimation of Reduction Error....18
2.7 Linear Constraints....20
2.7.1 Matrix Transformations....20
2.7.2 Constraint Matrices....21
3 Elements in Solid Mechanics....24
3.1 The Beam Element....24
3.1.1 Assumptions....24
3.1.2 Definitions....24
3.1.3 Kinematics....25
3.1.4 Stiffness Matrix....29
3.1.5 Mass Matrix....32
3.1.6 Stress Resultants....34

3.2 Membrane Elements....36
3.3 Membrane Elements with Drilling Dofs....39
3.4 Solid Elements....41
3.5 Shell Elements....41
3.5.1 The Element Coordinate System....42
3.5.2 Warping Correction....43
3.5.3 The Reissner-Mindlin Plate Theory....44
3.5.4 Stiffness Matrix....46
3.5.5 Mass Matrix....55
3.5.6 Stresses and Stress Resultants....55
4 Aerodynamic Methods....56
4.1 The Discrete Vortex Method....56
4.1.1 The Steady Discrete Vortex Method....56
4.1.2 The Time-Harmonic Discrete Vortex Method....57
4.2 The Vortex Lattice Method....61
4.2.1 The Horseshoe Vortex....61
4.2.2 The Steady Vortex Lattice Method....63
4.2.3 The Time-Harmonic Vortex Lattice Method....64
4.2.4 Evaluation of the Wake Integrals....68
4.3 Rigid Trim Analysis....71
5 Methods in Aeroelasticity....73
5.1 Splines....73
5.2 Steady Aerodynamic Matrices....76
5.3 Static Response....78
5.4 Static Divergence....80
5.5 Trim Analysis....80
5.5.1 Restrained Trim Analysis....81
5.5.2 Unrestrained Trim Analysis....82
5.6 Unsteady Aerodynamic Matrices....83
5.7 Flutter Analysis....84
5.7.1 The Flutter Equation....84
5.7.2 The k-Method....85
5.7.3 The pk-Method....86
5.8 Frequency Response....88

5.8.1 Gusts.....90
5.8.2 Manoeuvres.....91
References.....94

1 Introduction

This manual briefly describes the solution methods implemented in Mefisto as well as the formulations of the more sophisticated elements, the vortex lattice method and the splines. This information may be useful if you are interested in a deeper understanding of the theoretical background of Mefisto, especially if you want to modify or extend Mefisto.

The Mefisto software is a companion software of the graduate courses on structural dynamics and on aeroelasticity. A detailed description of the theory is given in the lecture notes of these courses which can be found at http://wandinger.userweb.mwn.de/index.html.

2 Methods in Solid Mechanics

2.1 Notation

Vectors and Matrices

Vectors are printed in bold, e.g. $\boldsymbol{n}$, $\boldsymbol{e}_x$. This notation is used in computations that do not use a coordinate system.

Matrices are indicated by letters in brackets, e.g. $[K]$, $[u]$. Matrices that contain the coordinates of a vector with respect to the coordinate system are indicated by bold letters in brackets, e.g. matrix $[\boldsymbol{n}]$ contains the coordinates of vector $\boldsymbol{n}$ with respect to a coordinate system. If there are several coordinate systems, a right lower index indicates the coordinate system the coordinates within the matrix refer to, e.g. matrix $[\boldsymbol{v}]_L$ contains the coordinates of vector $\boldsymbol{v}$ with respect to a local coordinate system denoted by L.

The transpose of a matrix is indicated by superscript T and the conjugate transpose by superscript H, e.g. $[X]^T$ or $[U]^H$.

Degrees of Freedom

- Index *G* denotes global degrees of freedom.
- Index *L* denotes local degrees of freedom.
- Index *P* denotes prescribed degrees of freedom.
- Index *D* denotes dependent degrees of freedom.
- Index *I* denotes the independent degrees of freedom.
- Index *A* denotes autonomous degrees of freedom.
- The set of global degrees of freedom contains $mxdofpnt$ degrees of freedom for each nodal point. $mxdofpnt$ is the maximum number of degrees of freedom at a nodal point. It depends on the dimension of the problem and the elements used.
- The displacements at prescribed degrees of freedom are prescribed. They are used to model bearings.
- The displacements at local degrees of freedom are unknown. They are obtained as results of the analysis.
- The displacements at dependent degrees of freedom can be computed from a linear relation between the displacements at a subset of the in-

dependent degrees of freedom. The independent degrees of freedom are all degrees of freedom that are not dependent: $I = G \setminus D, G = I \cup D$

- Those independent degrees of freedom that are involved in linear constraints are called autonomous degrees of freedom: $A \subset I$
- To simplify notation, the index *G* is omitted where no confusion can occur.

2.2 Static Response

In a linear static analysis, the equation to be solved reads

$$[K][u] = [l] \tag{2.2-1}$$

where $[K]$ is the stiffness matrix, $[u]$ is the displacement matrix and $[l]$ is the load matrix.

The displacement matrix $[u]$ can be partitioned into the the matrix $[u_P]$ of prescribed displacements and the matrix $[u_L]$ of local displacements. Accordingly, the load matrix $[l]$ is partitioned into the matrix $[l_P]$ of reaction loads due to the prescribed displacements, and the matrix $[l_L]$ of the loads applied at the local degrees of freedom.

Then, Equation (2.2-1) reads

$$\begin{bmatrix} [K_{LL}] & [K_{LP}] \\ [K_{LP}]^T & [K_{PP}] \end{bmatrix} \begin{bmatrix} [u_L] \\ [u_P] \end{bmatrix} = \begin{bmatrix} [l_L] \\ [l_P] \end{bmatrix}. \tag{2.2-2}$$

The prescribed displacements $[u_P]$ and the loads $[l_L]$ applied at the local degrees of freedom are known, whereas the local displacements $[u_L]$ and the reaction loads $[l_P]$ are unknown.

The local displacements can be obtained from the first row of equation (2.2-2) reading

$$[K_{LL}][u_L] = [l_L] - [K_{LP}][u_P]. \tag{2.2-3}$$

Subsequently, the reaction loads can be computed from the second row of Equation (2.2-3) reading

$$[l_P] = [K_{LP}]^T [u_L] + [K_{PP}][u_P]. \tag{2.2-4}$$

The strain energy is computed from

$$E^S = \frac{1}{2} [u]^T [K][u]. \tag{2.2-5}$$

Finally, the residual is computed from

$$[r] = [K][u] - [l]. \tag{2.2-6}$$

The work of the residual,

$$W^R = \frac{1}{2}[u]^T[r], \tag{2.2-7}$$

should be small compared to the strain energy.

2.3 Normal Modes

Normal modes are solutions of the general eigenvalue problem

$$[K_{LL}][x_L] = \omega^2[M_{LL}][x_L] \tag{2.3-1}$$

where $[K_{LL}]$ is the stiffness matrix and $[M_{LL}]$ is the mass matrix. Both the stiffness and the mass matrix are sparse symmetric matrices that are at least positive semi-definite.

If the structure has no rigid body modes the stiffness matrix is positive definite. Then, its Cholesky factor $[L_{LL}]$ can be computed and used to factorize it:

$$[K_{LL}] = [L_{LL}][L_{LL}]^T \tag{2.3-2}$$

Equation (2.3-1) then reads

$$[L_{LL}][L_{LL}]^T[x_L] = \omega^2[M_{LL}][L_{LL}]^{-T}[L_{LL}]^T[x_L]. \tag{2.3-3}$$

With the substitution

$$[y_L] = [L_{LL}]^T[x_L] \tag{2.3-4}$$

the standard symmetric eigenvalue problem

$$\frac{1}{\omega^2}[y_L] = [L_{LL}]^{-1}[M_{LL}][L_{LL}]^{-T}[y_L] \tag{2.3-5}$$

is obtained.

If the structure has rigid body modes the stiffness matrix can be partitioned according to

$$[K_{LL}] = \begin{bmatrix} [K_{EE}] & [K_{ER}] \\ [K_{KR}]^T & [K_{RR}] \end{bmatrix} \tag{2.3-6}$$

where index *E* denotes elastic and index *R* rigid degrees of freedom. The rigid degrees of freedom are selected such that the structure has no rigid body modes if the displacements at the rigid degrees of freedom are required to be zero. Then, matrix $[K_{EE}]$ is positive definite.

The rigid degrees of freedom can be detected automatically by performing a LU-decomposition of matrix $[K_{LL}]$ and looking at the diagonal elements of the upper triangular factor [Wandinger, 1990].

The matrix

$$\left[\widetilde{X}_R\right]=\begin{bmatrix}\left[K_{EE}\right]^{-1}\left[K_{ER}\right]\\ -\left[I_{RR}\right]\end{bmatrix} \tag{2.3-7}$$

where $[I_{RR}]$ is a unit matrix satisfies

$$\left[K_{LL}\right]\left[\widetilde{X}_R\right]=\begin{bmatrix}[0]\\ \left[K_{ER}^T\right]\left[K_{EE}\right]^{-1}\left[K_{ER}\right]-\left[K_{RR}\right]\end{bmatrix}=\begin{bmatrix}[0]\\ [0]\end{bmatrix}\ , \tag{2.3-8}$$

i.e. its columns are rigid body modes. The last identity in Equation (2.3-8) follows from the fact that the equation

$$\left[K_{LL}\right]\left[x_L\right]=[0] \tag{2.3-9}$$

must have as many non-trivial solutions as there are rigid body modes.

The rigid body modes can be orthonormalized with respect to the mass matrix using the Cholesky factor $[C_M]$ of the rigid body mass matrix:

$$\left[\widetilde{X}_R\right]^T\left[M_{LL}\right]\left[\widetilde{X}_R\right]=\left[M_{RR}\right]=\left[C_M\right]^T\left[C_M\right] \tag{2.3-10}$$

The rigid body modes

$$\left[X_R\right]=\left[\widetilde{X}_R\right]\left[C_M\right]^{-1} \tag{2.3-11}$$

satisfy

$$\left[X_R\right]^T\left[M_{LL}\right]\left[X_R\right]=\left[C_M\right]^{-T}\left[\widetilde{X}_R\right]^T\left[M_{LL}\right]\left[\widetilde{X}_R\right]\left[C_M\right]=\left[I_{RR}\right]. \tag{2.3-12}$$

Now, let $[X_E]$ be a matrix whose columns span a complement of the space spanned by the rigid body modes $[X_R]$. Then, each displacement vector can be expressed as a linear combination of the columns of $[X_R]$ and the columns of $[X_E]$:

$$\left[x_L\right]=\left[X_R\right]\left[x_R\right]+\left[X_E\right]\left[x_E\right]=\begin{bmatrix}\left[X_R\right] & \left[X_E\right]\end{bmatrix}\begin{bmatrix}\left[x_R\right]\\ \left[x_E\right]\end{bmatrix}=\left[T\right]\begin{bmatrix}\left[x_R\right]\\ \left[x_E\right]\end{bmatrix} \tag{2.3-13}$$

A congruence transformation of the eigenvalue problem (2.3-1) using matrix $[T]$ results in

$$\begin{bmatrix}[0_{RR}] & [0_{RE}]\\ [0_{ER}] & \left[X_E\right]^T\left[K_{LL}\right]\left[X_E\right]\end{bmatrix}\begin{bmatrix}\left[x_R\right]\\ \left[x_E\right]\end{bmatrix} =\omega^2\begin{bmatrix}\left[I_{RR}\right] & \left[X_R\right]^T\left[M_{LL}\right]\left[X_E\right]\\ \left[X_E\right]^T\left[M_{LL}\right]\left[X_R\right] & \left[X_E\right]^T\left[M_{LL}\right]\left[X_E\right]\end{bmatrix}\begin{bmatrix}\left[x_R\right]\\ \left[x_E\right]\end{bmatrix}. \tag{2.3-14}$$

Now, if a matrix $[X_E]$ is selected that is mass-orthogonal on the rigid body modes $[X_R]$, i.e.

$$\left[X_R\right]^T\left[M_{LL}\right]\left[X_E\right]=[0], \tag{2.3-15}$$

then the following decoupled equations are obtained:

$$[0]=\omega^2[x_R] \tag{2.3-16}$$

$$[X_E]^T[K_{LL}][X_E][x_E]=\omega^2[X_E]^T[M_{LL}][X_E] \tag{2.3-17}$$

Matrix $[X_E]$ is not uniquely defined by Equation (2.3-15). Thus it can be selected such that the sparsity of the matrices is not destroyed. To this end, let

$$[J_{LE}]=\begin{bmatrix}[I_{EE}]\\ [0_{RE}]\end{bmatrix}. \tag{2.3-18}$$

The columns of this matrix are linearly independent of the rigid body modes because the latter have non-zero values at the rigid degrees of freedom. Mass-orthogonalizing matrix $[J_{LE}]$ with respect to the rigid body modes results in

$$[X_E]=\left([I_{LL}]-[X_R][X_R]^T[M_{LL}]\right)[J_{LE}]. \tag{2.3-19}$$

It is easy to check that this matrix satisfies Equation (2.3-15).

With $[X_E]$ defined by Equation (2.3-19) the transformed stiffness matrix reads

$$[X_E]^T[K_{LL}][X_E]=[J_{EE}]^T[K_{LL}][J_{EE}]=[K_{EE}] \tag{2.3-20}$$

which is a sparse matrix. Transformation of the mass matrix yields

$$[X_E]^T[M_{LL}][X_E]=[J_{LE}]^T[M_{LL}]\left([I_{LL}]-[X_R][X_R]^T[M_{LL}]\right)[J_{LE}]. \tag{2.3-21}$$

With Equations (2.3-20) and (2.3-21), the eigenvalue problem (2.3-17) reads

$$[K_{EE}][x_E]=\omega^2[J_{LE}]^T[M_{LL}]\left([I_{LL}]-[X_R]^T[X_R][M_{LL}]\right)[J_{LE}][x_E]. \tag{2.3-22}$$

With the Cholesky factor $[L_{EE}]$ of matrix $[K_{EE}]$, the substitution

$$[y_E]=[L_{EE}]^T[x_E] \tag{2.3-23}$$

results in the standard symmetric eigenvalue problem

$$\frac{1}{\omega^2}[y_E]=[L_{EE}]^{-1}[J_{LE}]^T[M_{LL}]\left([I_{LL}]-[X_R]^T[X_R][M_{LL}]\right)[J_{LE}][L_{EE}]^{-T}[y_E]. \tag{2.3-24}$$

The eigenvalue problems (2.3-1) respectively (2.3-22) can be solved by function **`eigs`** where the power step is performed according to Equations (2.2-5) respectively (2.3-24). The result is the eigenvectors $[y_L]$ respectively $[y_E]$. Then the eigenvectors $[x_L]$ can be computed from

$$[x_L]=[L_{LL}]^{-T}[y_L] \tag{2.3-25}$$

respectively

$$[x_L]=\left([I_{LL}]-[X_R][X_R]^T[M_{LL}]\right)[J_{LE}][L_{EE}]^{-T}[y_E]. \tag{2.3-26}$$

Finally, the eigenvectors are normalized with respect to the mass matrix.

2.4 Frequency Response

The dynamic equation of a linear structure reads

$$[M]\left[\ddot{u}(t)\right]+[D]\left[\dot{u}(t)\right]+[K]\left[u(t)\right]=\left[l(t)\right] \tag{2.4-1}$$

where $[M]$ is the mass matrix, $[D]$ is the damping matrix, $[K]$ is the stiffness matrix and $[l]$ is the load matrix.

The load matrix can be expressed as a linear combination of load patterns $[l_k]$ with time-dependent coefficients $\phi_k(t)$:

$$\left[l(t)\right]=\sum_k [l_k]\phi_k(t) \tag{2.4-2}$$

In case of a harmonic excitation, the response is harmonic, too. In complex notation, the load matrix and the displacement matrix read

$$\left[l(t)\right]=\Re\left(\left[L(\Omega)\right]e^{i\Omega t}\right),\ \left[u(t)\right]=\Re\left(\left[U(\Omega)\right]e^{i\Omega t}\right). \tag{2.4-3}$$

Inserting of (2.4-3) into (2.4-1) gives

$$\left(-\Omega^2[M]+i\,\Omega[D]+[K]\right)\left[U(\Omega)\right]=\left[L(\Omega)\right]. \tag{2.4-4}$$

From this equation, the response $[U]$ can be computed for any excitation frequency Ω.

In Mefisto, load patterns correspond to load cases. In one frequency response analysis, only one load case can be processed. Actually, function **`mfs_freqresp`** solves the equation

$$\left(-\Omega^2[M]+i\,\Omega[D]+[K]\right)\left[U(\Omega)\right]=\left[L_k\right]. \tag{2.4-5}$$

In partitioned form, Equation (2.4-5) reads

$$\left(-\Omega^2\begin{bmatrix}[M_{LL}] & [M_{LP}]\\ [M_{LP}]^T & [M_{PP}]\end{bmatrix}+i\,\Omega\begin{bmatrix}[D_{LL}] & [D_{LP}]\\ [D_{LP}]^T & [D_{PP}]\end{bmatrix}+\begin{bmatrix}[K_{LL}] & [K_{LP}]\\ [K_{LP}]^T & [K_{PP}]\end{bmatrix}\right)\begin{bmatrix}[U_L]\\ [U_P]\end{bmatrix}=\begin{bmatrix}[L_L]\\ [L_P]\end{bmatrix} \tag{2.4-6}$$

where the subscript k has been omitted.

In case of a force excitation, the loads $[L_L]$ are given and the displacements $[U_P]$ are zero. The unknown displacements $[U_L]$ are obtained from

$$\left(-\Omega^2[M_{LL}]+i\,\Omega[D_{LL}]+[K_{LL}]\right)\left[U_L(\Omega)\right]=\left[L_L\right]. \tag{2.4-7}$$

In case of a base motion excitation, the displacements $[U_P]$ are given and the loads $[L_L]$ are zero. The unknown displacements $[U_L]$ are obtained from

$$\begin{aligned}&\left(-\Omega^2[M_{LL}]+i\Omega[D_{LL}]+[K_{LL}]\right)[U_L(\Omega)]\\&\quad=-\left(-\Omega^2[M_{LP}]+i\Omega[D_{LP}]+[K_{LP}]\right)[U_P(\Omega)].\end{aligned} \tag{2.4-8}$$

In Mefisto, force excitation and base motion excitation cannot be mixed within one load case.

The base motion can be defined by prescribed displacements, prescribed velocities or prescribed accelerations. A frequency dependence of these values cannot be defined. However, constant prescribed velocities or accelerations will of course result in frequency dependent prescribed displacements.

2.4.1 Direct Frequency Response Analysis

In a direct frequency response analysis, Equations (2.4-7) and (2.4-8) are solved for each excitation frequency. The strain energy is computed from

$$E^S=\frac{1}{4}[U]^H[K][U]. \tag{2.4-9}$$

Actually, this is the mean value of the strain energy, taken over one period.

The residual is computed from

$$[R_L(\Omega)]=\left(-\Omega^2[M_{LL}]+i\Omega[D_{LL}]+[K_{LL}]\right)[U_L(\Omega)]-[L_L] \tag{2.4-10}$$

and

$$\begin{aligned}[R_L(\Omega)]=&\left(-\Omega^2[M_{LL}]+i\Omega[D_{LL}]+[K_{LL}]\right)[U_L(\Omega)]\\&+\left(-\Omega^2[M_{LP}]+i\Omega[D_{LP}]+[K_{LP}]\right)[U_P(\Omega)]\end{aligned} \tag{2.4-11}$$

respectively. The work of the residual

$$W^R=\frac{1}{4}[U_L]^H[R_L] \tag{2.4-12}$$

should be small compared to the strain energy.

2.4.2 Modal Frequency Response Analysis

In a modal frequency response analysis, the response is approximated by a superposition of the computed normal modes.

In case of a force excitation, the displacements are approximated by

$$[U_L]\approx[U_L^p]=\sum_{n=1}^{p}[x_n]Q_n=[X^p][U]_p \tag{2.4-13}$$

where $[x_n]$ are the eigenvectors of

$$[K_{LL}][x_n]=\omega_n^2[M_{LL}][x_n] \tag{2.4-14}$$

and

$$\left[X^p\right]=\left[\left[x_1\right] \quad \ldots \quad \left[x_p\right]\right], \quad \left[U\right]_p=\left[Q_1 \quad \ldots \quad Q_p\right]^T. \tag{2.4-15}$$

Currently, all types of damping that can be defined in Mefisto result in a modal damping matrix. Thus, insertion of (2.4-13) into (2.4-7) and subsequent projection onto the eigenvectors leads to p uncoupled equations

$$\left(-\Omega^2+2\,i\,D_n\omega_n\Omega+\omega_n^2\right)Q_n=\left[x_n\right]^T\left[L_L\right], \quad n=1,\ldots p \tag{2.4-16}$$

where

$$D_n=\frac{\left[x_n\right]^T\left[D_{LL}\right]\left[x_n\right]}{2\,\omega_n} \tag{2.4-17}$$

are the modal damping ratios.

The solution of Equation (2.4-16) is

$$Q_n(\Omega)=\frac{\left[x_n\right]^T\left[L_L\right]}{\omega_n^2-\Omega^2+2\,i\,D_n\omega_n\Omega}=G_n\left[x_n\right]^T\left[L_L\right] \tag{2.4-18}$$

where

$$G_n=\frac{1}{\omega_n^2-\Omega^2+2\,i\,D_n\omega_n\Omega}=\frac{1}{4\,\pi^2}\,\frac{1}{f_n^2-f^2+2\,i\,D_n f_n f} \quad . \tag{2.4-19}$$

The strain energy can be computed from

$$E^S=\frac{1}{4}\sum_{n=1}^{p}\omega_n^2\left|Q_n\right|^2. \tag{2.4-20}$$

In case of a base motion excitation, first the base motion is computed from

$$\left[U_L^B\right]=-\left[K_{LL}\right]^{-1}\left[K_{LP}\right]\left[U_P\right]. \tag{2.4-21}$$

It describes the static response to the prescribed displacements.

If the structure has rigid body modes, the solution of Equation (2.4-21) is made unique by the additional constraint

$$\left[X_R\right]^T\left[M_{LL}\right]\left[U_L^B\right]=\left[0\right] \tag{2.4-22}$$

where matrix $[X_R]$ contains the rigid body modes.

Then, the motion relative to the base motion is approximated by a superposition of the computed eigenvectors. Thus, the displacements $[U_L]$ are approximated by

$$[U_L] \approx [U_L^p] = [U_L^B] + [X^p][U]_p. \tag{2.4-23}$$

Insertion of (2.4-23) into (2.4-8) and subsequent projection on the eigenvectors leads to the p uncoupled equations

$$\begin{aligned}\left(-\Omega^2 + 2i\Omega\omega_n D_n + \omega_n^2\right) Q_n = \Omega^2 [x_n]^T \left([M_{LL}][U_L^B] + [M_{LP}][U_P]\right) \\ - i\Omega [x_n]^T \left([D_{LL}][U_L^B] + [D_{LP}][U_P]\right), \quad n = 1, \ldots p\end{aligned} \tag{2.4-24}$$

If the damping is defined by modal damping ratios D_n, the relation

$$[x_n]^T [D_{LL}] = 2\omega_n D_n [x_n]^T [M_{LL}] \tag{2.4-25}$$

is used.

The strain energy contains a contribution from the base motion:

$$E^S = \frac{1}{4}\left([U^B]^H [K][U^B] + \sum_{n=1}^{p} \omega_n^2 |Q_n|^2 \right) \tag{2.4-26}$$

2.4.3 Enhanced Modal Reduction

The accuracy of the modal reduction can be improved if the static response of the neglected modes is added:

$$[U_L] = [U_L^p] + [\Delta U_L] \tag{2.4-27}$$

If the structure does not have rigid body modes, it is easy to compute the correction term. In case of a force excitation, it is obtained from

$$[K_{LL}][\Delta U_L] = [L_L] - [M_{LL}][X^p][X^p]^T [L_L]. \tag{2.4-28}$$

It does not depend on the excitation frequency.

In case of a base motion excitation, first matrix

$$[Y_L] = -\begin{bmatrix}[M_{LL}] & [M_{LP}]\end{bmatrix} \begin{bmatrix}[U_L^B] \\ [U_P]\end{bmatrix} \tag{2.4-29}$$

is computed. Then, the equation

$$[K_{LL}][Z_L] = [Y_L] - [M_{LL}][X^p][X^p]^T [Y_L] \tag{2.4-30}$$

is solved for $[Z_L]$. This matrix does not depend on the excitation frequency. Finally, the frequency dependent correction is

$$[\Delta U_L] = \Omega^2 [Z_L]. \tag{2.4-31}$$

If the structure has rigid body modes, the solution of Equations (2.4-28) and (2.4-30) is made unique by the additional constraint

$$[X_R]^T[M_{LL}][\Delta U_L]=[0] \tag{2.4-32}$$

where matrix $[X_R]$ contains the rigid body modes.

2.5 Transient Response

The dynamic equation of a linear structure reads

$$[M][\ddot{u}(t)]+[D][\dot{u}(t)]+[K][u(t)]=[l(t)] \tag{2.5-1}$$

where $[M]$ is the mass matrix, $[D]$ is the damping matrix, $[K]$ is the stiffness matrix and $[l]$ is the load matrix. In partitioned form, Equation (2.5-1) reads

$$[M_{LL}][\ddot{u}_L]+[D_{LL}][\dot{u}_L]+[K_{LL}][u_L]=[l_L]-[K_{LP}][u_P]-[D_{LP}][\dot{u}_P]-[M_{LP}][\ddot{u}_P] \tag{2.5-2}$$

and

$$[M_{LP}]^T[\ddot{u}_L]+[M_{PP}][\ddot{u}_P]+[D_{LP}]^T[\dot{u}_L]+[D_{PP}][\dot{u}_P]+[K_{LP}]^T[u_L]+[K_{PP}][u_P]=[l_P]. \tag{2.5-3}$$

Equation (2.5-2) is a system of coupled linear differential equations of second order the solution of which yields the displacement matrix $[u_L]$. Subsequently, the reaction loads $[l_P]$ can be determined from Equation (2.5-3).

The load matrix $[l_L]$ and the matrix of prescribed displacements $[u_P]$ can be expressed as a linear combination of load patterns with time-dependent coefficients:

$$\begin{aligned}[l_L(t)]&=\sum_k [l_{Lk}]\phi_k(t)\\ [u_P(t)]&=\sum_k [u_{Pk}]\psi_k(t)\end{aligned} \tag{2.5-4}$$

In Mefisto, load patterns are defined by load cases. The time-dependent coefficients are assigned to the load patterns in the transient response analysis. In contrast to a frequency response analysis, in a transient response analysis several load patterns can be combined. It is also possible to combine prescribed forces with prescribed displacements. If displacements are prescribed, also the first and second derivatives of the functions $\psi_k(t)$ must be defined.

2.5.1 Direct Transient Response Analysis

In a direct transient response analysis, Mefisto uses the Newmark method to solve Equation (2.5-2).

Let $[u_L^n]=[u_L(n\Delta t)]$, $[\dot{u}_L^n]=[\dot{u}_L(n\Delta t)]$ and $[\ddot{u}_L^n]=[\ddot{u}_L(n\Delta t)]$. The displacements $[u_L^0]$ and the velocities $[\dot{u}_L^0]$ are known from the initial conditions. The initial accelerations $[\ddot{u}_L^0]$ can be computed from the initial conditions (see p. 15).

The Newmark algorithm [Newmark, 1959] uses the following approach for the displacements and velocities at time t_{n+1}:

$$\begin{aligned}\left[\dot{u}_L^{n+1}\right] &= \left[\dot{u}_L^{n}\right] + \left((1-\beta)\left[\ddot{u}_L^{n}\right] + \beta\left[\ddot{u}_L^{n+1}\right]\right)\Delta t \\ \left[u_L^{n+1}\right] &= \left[u_L^{n}\right] + \left[\dot{u}_L^{n}\right]\Delta t + \left(\frac{1}{2}-\alpha\right)\left[\ddot{u}_n^{L}\right] + \alpha\left[\ddot{u}_L^{n+1}\right]\Delta t^2\end{aligned} \tag{2.5-5}$$

Together with Equation (2.5-2), applied at time t_{n+1}, the following equations are obtained to compute the displacements, velocities and accelerations at time t_{n+1} (cf. [Bathe, 1996]):

1. Compute the coefficients
$$a_0 = \frac{1}{\alpha \Delta t^2},\quad a_1 = \frac{\beta}{\alpha \Delta t},\quad a_2 = \frac{1}{\alpha \Delta t},\quad a_3 = \frac{1}{2\alpha} - 1$$
$$a_4 = \frac{\beta}{\alpha} - 1,\quad a_5 = \frac{\Delta t}{2}(a_4 - 1),\quad a_6 = (1-\beta)\Delta t,\quad a_7 = \beta \Delta t$$
2. Compute and factorize the dynamic stiffness matrix:
$$\left[K_{LL}^{D}\right] = a_0\left[M_{LL}\right] + a_1\left[D_{LL}\right] + \left[K_{LL}\right] = \left[U_{LL}\right]\left[L_{LL}\right]$$
3. Compute the right-hand side:
$$\begin{aligned}\left[R_L^{n+1}\right] = \left[l_L^{n+1}\right] &- \left[K_{LP}\right]\left[u_P^{n+1}\right] - \left[D_{LP}\right]\left[\dot{u}_P^{n+1}\right] - \left[M_{LP}\right]\left[\ddot{u}_P^{n+1}\right] \\ &+ \left[M_{LL}\right]\left(a_0\left[u_L^{n}\right] + a_2\left[\dot{u}_L^{n}\right] + a_3\left[\ddot{u}_L^{n}\right]\right) \\ &+ \left[D_{LL}\right]\left(a_1\left[u_L^{n}\right] + a_4\left[\dot{u}_L^{n}\right] + a_5\left[\ddot{u}_L^{n}\right]\right)\end{aligned}$$
4. Solve for the displacements:
$$\left[u_L^{n+1}\right] = \left[U_{LL}\right]^{-1}\left[L_{LL}\right]^{-1}\left[R_L^{n+1}\right]$$
5. Compute accelerations and velocities:
$$\left[\ddot{u}_L^{n+1}\right] = a_0\left(\left[u_L^{n+1}\right] - \left[u_L^{n}\right]\right) - a_2\left[\dot{u}_L^{n}\right] - a_3\left[\ddot{u}_L^{n}\right]$$
$$\left[\dot{u}_L^{n+1}\right] = \left[\dot{u}_L^{n}\right] + a_6\left[\ddot{u}_L^{n}\right] + a_7\left[\ddot{u}_L^{n+1}\right]$$

With the standard values $\alpha = 0.25$ and $\beta = 0.5$ the algorithm is unconditionally stable.

The initial accelerations $\left[\ddot{u}_L^{0}\right]$ could be obtained from

$$\left[M_{LL}\right]\left[\ddot{u}_L^{0}\right] = \left[l_L^{0}\right] - \left[K_{LP}\right]\left[u_P^{0}\right] - \left[D_{LP}\right]\left[\dot{u}_P^{0}\right] - \left[M_{LP}\right]\left[\ddot{u}_P^{0}\right] - \left[D_{LL}\right]\left[\dot{u}_L^{0}\right] - \left[K_{LL}\right]\left[u_L^{0}\right]. \tag{2.5-6}$$

Unfortunately, however, the mass matrix $\left[M_{LL}\right]$ may be singular so that Equation (2.5-6) cannot be solved. This problem can be circumvented by the following approach which is implemented in Mefisto:

First, intermediate results $\left[u_L^{I}\right]$, $\left[\dot{u}_L^{I}\right]$ and $\left[\ddot{u}_L^{I}\right]$ are computed with a time step $\Delta\tau = \gamma \Delta t$ where $0 < \gamma \le 1$ (default: $\gamma = 0.1$). This computation is performed with $\beta = 1$ and $\alpha = 0.5$. With these values of the Newmark parameters, the ini-

tial accelerations are not needed.

Subsequently, using the given value of parameter β, the initial accelerations are obtained by solving the first of Equations (2.5-5) for $\left[\ddot{u}_L^0\right]$:

$$\left[\ddot{u}_L^0\right]=\frac{1}{(1-\beta)\Delta\tau}\left(\left[\dot{u}_L^I\right]-\left[\dot{u}_L^0\right]\right)-\frac{\beta}{1-\beta}\left[\ddot{u}_L^I\right] \tag{2.5-7}$$

2.5.2 Modal Transient Response Analysis

In a modal transient response analysis, the response is approximated by a superposition of the computed normal modes.

If there are prescribed displacements, first the base motion is computed from

$$\left[u_{Lk}^B\right]=-\left[K_{LL}\right]^{-1}\left[K_{LP}\right]\left[u_{Pk}\right]. \tag{2.5-8}$$

The base motion describes the static response to the prescribed displacements.

If the structure has rigid body modes, the solution of Equation (2.5-8) is made unique by the additional constraint

$$\left[X_R\right]^T\left[M_{LL}\right]\left[u_{Lk}^B\right]=[0] \tag{2.5-9}$$

where matrix $[X_R]$ contains the rigid body modes.

The motion relative to the base motion is approximated by a superposition of the computed eigenvectors, i.e.

$$\left[u_L(t)\right]\approx\left[u_L^p(t)\right]=\sum_k\left[u_{Lk}^B\right]\psi_k(t)+\left[X^p\right]\left[q(t)\right] \tag{2.5-10}$$

with

$$\left[X^p\right]=\left[\left[x_1\right]\quad\ldots\quad\left[x_p\right]\right],\ \ [u]_p=\left[q_1\quad\ldots\quad q_p\right]^T \tag{2.5-11}$$

where $\left[x_n\right],\ \ n=1,\ldots,p$ are the computed eigenvectors (cf. Equations (2.4-14) and (2.4-15)).

Insertion of (2.5-10) into (2.5-2) and subsequent projection on the eigenvectors leads to the p uncoupled equations

$$\begin{aligned}\ddot{q}_n(t)+2\omega_n D_n\dot{q}_n(t)+\omega_n^2 q_n(t)=&\left[x_n\right]^T\sum_k\left[l_{Lk}\right]\phi_k(t)\\&-\left[x_n\right]^T\sum_k\left(\left[M_{LL}\right]\left[u_{Lk}^B\right]+\left[M_{LP}\right]\left[u_{Pk}\right]\right)\ddot{\psi}_k(t)\\&-\left[x_n\right]^T\sum_k\left(\left[D_{LL}\right]\left[u_{Lk}^B\right]+\left[D_{LP}\right]\left[u_{Pk}\right]\right)\dot{\psi}_k(t)\end{aligned} \tag{2.5-12}$$

where D_n are the modal damping ratios and ω_n the circular eigenfrequencies.

If the damping is defined by modal damping ratios D_n, the equation

$$[x_n]^T[D_{LL}] = 2\,\omega_n D_n [x_n]^T[M_{LL}] \tag{2.5-13}$$

is used. In case of Rayleigh damping, the modal damping ratios of the elastic modes are obtained from

$$D_n = \frac{1}{2}\left(\alpha_K \omega_n + \frac{\alpha_M}{\omega_n}\right). \tag{2.5-14}$$

The rigid body modes, if any, are assumed to be undamped.

As in the case of the direct transient response analysis, the Newmark method is used to solve the system of equations (2.5-12). The initial conditions of the modal coordinates q_n are obtained from the initial displacements and velocities by

$$q_n^0 = [x_n]^T\left([u_L^0] - \sum_k [u_{Lk}^B]\psi_k^0\right) \tag{2.5-15}$$

and

$$\dot{q}_n^0 = [x_n]^T\left([\dot{u}_L^0] - \sum_k [u_{Lk}^B]\dot{\psi}_k^0\right). \tag{2.5-16}$$

The initial modal accelerations $[\ddot{q}_n^0]$ are obtained from Equation (2.5-12) applied at $t = 0$ and solved for the accelerations.

2.5.3 Enhanced Modal Reduction

The accuracy of the modal reduction can be improved if the modal basis is supplemented by a set of static mode shapes that ensure that the static response can be represented exactly.

First, the load patterns are collected into a single matrix

$$[P_L] = \left[[l_{L1}] \quad \ldots \quad [l_{Ll}] \quad -[M_{LL}][u_{L1}^B] \quad \ldots \quad -[M_{LL}][u_{Lm}^B]\right]. \tag{2.5-17}$$

Then, static displacements are obtained from

$$[K_{LL}][U_L^S] = [P_L]. \tag{2.5-18}$$

If the structure has rigid body modes, the static displacements are given by

$$[U_L^S] = \begin{bmatrix}[U_E^S] \\ [0]\end{bmatrix} \tag{2.5-19}$$

where

$$[K_{EE}][U_E^S] = [J_E]^T\left([P_L] - [M_{LL}][X_R][X_R]^T[P_L]\right) \tag{2.5-20}$$

(cf. section 2.3).

Next, a set of vectors that are mass-orthogonal to the normal modes is com-

puted from

$$[\widetilde{X}^S]=[U_L^S]-[X^p][X^p]^T[M_{LL}][U_L^S]. \tag{2.5-21}$$

Subsequently, the projected eigenvalue problem

$$[\widetilde{X}^S]^T[K_{LL}][\widetilde{X}^S][q^S]=[\widetilde{X}^S]^T[M_{LL}][\widetilde{X}^S][q^S][\Omega^S]^2 \tag{2.5-22}$$

is solved for $[q^S]$. Finally, the static mode shapes are obtained from

$$[X^S]=[\widetilde{X}^S][q^S]. \tag{2.5-23}$$

The static mode shapes have the following properties:

1. $[X^p]^T[M_{LL}][X^S]=[0],\ [X^p]^T[K_{LL}][X^S]=[0]$
2. $[X^S]^T[M_{LL}][X^S]=[I],\ [X^S]^T[K_{LL}][X^S]=[\Omega^S]^2$ where $[\Omega^S]$ is a diagonal matrix.

Thus, the augmented modal basis $[[X]\ \ [X^S]]$ has the same properties as the original modal basis. The static solution is contained in the span of this basis.

2.6 Estimation of Reduction Error

The accuracy of the solution obtained with a modal frequency response analysis can be assessed by looking at the error of the strain energy. This error reads

$$\Delta E^{Sp}=\frac{1}{4}\left([U_L]^H[K_{LL}][U_L]-[U_L^p]^H[K_{LL}][U_L^p]\right). \tag{2.6-1}$$

In case of force excitation, the error without static correction is

$$\Delta E^{Sp}=\frac{1}{4}\sum_{n=p+1}^{N}\omega_n^2|Q_n|^2=\frac{1}{4}\sum_{n=p+1}^{N}|H_n|^2\left(\frac{[x_n]^T[L_L]}{\omega_n}\right)^2 \tag{2.6-2}$$

where N is the total number of eigenvectors, and

$$H_n=\omega_n^2G_n=\frac{1}{1-\left(\frac{\Omega}{\omega_n}\right)^2+2i\,D_n\left(\frac{\Omega}{\omega_n}\right)}\ . \tag{2.6-3}$$

An upper bound of the error is

$$\Delta E^{Sp}<\frac{1}{4}|H_p|^2\sum_{n=p+1}^{N}\left(\frac{[x_n]^T[L_L]}{\omega_n}\right)^2. \tag{2.6-4}$$

If the structure does not have rigid body modes, a static solution

$$[u_L]=[K_{LL}]^{-1}[L_L] \tag{2.6-5}$$

can be computed. This static solution equals the frequency response at the excitation frequency $\Omega = 0$:

$$[u_L] = \sum_{n=1}^{N} \frac{1}{\omega_n^2} [x_n] [x_n]^T [L_L] \tag{2.6-6}$$

The strain energy of the static solution is

$$E_S^S = \frac{1}{2} [u_L]^T [K_{LL}] [u_L] = \sum_{n=1}^{p} \frac{1}{2} \left(\frac{[x_n]^T [L_L]}{\omega_n} \right)^2 + \sum_{n=p+1}^{N} \frac{1}{2} \left(\frac{[x_n]^T [L_L]}{\omega_n} \right)^2 . \tag{2.6-7}$$

Thus,

$$\sum_{n=p+1}^{N} \left(\frac{[x_n]^T [L_L]}{\omega_n} \right)^2 = 2 E_S^S - \sum_{n=1}^{p} \left(\frac{[x_n]^T [L_L]}{\omega_n} \right)^2 . \tag{2.6-8}$$

With the modal strain energies

$$E_n^S = \frac{1}{2} \left(\frac{[x_n]^T [L_L]}{\omega_n} \right)^2 \tag{2.6-9}$$

the strain energy error satisfies

$$\Delta E^{Sp} < \frac{1}{2} |H_p|^2 \left(E_S^S - \sum_{n=1}^{p} E_n^S \right). \tag{2.6-10}$$

The relative error is

$$e_S^p = \frac{\Delta E^{Sp}}{E_S^S} < \frac{1}{2} |H_p|^2 \left(1 - \sum_{n=1}^{p} \frac{E_n^F}{E_S^F} \right). \tag{2.6-11}$$

With static correction, the static response of the neglected modes is included in the solution. Thus, the error is

$$\Delta E^{Spc} = \frac{1}{4} \sum_{n=p+1}^{N} \left(|H_n|^2 - 1 \right) \left(\frac{[x_n]^T [L_L]}{\omega_n} \right)^2 . \tag{2.6-12}$$

The relative error satisfies

$$e_S^{pc} < \frac{1}{2} \left(|H_p|^2 - 1 \right) \left(1 - \sum_{n=1}^{p} \frac{E_n^S}{E_S^S} \right). \tag{2.6-13}$$

In case of a base motion excitation the same relations are obtained, with

$$[L_L] = \Omega^2 \left([M_{LL}] \left[U_L^B \right] + [M_{LP}] [U_P] \right). \tag{2.6-14}$$

Both the modal strain energies E_n^S and the static strain energy E_S^S are proportional to Ω^4. Thus, this factor cancels out when computing the relative er-

ror.

If the structure has rigid body modes, the static solution is the solution of the inertia relief problem

$$[K_{LL}][u_L]=[L_L]-[M_{LL}][X_R][X_R]^T[L_L] \tag{2.6-15}$$

where matrix $[X_R]$ contains the rigid body modes. Equation (2.6-15) means that the structure is loaded by the applied loads and the inertia loads due to the rigid body acceleration caused by the applied loads.

The solution of Equation (2.6-15) is unique only up to a rigid body motion. Because a rigid body motion does not contribute to the strain energy, Equation (2.6-15) can be solved for any arbitrary set of fictitious supports that prevent a rigid body motion.

Because the elastic modes are mass orthogonal with respect to the rigid body modes, the modal strain energies can still be computed from Equation (2.6-9).

2.7 Linear Constraints

2.7.1 Matrix Transformations

The displacements $[u_D]$ at the dependent degrees of freedom depend linearly on the displacements $[u_I]$ at the independent degrees of freedom:

$$[u_D]=[C_{DI}][u_I] \tag{2.7-1}$$

This equation can be expanded to

$$\begin{bmatrix}[u_I]\\[u_D]\end{bmatrix}=\begin{bmatrix}[I_{II}]\\[C_{DI}]\end{bmatrix}[u_I]=[C_{Gi}][u_I] \tag{2.7-2}$$

where $[I_{II}]$ is the unit matrix related to the independent degrees of freedom.

With the partitioning

$$[K]=\begin{bmatrix}[K_{II}] & [K_{ID}]\\ [K_{ID}]^T & [K_{DD}]\end{bmatrix} \tag{2.7-3}$$

the transformed stiffness matrix reads

$$\begin{aligned}[\bar{K}_{II}]&=[C_{GI}]^T[K][C_{GI}]\\ &=[K_{II}]+[K_{ID}][C_{DI}]+[C_{DI}]^T[K_{ID}]^T+[C_{DI}]^T[K_{DD}][C_{DI}].\end{aligned} \tag{2.7-4}$$

With the augmented constraint matrix

$$[C]=\begin{bmatrix}[I_{II}] & [0_{ID}]\\ [C_{DI}] & [0_{DD}]\end{bmatrix} \tag{2.7-5}$$

the transformation reads

$$[\bar{K}]=[C]^T[K][C]=\begin{bmatrix}[\bar{K}_{II}] & [0_{ID}]\\ [0_{DI}] & [0_{DD}]\end{bmatrix}. \tag{2.7-6}$$

From $[\bar{K}]$, the *L*- and *P*-partitions can be obtained in the usual way.

The mass matrix is transformed in the same way:

$$[\bar{M}]=[C]^T[M][C] \tag{2.7-7}$$

Finally the transformation of the load matrix is

$$[\bar{l}]=[C]^T[l]. \tag{2.7-8}$$

All equations of sections 2.2 to 2.6 also apply in the presence of linear constraints. It is only necessary to replace $[K]$ by $[\bar{K}]$, $[M]$ by $[\bar{M}]$ and $[l]$ by $[\bar{l}]$.

2.7.2 Constraint Matrices

The constraint matrix $[C]$ is assembled from the constraint matrices of the different linear constraints. The contributions depend on the type of the linear constraint.

connect

The displacements at the connected pairs of degrees of freedom are identical. The constraint matrix is therefore simply an identity matrix.

rigbdy

The displacements at the dependent degrees of freedom follow a rigid body motion defined by the displacements at the autonomous degrees of freedom. So there are always six autonomous degrees of freedom in a three-dimensional problem and three in a two-dimensional problem.

In three dimensions, the rigid body motion is described by

$$\begin{bmatrix}[u_D]\\ [r_D]\end{bmatrix}=\begin{bmatrix}[I_{33}] & [R_{33}]\\ [0_{33}] & [I_{33}]\end{bmatrix}\begin{bmatrix}[u_A]\\ [r_A]\end{bmatrix} \tag{2.7-9}$$

where

$$[u]=[u_x \quad u_y \quad u_z]^T,\ [r]=[r_x \quad r_y \quad r_z]^T \tag{2.7-10}$$

are the translations and rotations, $[I_{33}]$ is the three-dimensional unit matrix,

$[0_{33}]$ is the three-dimensional null matrix and

$$[R_{33}]=\begin{bmatrix} 0 & z_D-z_A & -(y_D-y_A) \\ -(z_D-z_A) & 0 & x_D-x_A \\ y_D-y_A & -(x_D-x_A) & 0 \end{bmatrix} \tag{2.7-11}$$

is the three-dimensional rotation matrix. In two dimensions, columns 3 to 5 and rows 3 to 5 are removed.

The constraint matrix $[C]$ is assembled from the rows of Equation (2.7-9) that correspond to the dependent degrees of freedom.

rigfit

This constraint is mainly used to apply loads of which only the resultants with respect to a certain point are known. The load is distributed to a set of nodal points so that the resultants of these distributed loads agree with the resultants of the given load.

This constraint is closely related to the rigid body constraint, but now the degrees of freedom that control the rigid body motion are dependent degrees of freedom. The loads are applied at the dependent degrees of freedom and distributed to the autonomous degrees of freedom.

Let $[X_{AD}]$ be the rigid body matrix that describes the motion of the autonomous degrees of freedom due to a unit rigid body motion of the dependent degrees of freedom. This matrix is the same as the constraint matrix of the rigid body constraint.

The condition that the resultants of the loads at the autonomous degrees of freedom with respect to the nodal point with the dependent degrees of freedom are identical with the resultants of the loads at the dependent degrees of freedom reads

$$[X_{AD}]^T[l_A]=[l_D]. \tag{2.7-12}$$

With

$$[l_A]=[C_{DA}]^T[l_D] \tag{2.7-13}$$

Equation (2.7-12) reads

$$[X_{AD}]^T[C_{DA}]^T[l_D]=[l_D]. \tag{2.7-14}$$

Thus,

$$[X_{AD}]^T[C_{DA}]^T=[I_{AA}] \tag{2.7-15}$$

or

$$[C_{DA}][X_{AD}]=[I_{AA}]. \tag{2.7-16}$$

Hence, the constraint matrix $[C_{DA}]$ is the generalized inverse of matrix $[X_{AD}]$. With the QR-decomposition

$$[X_{AD}]=[Q_{AD}][R_{DD}] \tag{2.7-17}$$

where $[Q_{AD}]$ is an orthonormal matrix and $[R_{DD}]$ an upper triangular matrix, the constraint matrix $[C_{DA}]$ can be computed from

$$[C_{DA}]=[R_{DD}]^{-1}[Q_{AD}]^T. \tag{2.7-18}$$

There is also a kinematic interpretation of this constraint. The displacements

$$[u_D]=[C_{DA}][u_A]$$

solve the minimization problem

$$\|[u_A]-[X_{AD}][u_D]\|=\text{Min}. \tag{2.7-19}$$

The displacements at the dependent degrees of freedom thus define a rigid body motion that best matches the displacements at the autonomous degrees of freedom. Therefore, this constraint is called rigfit.

3 Elements in Solid Mechanics

3.1 The Beam Element

3.1.1 Assumptions

The current Mefisto beam element has a constant cross section and satisfies the assumptions of the Euler-Bernoulli theory, i.e. shear deformations are neglected.

3.1.2 Definitions

The x_E-axis of the element coordinate system points from the centre of area of cross section 1 to the centre of area of cross section 2. The z_E-axis is in the plane spanned by the x_E-axis and the user defined vector $\boldsymbol{v}$. The y_E-axis complements these two axes to form a right-handed coordinate system (see Figure 3.1-1).

The unit vectors of the beam coordinate system can be computed from

$$\boldsymbol{b}_x=\frac{\boldsymbol{r}_2-\boldsymbol{r}_1}{\|\boldsymbol{r}_2-\boldsymbol{r}_1\|},\quad \boldsymbol{c}_z=\boldsymbol{v}-(\boldsymbol{v}\cdot\boldsymbol{b}_x)\boldsymbol{b}_x,\quad \boldsymbol{b}_z=\frac{\boldsymbol{c}_z}{\|\boldsymbol{c}_z\|},\quad \boldsymbol{b}_y=\boldsymbol{b}_z\times\boldsymbol{b}_x \tag{3.1-1}$$

where $\boldsymbol{r}_1$ and $\boldsymbol{r}_2$ are the position vectors of the two nodal points.

Each of the two nodal points of the element has six degrees of freedom:

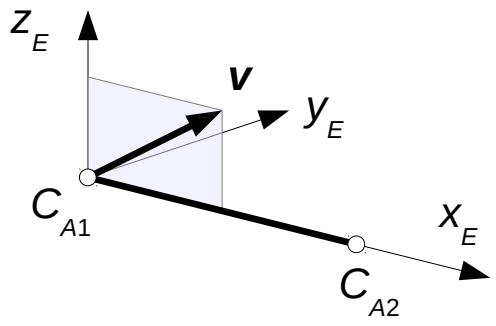


Figure 3.1-1: Beam Coordinate System

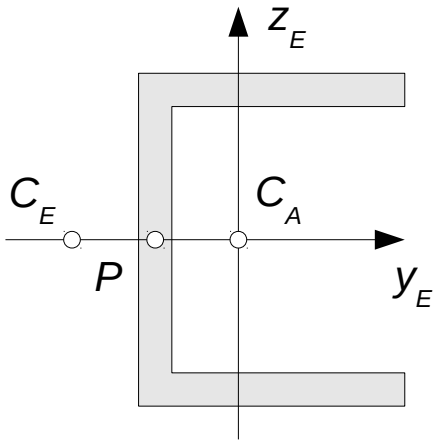


Figure 3.1-2: Centre of Area C_A, Shear Centre C_E and Nodal Point P

- Translation u in x_E-direction
- Translation v in y_E-direction
- Translation w in z_E-direction
- Rotation θ about the x_E-axis
- Rotation ϕ about the y_E-axis
- Rotation ψ about the z_E-axis

The shear centre C_E is the centre of the resultant shear forces. It is also the point about which the cross section rotates in pure torsion.

The location of the shear centre as well as of the nodal points the element is connected to are defined with respect to the element coordinate system (see Figure 3.1-2). If these points are undefined, they are assumed to coincide with the centre of area.

3.1.3 Kinematics

Transformation matrices

Let matrices $[\boldsymbol{b}_x]$, $[\boldsymbol{b}_y]$ and $[\boldsymbol{b}_z]$ contain the coordinates of the basis vectors of the element coordinate system with respect to the global coordinate system. Then, the transformation of the displacement vector from the element coordinate system to the structural coordinate system reads

$$[\boldsymbol{u}]=\begin{bmatrix}u_x\\u_y\\u_z\end{bmatrix}=[\boldsymbol{b}_x]u+[\boldsymbol{b}_y]v+[\boldsymbol{b}_z]w=\begin{bmatrix}[\boldsymbol{b}_x] & [\boldsymbol{b}_y] & [\boldsymbol{b}_z]\end{bmatrix}\begin{bmatrix}u\\v\\w\end{bmatrix}=[T]_E^T[\boldsymbol{u}]_E \tag{3.1-2}$$

where

$$[T]_E=\begin{bmatrix}[\boldsymbol{b}_x]^T\\[\boldsymbol{b}_y]^T\\[\boldsymbol{b}_z]^T\end{bmatrix} \tag{3.1-3}$$

is the transformation matrix from the structural coordinate system to the element coordinate system. Likewise, the transformation of the rotations reads

$$[\boldsymbol{\phi}]=\begin{bmatrix}\phi_x\\\phi_y\\\phi_z\end{bmatrix}=[\boldsymbol{b}_x]\theta+[\boldsymbol{b}_y]\phi+[\boldsymbol{b}_z]\psi=\begin{bmatrix}[\boldsymbol{b}_x] & [\boldsymbol{b}_y] & [\boldsymbol{b}_z]\end{bmatrix}\begin{bmatrix}\theta\\\phi\\\psi\end{bmatrix}=[T]_E^T[\boldsymbol{\phi}]_E \quad . \tag{3.1-4}$$

If the centre of area does not coincide with the nodal point, the displacement vector $\boldsymbol{u}_A$ of the centre of area can be computed from

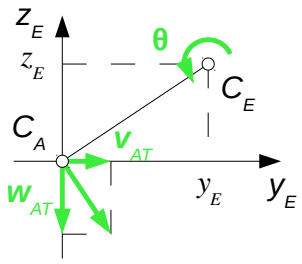


Figure 3.1-3: Rotation about Shear Centre

$$\boldsymbol{u}_A = \boldsymbol{u}_P + \boldsymbol{\phi} \times \boldsymbol{r}_{PA} \tag{3.1-5}$$

where $\boldsymbol{u}_P$ is the displacement vector of the nodal point, $\boldsymbol{\phi}$ is the rotation vector and $\boldsymbol{r}_{PA}$ is the vector from the nodal point to the centre of area. If y_P and z_P are the coordinates of the nodal point with respect to the element coordinate system, then Equation (3.1-5) reads

$$\begin{bmatrix} u_A \\ v_A \\ w_A \end{bmatrix} = \begin{bmatrix} u \\ v \\ w \end{bmatrix} - \begin{bmatrix} \theta \\ \phi \\ \psi \end{bmatrix} \times \begin{bmatrix} 0 \\ y_P \\ z_P \end{bmatrix} = \begin{bmatrix} u \\ v \\ w \end{bmatrix} + \begin{bmatrix} 0 & -z_P & y_P \\ z_P & 0 & 0 \\ -y_P & 0 & 0 \end{bmatrix} \begin{bmatrix} \theta \\ \phi \\ \psi \end{bmatrix}. \tag{3.1-6}$$

The motion of a cross section can be subdivided into a motion due to extension, a motion due to bending and a motion due to rotation. As the cross section rotates about the shear centre, the corresponding motion of the centre of area is, see Figure 3.1-3,

$$\begin{bmatrix} v_{AT} \\ w_{AT} \end{bmatrix} = \begin{bmatrix} z_E \\ -y_E \end{bmatrix} \theta \tag{3.1-7}$$

where x_E and y_E are the coordinates of the shear centre with respect to the element coordinate system. The motion due to bending is

$$\begin{bmatrix} v_{AB} \\ w_{AB} \end{bmatrix} = \begin{bmatrix} v_A \\ w_A \end{bmatrix} - \begin{bmatrix} v_{AT} \\ w_{AT} \end{bmatrix} = \begin{bmatrix} 1 & 0 & -z_E \\ 0 & 1 & y_E \end{bmatrix} \begin{bmatrix} v_A \\ w_A \\ \theta \end{bmatrix}. \tag{3.1-8}$$

Displacements

The total displacements of an arbitrary point of the cross section can be subdivided into the displacements due to extension, due to bending and due to rotation:

$$\begin{bmatrix} u \\ v \\ w \end{bmatrix} = \begin{bmatrix} u_E \\ 0 \\ 0 \end{bmatrix} + \begin{bmatrix} u_B \\ v_B \\ w_B \end{bmatrix} + \begin{bmatrix} u_T \\ v_T \\ w_T \end{bmatrix}. \tag{3.1-9}$$

The displacements due to extension are constant over the cross section:

$$u_E(x)=u_A(x) \tag{3.1-10}$$

In the Euler-Bernoulli theory, bending causes the cross sections to perform a rigid rotation about an axis in the *yz*-plane through the centre of area. Hence,

$$u_B(x,y,z)=\phi(x)z-\psi(x)y. \tag{3.1-11}$$

The shear strains are

$$\gamma_{xy}=\frac{\partial u_B}{\partial y}+\frac{\partial v_B}{\partial x}=-\psi(x)+\frac{dv_B}{dx},\quad \gamma_{xz}=\frac{\partial u_B}{\partial z}+\frac{\partial w_B}{\partial x}=\phi(x)+\frac{dw_B}{dx}. \tag{3.1-12}$$

In the Euler-Bernoulli theory, the shear strains are neglected:

$$\gamma_{xy}=0 \;\rightarrow\; \psi(x)=\frac{dv_B}{dx}\;,\ \gamma_{xz}=0 \;\rightarrow\; \phi(x)=-\frac{dw_B}{dx} \tag{3.1-13}$$

The longitudinal strains are

$$\epsilon_x=\frac{du}{dx}=\frac{du_A}{dx}+\frac{d\phi}{dx}z-\frac{d\psi}{dx}y=\frac{du_A}{dx}-\frac{d^2w_B}{dx^2}z-\frac{d^2v_B}{dx^2}y. \tag{3.1-14}$$

Interpolation

For interpolation, the non-dimensional coordinate $\xi = x/L$ is used where L is the length of the beam. Then, $\xi = 0$ corresponds to nodal point 1 and $\xi = 1$ to nodal point 2.

For the longitudinal displacement u_A a linear interpolation is sufficient:

$$u_A(\xi)=(1-\xi)u_{A1}+\xi u_{A2}\ . \tag{3.1-15}$$

For bending, displacements and rotations must be continuous at the nodal points. Thus, Hermite interpolation has to be used:

$$\begin{aligned} v_B(\xi)&=H_1(\xi)v_{B1}+H_2(\xi)\psi_1+H_3(\xi)v_{B2}+H_4(\xi)\psi_2\\ w_B(\xi)&=H_1(\xi)w_{B1}-H_2(\xi)\phi_1+H_3(\xi)w_{B2}-H_4(\xi)\phi_2 \end{aligned} \tag{3.1-16}$$

The Hermite polynomials read:

$$\begin{aligned} H_1(\xi)&=2\xi^3-3\xi^2+1 & H_3(\xi)&=-2\xi^3+3\xi^2\\ H_2(\xi)&=L(\xi^3-2\xi^2+\xi) & H_4(\xi)&=L(\xi^3-\xi^2) \end{aligned} \tag{3.1-17}$$

They satisfy

$$\begin{aligned} &H_1(0)=1,\ H_1(1)=0,\ H_3(0)=0,\ H_3(1)=1,\\ &H_2(0)=0,\ H_2(1)=0,\ H_4(0)=0,\ H_4(1)=0\ . \end{aligned} \tag{3.1-18}$$

The derivatives read:

$$\begin{aligned} \frac{dH_1}{d\xi} &= 6\xi^2 - 6\xi & \frac{dH_3}{d\xi} &= -6\xi^2 + 6\xi \\ \frac{dH_2}{d\xi} &= L\left(3\xi^2 - 4\xi + 1\right) & \frac{dH_4}{d\xi} &= L\left(3\xi^2 - 2\xi\right) \end{aligned} \tag{3.1-19}$$

They satisfy

$$\begin{aligned} &\frac{dH_1}{d\xi}(0) = 0, \quad \frac{dH_1}{d\xi}(1) = 0, \quad \frac{dH_3}{d\xi}(0) = 0, \quad \frac{dH_3}{d\xi}(1) = 0, \\ &\frac{dH_2}{d\xi}(0) = L, \quad \frac{dH_2}{d\xi}(1) = 0, \quad \frac{dH_4}{d\xi}(0) = 0, \quad \frac{dH_4}{d\xi}(0) = L \quad . \end{aligned} \tag{3.1-20}$$

Thus,

$$\begin{aligned} &v_B(0) = v_{B1}, \quad v_B(1) = v_{B2}, \quad w_B(0) = w_{B1}, \quad w_B(1) = w_{B2}, \\ &\frac{dv_B}{dx}(0) = \frac{1}{L}\frac{dv_B}{d\xi}(0) = \psi_1, \quad \frac{dv_B}{dx}(1) = \frac{1}{L}\frac{dv_B}{d\xi}(1) = \psi_2, \\ &\frac{dw_B}{dx}(0) = \frac{1}{L}\frac{dw_B}{d\xi}(0) = -\phi_1, \quad \frac{dw_B}{dx}(1) = \frac{1}{L}\frac{dw_B}{d\xi}(1) = -\phi_2 \end{aligned} \tag{3.1-21}$$

as required.

To compute the strains, also the second derivatives of the Hermite polynomials are needed. They read:

$$\begin{aligned} &\frac{d^2H_1}{d\xi^2} = 12\xi - 6, \quad \frac{d^2H_3}{d\xi^2} = -12\xi + 6, \\ &\frac{d^2H_2}{d\xi^2} = L(6\xi - 4), \quad \frac{d^2H_4}{d\xi^2} = L(6\xi - 2) \end{aligned} \tag{3.1-22}$$

Then, the longitudinal strains due to bending read:

$$\begin{aligned} \epsilon_{Bx} &= -\frac{1}{L^2}\left(\frac{d^2w_B}{d\xi^2}z + \frac{d^2v_B}{d\xi^2}y\right) \\ &= -\frac{z}{L^2}\left[(12\xi - 6)w_{B1} - L(6\xi - 4)\phi_1 + (-12\xi + 6)w_{B2} - L(6\xi - 2)\phi_2\right] \\ &\quad -\frac{y}{L^2}\left[(12\xi - 6)v_{B1} + L(6\xi - 4)\psi_1 + (-12\xi + 6)v_{B2} - L(6\xi - 2)\psi_2\right] \end{aligned} \tag{3.1-23}$$

With the matrices

$$\left[B_z\right] = \left[12\xi - 6 \quad -L(6\xi - 4) \quad -12\xi + 6 \quad -L(6\xi - 2)\right], \quad [w] = \begin{bmatrix} w_{B1} \\ \phi_1 \\ w_{B2} \\ \phi_2 \end{bmatrix} \tag{3.1-24}$$

and

$$[B_y]=\begin{bmatrix}12\xi-6 & L(6\xi-4) & -12\xi+6 & L(6\xi-2)\end{bmatrix},\quad [v]=\begin{bmatrix}v_{B1}\\ \psi_1\\ v_{B2}\\ \psi_2\end{bmatrix} \tag{3.1-25}$$

Equation (3.1-23) reads

$$\epsilon_{Bx}=-\frac{z}{L^2}[B_z][w]-\frac{y}{L^2}[B_y][v]. \tag{3.1-26}$$

3.1.4 Stiffness Matrix

Extensional Stiffness Matrix

The extensional stiffness matrix relates the normal forces to the displacements in longitudinal direction:

$$\begin{bmatrix}N_1\\ N_2\end{bmatrix}=\frac{EA}{L}\begin{bmatrix}1 & -1\\ -1 & 1\end{bmatrix}\begin{bmatrix}u_{A1}\\ u_{A2}\end{bmatrix} \tag{3.1-27}$$

Bending Stiffness Matrix

The bending stiffness matrix relates the shear forces and the bending moments to the motion in the *xy*- and the *xz*-planes.

With $\sigma_y=\sigma_z=\tau_{xy}=\tau_{xz}=\tau_{yz}=0$ and $\sigma_x=E\,\epsilon_{Bx}$, the virtual strain energy per volume is

$$\begin{aligned}\delta\epsilon_x\sigma_x&=\left(-\frac{z}{L^2}[B_z][\delta w]-\frac{y}{L^2}[B_y][\delta v]\right)^T E\left(-\frac{z}{L^2}[B_z][w]-\frac{y}{L^2}[B_y][v]\right)\\ &=\frac{Ez^2}{L^4}[\delta w]^T[B_z]^T[B_z][w]+\frac{Eyz}{L^4}\left([\delta w]^T[B_z]^T[B_y][v]+[\delta v]^T[B_y]^T[B_z][w]\right)\\ &\quad+\frac{Ey^2}{L^4}[\delta v]^T[B_y]^T[B_y][v]\\ &=\frac{E}{L^4}\begin{bmatrix}[\delta v]^T & [\delta w]^T\end{bmatrix}\begin{bmatrix}y^2[B_y]^T[B_y] & yz[B_y]^T[B_z]\\ yz[B_z]^T[B_y] & z^2[B_z]^T[B_z]\end{bmatrix}\begin{bmatrix}[v]\\ [w]\end{bmatrix}.\end{aligned} \tag{3.1-28}$$

Integration over the volume gives

$$\delta\epsilon_x\sigma_x=\frac{E}{L^3}\begin{bmatrix}[\delta v]^T & [\delta w]^T\end{bmatrix}\int_0^1\begin{bmatrix}I_z[B_y]^T[B_y] & -I_{yz}[B_y]^T[B_z]\\ -I_{yz}[B_z]^T[B_y] & I_y[B_z]^T[B_z]\end{bmatrix}d\xi\begin{bmatrix}[v]\\ [w]\end{bmatrix} \tag{3.1-29}$$

where

$$I_y = \int_A z^2\,dA\,,\quad I_z = \int_A y^2\,dA \text{ and } I_{yz} = -\int_A y\,z\,dA$$

are the area moments of inertia.

Thus, the bending stiffness matrix reads

$$[k_B]_E = \frac{E}{L^3}\begin{bmatrix} I_z \int_0^1 [B_y]^T [B_y]\,d\xi & -I_{yz} \int_0^1 [B_y]^T [B_z]\,d\xi \\ -I_{yz} \int_0^1 [B_z]^T [B_y]\,d\xi & I_y \int_0^1 [B_z]^T [B_z]\,d\xi \end{bmatrix}. \tag{3.1-30}$$

Evaluation of the integrals gives:

$$[B_{yy}] = \int_0^1 [B_y]^T [B_y]\,d\xi = \begin{bmatrix} 12 & 6L & -12 & 6L \\ 6L & 4L^2 & -6L & 2L^2 \\ -12 & -6L & 12 & -6L \\ 6L & 2L^2 & -6L & 4L^2 \end{bmatrix} \tag{3.1-31}$$

$$[B_{yz}] = \int_0^1 [B_y]^T [B_z]\,d\xi = \begin{bmatrix} 12 & -6L & -12 & -6L \\ 6L & -4L^2 & -6L & -2L^2 \\ -12 & 6L & 12 & 6L \\ 6L & -2L^2 & -6L & -4L^2 \end{bmatrix} \tag{3.1-32}$$

$$[B_{zz}] = \int_0^1 [B_z]^T [B_z]\,d\xi = \begin{bmatrix} 12 & -6L & -12 & -6L \\ -6L & 4L^2 & 6L & 2L^2 \\ -12 & 6L & 12 & 6L \\ -6L & 2L^2 & 6L & 4L^2 \end{bmatrix} \tag{3.1-33}$$

Torsional Stiffness Matrix

The torsional stiffness matrix relates the torsional moments to the rotations about the *x*-axis:

$$\begin{bmatrix} M_{x1} \\ M_{x2} \end{bmatrix} = \frac{G I_T}{L}\begin{bmatrix} 1 & -1 \\ -1 & 1 \end{bmatrix}\begin{bmatrix} \theta_1 \\ \theta_2 \end{bmatrix} \tag{3.1-34}$$

Complete Stiffness Matrix in the Element Coordinate System

The order of the element degrees of freedom is

1	2	3	4	5	6	7	8	9	10	11	12
u_{A1}	v_{B1}	w_{B1}	θ_1	ϕ_1	ψ_1	u_{A2}	v_{B2}	w_{B2}	θ_2	ϕ_2	ψ_2

Thus, the extensional, bending and torsional stiffness matrices are inserted into the complete stiffness matrix as follows:

```
k([1,7],[1,7])             = kE
k([2,6,8,12],[2,6,8,12]) = E * Iz * Byy / L^3
k([2,6,8,12],[3,5,9,11]) = -E * Iyz* Byz / L^3
k([3,5,9,11],[2,6,8,12]) = k([2,6,8,12],[3,5,9,11])'
k([3,5,9,11],[2,5,9,11]) = E * Iy * Bzz / L^3
k([4,10],[4,10])           = kT
```

Transformation to the Structural Coordinate System

The displacements of the nodal points, in the element coordinate system, are obtained from the displacements of the nodal points, in the structural coordinate system, by

$$\begin{bmatrix} [u_1]_E \\ [\phi_1]_E \\ [u_2]_E \\ [\phi_2]_E \end{bmatrix} = \begin{bmatrix} [T]_E & [0] & [0] & [0] \\ [0] & [T]_E & [0] & [0] \\ [0] & [0] & [T]_E & [0] \\ [0] & [0] & [0] & [T]_E \end{bmatrix} \begin{bmatrix} [u_1] \\ [\phi_1] \\ [u_2] \\ [\phi_2] \end{bmatrix} \tag{3.1-35}$$

where $[T]_E$ is given by Equation (3.1-3) and

$$[u_n]_E = \begin{bmatrix} u_n \\ v_n \\ w_n \end{bmatrix}, \quad [\phi_n]_E = \begin{bmatrix} \theta_n \\ \phi_n \\ \psi_n \end{bmatrix}, \quad [u_n] = \begin{bmatrix} u_{nx} \\ u_{ny} \\ u_{nz} \end{bmatrix}, \quad [\phi_n] = \begin{bmatrix} \phi_{nx} \\ \phi_{ny} \\ \phi_{nz} \end{bmatrix}, \quad n = 1,2. \tag{3.1-36}$$

The displacements of the centre of area are

$$\begin{bmatrix} [u_{A1}]_E \\ [\phi_1]_E \\ [u_{A2}]_E \\ [\phi_2]_E \end{bmatrix} = \begin{bmatrix} [I] & [T_A] & [0] & [0] \\ [0] & [I] & [0] & [0] \\ [0] & [0] & [I] & [T_A] \\ [0] & [0] & [0] & [I] \end{bmatrix} \begin{bmatrix} [u_1]_E \\ [\phi_1]_E \\ [u_2]_E \\ [\phi_2]_E \end{bmatrix} \tag{3.1-37}$$

where $[T_A]$ is defined by Equation (3.1-6) and

$$[u_{An}]_E = \begin{bmatrix} u_{An} \\ v_{An} \\ w_{An} \end{bmatrix}, \quad n = 1,2 \quad . \tag{3.1-38}$$

Finally, the bending deformation is obtained from

$$\begin{bmatrix} [u_{B1}]_E \\ [\phi_1]_E \\ [u_{B2}]_E \\ [\phi_2]_E \end{bmatrix} = \begin{bmatrix} [I] & [T_R] & [0] & [0] \\ [0] & [I] & [0] & [0] \\ [0] & [0] & [I] & [T_R] \\ [0] & [0] & [0] & [I] \end{bmatrix} \begin{bmatrix} [u_{A1}]_E \\ [\phi_1]_E \\ [u_{A2}]_E \\ [\phi_2]_E \end{bmatrix} \tag{3.1-39}$$

with

$$[T_R]=\begin{bmatrix} 0 & 0 & 0 \\ -z_E & 0 & 0 \\ y_e & 0 & 0 \end{bmatrix}, \tag{3.1-40}$$

cf. Equation (3.1-7).

3.1.5 Mass Matrix

Lumped Mass Matrix

In the element coordinate system, the lumped mass matrix reads

$$[m]_E=\frac{1}{2}\begin{bmatrix} m & 0 & 0 & 0 & 0 & 0 & 0 & 0 & 0 & 0 & 0 & 0 \\ 0 & m & 0 & 0 & 0 & 0 & 0 & 0 & 0 & 0 & 0 & 0 \\ 0 & 0 & m & 0 & 0 & 0 & 0 & 0 & 0 & 0 & 0 & 0 \\ 0 & 0 & 0 & J_x & 0 & 0 & 0 & 0 & 0 & 0 & 0 & 0 \\ 0 & 0 & 0 & 0 & 0 & 0 & 0 & 0 & 0 & 0 & 0 & 0 \\ 0 & 0 & 0 & 0 & 0 & 0 & 0 & 0 & 0 & 0 & 0 & 0 \\ 0 & 0 & 0 & 0 & 0 & 0 & m & 0 & 0 & 0 & 0 & 0 \\ 0 & 0 & 0 & 0 & 0 & 0 & 0 & m & 0 & 0 & 0 & 0 \\ 0 & 0 & 0 & 0 & 0 & 0 & 0 & 0 & m & 0 & 0 & 0 \\ 0 & 0 & 0 & 0 & 0 & 0 & 0 & 0 & 0 & J_x & 0 & 0 \\ 0 & 0 & 0 & 0 & 0 & 0 & 0 & 0 & 0 & 0 & 0 & 0 \\ 0 & 0 & 0 & 0 & 0 & 0 & 0 & 0 & 0 & 0 & 0 & 0 \end{bmatrix} \tag{3.1-41}$$

where

$$m=\rho A L \tag{3.1-42}$$

is the mass of the element and

$$J_x=\rho L(I_y+I_z) \tag{3.1-43}$$

is the mass moment of inertia about the *x*-axis.

Consistent Mass Matrix

With Equation (3.1-15), the mass matrix for the longitudinal motion is

$$[m_x]_E=\rho A L\int_0^1\begin{bmatrix}1-\xi\\ \xi\end{bmatrix}[1-\xi \quad \xi]\,d\xi=m\int_0^1\begin{bmatrix}(1-\xi)^2 & \xi(1-\xi)\\ \xi(1-\xi) & \xi^2\end{bmatrix}d\xi.$$

The result of the integration is

$$[m_x]_E=\frac{m}{6}\begin{bmatrix}2 & 1\\ 1 & 2\end{bmatrix}. \tag{3.1-44}$$

This matrix is inserted into the 1,7/1,7-partition of the complete mass matrix.

The motion of the centre of area in *y*-direction is

$$v_A(\xi)=\begin{bmatrix}H_1(\xi) & H_2(\xi) & H_3(\xi) & H_4(\xi)\end{bmatrix}\begin{bmatrix}v_{A1}\\ \psi_1\\ v_{A2}\\ \psi_2\end{bmatrix} \tag{3.1-45}$$

with the interpolation functions defined by Equation (3.1-17). The mass matrix is computed from

$$[m_y]_E=\rho A L\int_0^1\begin{bmatrix}H_1^2 & H_1H_2 & H_1H_3 & H_1H_4\\ H_2H_1 & H_2^2 & H_2H_3 & H_2H_4\\ H_3H_1 & H_3H_2 & H_3^2 & H_3H_4\\ H_4H_1 & H_4H_2 & H_4H_3 & H_4^2\end{bmatrix}d\xi$$

giving

$$[m_y]_E=\frac{m}{420}\begin{bmatrix}156 & 22L & 54 & -13L\\ 22L & 4L^2 & 13L & -3L^2\\ 54 & 13L & 156 & -22L\\ -13L & -3L^2 & -22L & 4L^2\end{bmatrix}. \tag{3.1-46}$$

This matrix is inserted into the 2,6,8,12/2,6,8,12-partition of the complete mass matrix.

The motion of the centre of area in *z*-direction is

$$w_A(\xi)=\begin{bmatrix}H_1(\xi) & -H_2(\xi) & H_3(\xi) & -H_4(\xi)\end{bmatrix}\begin{bmatrix}w_{A1}\\ \phi_1\\ w_{A2}\\ \phi_2\end{bmatrix}. \tag{3.1-47}$$

Thus,

$$[m_z]_E=\rho A L\int_0^1\begin{bmatrix}H_1^2 & -H_1H_2 & H_1H_3 & -H_1H_4\\ -H_2H_1 & H_2^2 & -H_2H_3 & H_2H_4\\ H_3H_1 & -H_3H_2 & H_3^2 & -H_3H_4\\ -H_4H_1 & H_4H_2 & -H_4H_3 & H_4^2\end{bmatrix}d\xi$$

resulting in

$$[m_z]_E=\frac{m}{420}\begin{bmatrix}156 & -22L & 54 & 13L\\ -22L & 4L^2 & -13L & -3L^2\\ 54 & -13L & 156 & 22L\\ 13L & -3L^2 & 22L & 4L^2\end{bmatrix}. \tag{3.1-48}$$

This matrix is inserted into the 3,5,9,11/3,5,9,11-partition of the complete mass matrix.

Finally, the mass matrix for the rotation about the *x*-axis reads

$$[m_\theta]_E = \frac{J_x}{6}\begin{bmatrix} 2 & 1 \\ 1 & 2 \end{bmatrix} \tag{3.1-49}$$

where $J_x = \rho L (I_y + I_z)$. This matrix is inserted into the 4,10/4,10-partition of the complete mass matrix.

Transformation

The transformation from the structural coordinate system to the element coordinate system is composed of the transformation defined in Equation (3.1-35) followed by the transformation defined in Equation (3.1-37).

3.1.6 Stress Resultants

The stress resultants are computed at the midpoint of the element. The positive directions of the stress resultants can be seen in Figure 3.1-4.

Normal Force

The normal force acts at the centre of area. It is computed from

$$N = E\,A \frac{du}{dx} = \frac{E\,A}{L}\frac{du}{d\xi} = \frac{E\,A}{L}(u_{A2} - u_{A1}) \tag{3.1-50}$$

(cf. Equation (3.1-15)) where u_A is the *x*-component of the displacement of the centre of area.

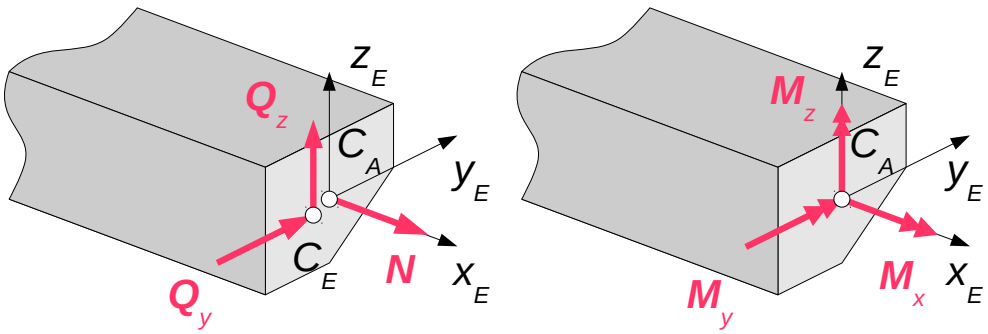


Figure 3.1-4: Positive Directions of Stress Resultants

Shear Forces

The shear forces act at the shear centre. They are computed from

$$Q_y = -\frac{dM_z}{dx} = -E\left(I_{yz}\frac{d^2\phi}{dx^2} + I_z\frac{d^2\psi}{dx^2}\right) \tag{3.1-51}$$

and

$$Q_z = \frac{dM_y}{dx} = E\left(I_y\frac{d^2\phi}{dx^2} + I_{yz}\frac{d^2\psi}{dx^2}\right) \tag{3.1-52}$$

respectively. With Equations (3.1-13) and (3.1-16), the rotations read

$$\phi(\xi) = -\frac{1}{L}\frac{dw_B}{d\xi} = -\frac{1}{L}\left(\frac{dH_1}{d\xi}w_{B1} - \frac{dH_2}{d\xi}\phi_1 + \frac{dH_3}{d\xi}w_{B2} - \frac{dH_4}{d\xi}\phi_2\right) \tag{3.1-53}$$

and

$$\psi(\xi) = \frac{1}{L}\frac{dv_B}{d\xi} = \frac{1}{L}\left(\frac{dH_1}{d\xi}v_{B1} + \frac{dH_2}{d\xi}\psi_1 + \frac{dH_3}{d\xi}v_{B2} + \frac{dH_4}{d\xi}\psi_2\right) \ . \tag{3.1-54}$$

With Equation (3.1-22), the second derivatives of the rotations read

$$\frac{d^2\phi}{dx^2} = \frac{1}{L^2}\frac{d^2\phi}{d\xi^2} = -\frac{1}{L^3}(12\,w_{B1} - 6L\,\phi_1 - 12\,w_{B2} - 6L\,\phi_2) \tag{3.1-55}$$

and

$$\frac{d^2\psi}{dx^2} = \frac{1}{L^2}\frac{d^2\psi}{d\xi^2} = \frac{1}{L^3}(12\,v_{B1} + 6L\,\psi_1 - 12\,v_{B2} + 6L\,\psi_2) \ . \tag{3.1-56}$$

Thus, the shear forces at the midpoint are given by

$$\begin{aligned} Q_y = \frac{E}{L^3}\big(&I_{yz}(12\,w_{B1} - 6L\,\phi_1 - 12\,w_{B2} - 6L\,\phi_2) \\ &- I_z(12\,v_{B1} + 6L\,\psi_1 - 12\,v_{B2} + 6L\,\psi_2)\big) \end{aligned} \tag{3.1-57}$$

and

$$\begin{aligned} Q_z = -\frac{E}{L^3}\big(&I_y(12\,w_{B1} - 6L\,\phi_1 - 12\,w_{B2} - 6L\,\phi_2) \\ &- I_{yz}(12\,v_{B1} + 6L\,\psi_1 - 12\,v_{B2} + 6L\,\psi_2)\big) \ . \end{aligned} \tag{3.1-58}$$

Bending Moments

The bending moments with respect to the centre of area can be computed from

$$M_y = E\left(I_y \frac{d\phi}{dx} + I_{yz} \frac{d\psi}{dx} \right) \tag{3.1-59}$$

and

$$M_z = E\left(I_{yz} \frac{d\phi}{dx} + I_z \frac{d\psi}{dx} \right) \tag{3.1-60}$$

respectively. At the midpoint, the derivatives of the rotations are given by

$$\frac{d\phi}{dx} = \frac{1}{L}\frac{d\phi}{d\xi} = -\frac{1}{L^2}\left(L\phi_1 - L\phi_2\right) = \frac{1}{L}\left(\phi_2 - \phi_1\right) \tag{3.1-61}$$

and

$$\frac{d\psi}{dx} = \frac{1}{L}\frac{d\psi}{d\xi} = \frac{1}{L^2}\left(-L\psi_1 + L\psi_2\right) = \frac{1}{L}\left(\psi_2 - \psi_1\right) \quad . \tag{3.1-62}$$

Thus, the bending moments at the midpoint can be computed from

$$M_y = \frac{E}{L}\left(I_y\left(\phi_2 - \phi_1\right) + I_{yz}\left(\psi_2 - \psi_1\right)\right) \tag{3.1-63}$$

and

$$M_z = \frac{E}{L}\left(I_{yz}\left(\phi_2 - \phi_1\right) + I_z\left(\psi_2 - \psi_1\right)\right) \quad . \tag{3.1-64}$$

Torque

The torque can be computed from

$$M_x = G I_T \frac{d\theta}{dx} = \frac{G I_T}{L}\left(\theta_2 - \theta_1\right) \quad . \tag{3.1-65}$$

3.2 Membrane Elements

The 2-dimensional membrane elements are standard isoparametric elements as can be found in any textbook on the Finite Element Method, see e.g. [Bathe, 1996, MacNeal, 1994]. The linear quadrilateral element **`q4`** uses selective integration, i.e. the shear is evaluated at the midpoint only.

The **`q4e`** element has an internal node located at the midpoint. The interpolation function for this node is the same as that related to the 9th node of the **`q9`** element. The degrees of freedom at the internal node are eliminated by static condensation at the element level. This makes the element more robust with respect to distortion, but increases the computation time.

The lumped mass matrix is obtained from the kinematically equivalent inertia forces due to unit accelerations. With this method, the lumped mass matrix,

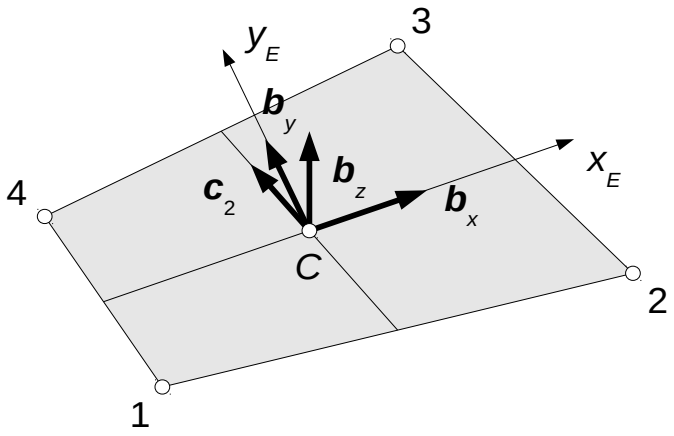


Figure 3.2-1: Coordinate System of q4-Element

like the consistent mass matrix, provides correct values for the centre of mass. However, the lumped mass matrix of the serendipity element **q8** has negative masses for the corner nodes.

The 3-dimensional membrane elements are formulated like the 2-dimensional membrane elements, but with respect to a 2-dimensional element coordinate system. Currently, only triangular and quadrilateral linear elements are available. These elements have no stiffness perpendicular to their plane, and no rotational stiffness.

The 3-dimensional quadrilateral membrane element is formulated in the plane tangential to the element in the midpoint *C* (see Figure 3.2-1).

The coordinates of the midpoint *C* are

$$[\boldsymbol{r}_C] = \sum_{n=1}^{4} [\boldsymbol{r}_n]. \tag{3.2-1}$$

The element coordinate system is defined as follows: Vector $\boldsymbol{b}_x$ points from the midpoint *C* to the midpoint of the edge 23. Vector $\boldsymbol{c}_2$ points from the midpoint *C* to the midpoint of the edge 34. Then,

$$\boldsymbol{b}_z = \frac{\boldsymbol{b}_x \times \boldsymbol{c}_2}{\|\boldsymbol{b}_x \times \boldsymbol{c}_2\|}, \quad \boldsymbol{b}_y = \boldsymbol{b}_z \times \boldsymbol{b}_x. \tag{3.2-2}$$

Likewise, the 3-dimensional triangular membrane element is formulated in the plane of the triangle. The origin coincides with node 1. Vector $\boldsymbol{b}_x$ points from node 1 to node 2, and vector $\boldsymbol{c}_2$ points from node 1 to node 3. As for the quadrilateral element, vectors $\boldsymbol{b}_y$ and $\boldsymbol{b}_z$ are computed from Equation (3.2-2).

Quadrilateral elements may be warped, i.e. the nodal points may not all be in the same plane. Then, the forces at the projected nodal points have to be

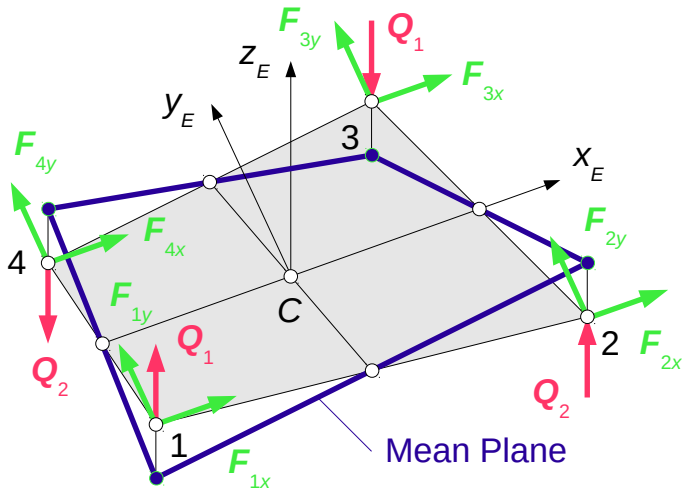


Figure 3.2-2: Forces of Warped Element

transferred to the actual nodal points. This will generate moments about the x_E- and y_E-axis that have to be balanced by two couples Q_1 and Q_2 (see Figure 3.2-2) [Naganarayana & Prathap, 1989].

The balance of moments requires

$$\begin{aligned} \sum M_x^C = 0 \;:\; (y_1 - y_3) Q_1 + (y_2 - y_4) Q_2 - \sum_{n=1}^{4} z_n F_{ny} = 0 \\ \sum M_y^C = 0 \;:\; -(x_1 - x_3) Q_1 - (x_2 - x_4) Q_2 + \sum_{n=1}^{4} z_n F_{nx} = 0 \end{aligned} \tag{3.2-3}$$

i.e.

$$\begin{bmatrix} Q_1 \\ Q_2 \end{bmatrix} = [C]^{-1} [Z] [F] \tag{3.2-4}$$

where

$$[C] = \begin{bmatrix} y_1 - y_3 & y_2 - y_4 \\ x_1 - x_3 & x_2 - x_4 \end{bmatrix} , \tag{3.2-5}$$

$$[Z] = \begin{bmatrix} 0 & z_1 & 0 & z_2 & 0 & z_3 & 0 & z_4 \\ z_1 & 0 & z_2 & 0 & z_3 & 0 & z_4 & 0 \end{bmatrix} \tag{3.2-6}$$

and

$$[F] = \begin{bmatrix} F_{1x} & F_{1y} & \cdots & F_{4x} & F_{4y} \end{bmatrix}^T . \tag{3.2-7}$$

The warping correction is applied if

$$|z| / L_{min} > wtol \tag{3.2-8}$$

where z is the z-coordinate of the nodal points in the element coordinate sys-

tem, L_{min} is the minimum edge length, and $wtol$ is the warping tolerance. The default of the warping tolerance is 10^{-3}.

3.3 Membrane Elements with Drilling Dofs

2-dimensional membrane elements can be given a rotational stiffness by adding the rotation about the *z*-axis as third degree of freedom at the nodal points. The triangular element **`t3r`** and the quadrilateral element **`q4r`** are obtained from elements **`t6`** and **`t8`** respectively by relating the displacements at the midpoints to the displacements and the rotation at the corner nodes.

To see how this transformation is defined, consider midpoint 4 of the triangular element shown in Figure 3.3-1. First, a local coordinate system for edge 12 is defined. Vector $\boldsymbol{e}_1$ points from node 1 to node 2, and vector $\boldsymbol{e}_2$ is perpendicular to vector $\boldsymbol{e}_1$ and points to the left. The vectors are given by

$$[\boldsymbol{e_1}]=\begin{bmatrix} e_{1x} \\ e_{1y} \end{bmatrix}=\frac{1}{L}\begin{bmatrix} x_2-x_1 \\ y_2-y_1 \end{bmatrix},\quad [\boldsymbol{e_2}]=\begin{bmatrix} -e_{1y} \\ e_{1x} \end{bmatrix} \tag{3.3-1}$$

where $L=\sqrt{(x_2-x_1)^2+(y_2-y_1)^2}$ is the length of the edge. Then, the transformation matrix from the global coordinate system to the edge coordinate system reads

$$[T_{12}]=\begin{bmatrix} e_{1x} & e_{1y} & 0 \\ -e_{1y} & e_{1x} & 0 \\ 0 & 0 & 1 \end{bmatrix}. \tag{3.3-2}$$

The displacements with respect to the edge coordinate system are given by

$$[u_a]_{12}=\begin{bmatrix} \bar{u}_a \\ \bar{v}_a \\ \psi_a \end{bmatrix}_{12}=[T_{12}][u_a],\quad a=1,2 \tag{3.3-3}$$

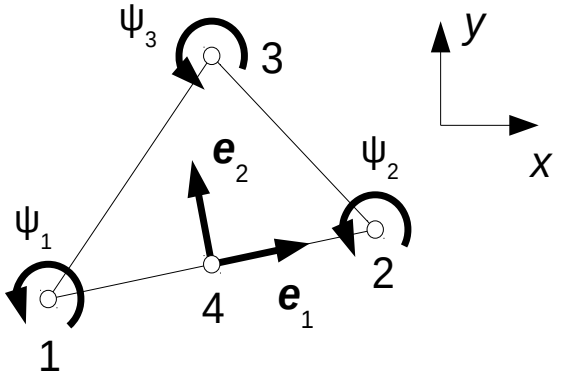


Figure 3.3-1: Edge Coordinate System

where

$$[u_a]=\begin{bmatrix} u_a \\ v_a \\ \psi_a \end{bmatrix} \tag{3.3-4}$$

are the displacements with respect to the global coordinate system.

The displacement component $\bar{u}_4$ tangential to the edge is the mean of the tangential displacements at the corner nodes of the edge:

$$\bar{u}_4=\frac{1}{2}(\bar{u}_1+\bar{u}_2) \tag{3.3-5}$$

To compute the displacement component $\bar{v}_4$ perpendicular to the edge, Hermite interpolation is used:

$$\bar{v}_4=H_1(0.5)\bar{v}_1+H_2(0.5)\psi_1+H_3(0.5)\bar{v}_2+H_4(0.5)\psi_2 \tag{3.3-6}$$

The Hermite polynomials are given by Equation (3.1-17). With

$$\begin{aligned} H_1(0.5)&=2\cdot\frac{1}{2^3}-3\cdot\frac{1}{2^2}+1=\frac{1}{2}, \quad H_2(0.5)=L\left(\frac{1}{2^3}-2\cdot\frac{1}{2^2}+\frac{1}{2}\right)=\frac{L}{8}, \\ H_3(0.5)&=-2\cdot\frac{1}{2^3}+3\cdot\frac{1}{2^2}=\frac{1}{2}, \quad H_4(0.5)=L\left(\frac{1}{2^3}-\frac{1}{2^2}\right)=-\frac{L}{8}, \end{aligned} \tag{3.3-7}$$

the displacement component perpendicular to the edge is

$$\bar{v}_4=\frac{1}{2}(\bar{v}_1+\bar{v}_2)+\frac{L}{8}(\psi_1-\psi_2). \tag{3.3-8}$$

In matrix notation, Equations (3.3-5) and (3.3-8) read

$$[u_4]_{12}=\begin{bmatrix} \bar{u}_4 \\ \bar{v}_4 \end{bmatrix}_{12}=\frac{1}{8}\begin{bmatrix} 4 & 0 & 0 & 4 & 0 & 0 \\ 0 & 4 & L & 0 & 4 & -L \end{bmatrix}_{12}\begin{bmatrix} \bar{u}_1 \\ \bar{v}_1 \\ \psi_1 \\ \bar{u}_2 \\ \bar{v}_2 \\ \psi_2 \end{bmatrix}_{12} \tag{3.3-9}$$

Finally, the displacements of the midpoint with respect to the global coordinate system are obtained from

$$[u_4]=\begin{bmatrix} u_4 \\ v_4 \end{bmatrix}=[\boldsymbol{e_1}]\bar{u}_4+[\boldsymbol{e_2}]\bar{v}_4=\begin{bmatrix} e_{1x} & -e_{1y} \\ e_{1y} & e_{1x} \end{bmatrix}\begin{bmatrix} \bar{u}_4 \\ \bar{v}_4 \end{bmatrix}. \tag{3.3-10}$$

Combining the equations, the following result is obtained:

$$\begin{bmatrix} u_4 \\ v_4 \end{bmatrix} = \frac{1}{8} \begin{bmatrix} 4 & 0 & -e_{1y}L & 4 & 0 & e_{1y}L \\ 0 & 4 & e_{1x}L & 0 & 4 & -e_{1x}L \end{bmatrix} \begin{bmatrix} u_1 \\ v_1 \\ \psi_1 \\ u_2 \\ v_2 \\ \psi_2 \end{bmatrix} \tag{3.3-11}$$

In the same way, the transformation matrices for the other edge points can be computed. They can be assembled into one single transformation matrix that relates the displacements at the nodes of a **t6** or **q8** element to those of the **t3r** or **q4r** element.

The formulation of 3-dimensional elements with drilling degrees of freedom is the same as of 2-dimensional elements. As in the case of standard membrane elements, the elements are formulated in a 2-dimensional local coordinate system and subsequently transformed to 3 dimensions.

The membrane elements with drilling degrees of freedom have one spurious mode where the rotations about the element normal at all nodes of the element have the same value. To prevent this spurious mode it is sufficient to constrain the rotation at one single node. The spurious mode is also prevented if at least one element is connected to a beam element.

3.4 Solid Elements

The 3-dimensional solid elements are standard isoparametric elements as described in any text book on the Finite Element Method, see e.g. [Bathe, 1996, MacNeal, 1994]. Both linear and quadratic hexahedral and pentahedral elements, including the serendipity elements, are available. None of the methods to improve the performance of the linear elements (see MacNeal, 1994] have been implemented because these methods are either time consuming or do not satisfy the patch test.

The lumped mass matrix is obtained from the kinematically equivalent nodal point forces due to unit accelerations. With this method, the lumped mass matrix, like the consistent mass matrix, provides correct values for the centre of mass. However, the lumped mass matrix of the serendipity elements **p15** and **h20** has negative masses for the corner nodes.

3.5 Shell Elements

The shell elements currently implemented in Mefisto are facetted shell elements, i.e. the curvature is neglected within the element. The elements can be considered a combination of membrane and plate elements. They are

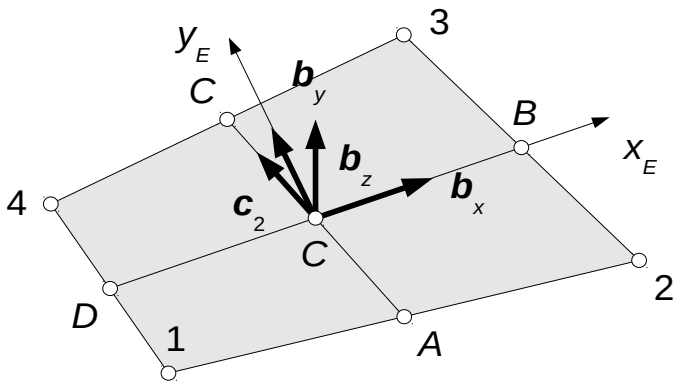


Figure 3.5-1: Coordinate System of Quadrilateral Shell Elements

based on the Reissner-Mindlin plate theory.

The membrane part of the stiffness and the mass matrix of the **s3** and **s4** element are taken from the **t3** and **q4** elements, respectively, whereas the **s3r** and **s4r** elements use the membrane part of the **t3r** and **q4r** elements. Thus, the **s3r** and **s4r** elements have a stiffness for the drilling degrees of freedom whereas the **s3** and **s4** elements do not. These elements need be stabilized by means of an artificial stiffness.

3.5.1 The Element Coordinate System

The element coordinate system is defined in the same way as for the corresponding 3-dimensional membrane elements. At each nodal point, matrix

$$[T_{33}]_{PE} = \begin{bmatrix} [\boldsymbol{b}_x]^T \\ [\boldsymbol{b}_y]^T \\ [\boldsymbol{b}_z]^T \end{bmatrix} \tag{3.5-1}$$

transforms the translations and the rotations to the element coordinate system. The vectors $\boldsymbol{b}_x$, $\boldsymbol{b}_y$ and $\boldsymbol{b}_z$ are as defined in Section 3.2.

The element may have a user-defined offset, i.e. the nodal points may have a distance z_O in z_E-direction from the warped shape of the element to the nodal point. In Mefisto, all nodal points of the element must have the same offset.

If the nodal points have an offset, the actual displacements are obtained from

$$\begin{bmatrix} u \\ v \\ w \end{bmatrix}_N = \begin{bmatrix} u \\ v \\ w \end{bmatrix}_P - \begin{bmatrix} \phi \\ \psi \\ \theta \end{bmatrix} \times \begin{bmatrix} 0 \\ 0 \\ z_O \end{bmatrix}_E = \begin{bmatrix} u - \psi z_O \\ v + \phi z_O \\ w \end{bmatrix} . \tag{3.5-2}$$

The rotations are not affected by the offset. Thus, matrix

$$[T_{66}]_{NP}=\begin{bmatrix}1&0&0&0&-z_O&0\\0&1&0&z_O&0&0\\0&0&1&0&0&0\\0&0&0&1&0&0\\0&0&0&0&1&0\\0&0&0&0&0&1\end{bmatrix} \tag{3.5-3}$$

computes the actual displacements and rotations.

Finally, with

$$[T_{66}]_{PE}=\begin{bmatrix}[T_{33}]_{PE}&[0_{33}]\\[0_{33}]&[T_{33}]_{PE}\end{bmatrix} \tag{3.5-4}$$

the transformation matrix for the displacements and rotations at one nodal point from the global coordinate system to the displacements and rotations at the projected node in the element coordinate system reads

$$[T_{66}]_E=[T_{66}]_{NP}[T_{66}]_{PE}. \tag{3.5-5}$$

3.5.2 Warping Correction

Quadrilateral elements may be warped. Then, the nodal points are projected into the plane spanned by vectors $\boldsymbol{b}_x$ and $\boldsymbol{b}_y$. In Figure 3.5-2 the contour of the projected element is shown in blue. The element matrices are formulated for the projected element.

To transfer the forces from the projected nodal points to the original nodal

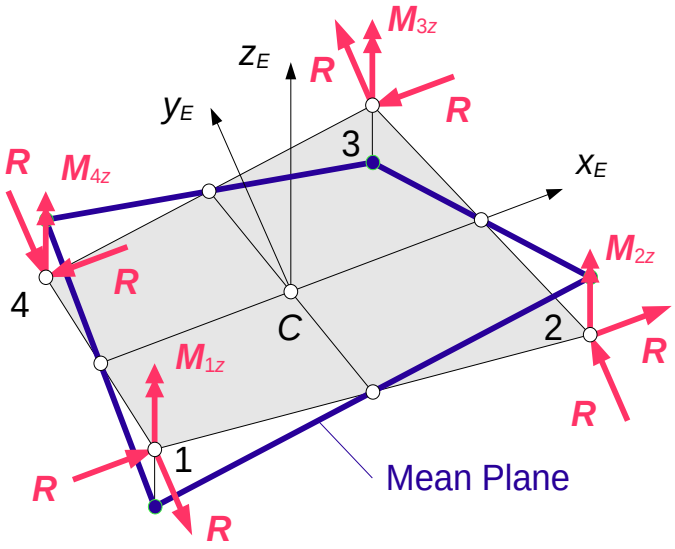


Figure 3.5-2: Warping Correction of s4 Element

points the same method as for the quadrilateral membrane element (cf. Section 3.2) is used. An additional correction is needed to align the moments at the nodal points along the element edges [Naganarayana & Prathap, 1989, MacNeal, 1994]. The correction adds an additional moment M_{nz} so that the resulting moment at each nodal point lies in the plane that is tangential to the warped element at the nodal point. These additional moments must be balanced by additional forces R.

Let $\boldsymbol{v}_n$ be a vector that is normal to the tangential plane at the n-th nodal point. This vector can be computed from the vectors along the edges joining at the corresponding nodal point. Then, the moment vector at this nodal point must satisfy

$$\left(M_{nx}\boldsymbol{b}_x+M_{ny}\boldsymbol{b}_y+M_{nz}\boldsymbol{b}_z\right)\cdot\boldsymbol{v}_n=0 \tag{3.5-6}$$

yielding

$$M_{nz}=-\frac{v_{nx}}{v_{nz}}M_{nx}-\frac{v_{ny}}{v_{nz}}M_{ny} \quad . \tag{3.5-7}$$

The balance of moments reads (cf. Figure 3.5-2)

$$\sum M_z^C=0 \;:\; \sum_{n=1}^{n} M_{nz}+\left(y_3+y_4-y_1-y_2+x_2+x_3-x_4-x_1\right)R=0 \quad , \tag{3.5-8}$$

i.e.

$$R=\frac{\sum_{n=1}^{4}\frac{v_{nx}}{v_{nz}}M_{nx}+\frac{v_{ny}}{v_{nz}}M_{ny}}{x_2+x_3-x_1-x_4+y_3+y_4-y_1-y_2} \quad . \tag{3.5-9}$$

3.5.3 The Reissner-Mindlin Plate Theory

The basic assumption of plate theory is that the displacements of cross sections perpendicular to the mid-surface of the plate are a superposition of a vertical translation and a rotation about an axis in the mid surface. Thus, in the element coordinate system,

$$[\boldsymbol{u}]=\begin{bmatrix}u(x,y,z)\\v(x,y,z)\\w(x,y)\end{bmatrix}=\begin{bmatrix}0\\0\\w(x,y)\end{bmatrix}+\begin{bmatrix}\phi(x,y)\\\psi(x,y)\\0\end{bmatrix}\times\begin{bmatrix}0\\0\\z\end{bmatrix}=\begin{bmatrix}\psi(x,y)z\\-\phi(x,y)z\\w(x,y)\end{bmatrix} \tag{3.5-10}$$

where ϕ and ψ are the rotations about the *x*- and *y*-axis respectively, and w is the displacement in *z*-direction.

The strains in a plane parallel to the mid-surface are

$$\epsilon_x=\frac{\partial u}{\partial x}=\frac{\partial \psi}{\partial x}z,\quad \epsilon_y=\frac{\partial v}{\partial y}=-\frac{\partial \phi}{\partial y}z,\quad \gamma_{xy}=\frac{\partial u}{\partial y}+\frac{\partial v}{\partial x}=\left(\frac{\partial \psi}{\partial y}-\frac{\partial \phi}{\partial x}\right)z\quad , \tag{3.5-11}$$

and the transverse shear strains are obtained from

$$\gamma_{xz}=\frac{\partial u}{\partial z}+\frac{\partial w}{\partial x}=\psi+\frac{\partial w}{\partial x},\quad \gamma_{yz}=\frac{\partial v}{\partial z}+\frac{\partial w}{\partial y}=-\phi+\frac{\partial w}{\partial y}\quad . \tag{3.5-12}$$

In matrix notation, the strain-displacement equations can be written

$$[\epsilon]=\begin{bmatrix}\epsilon_x\\ \epsilon_y\\ \gamma_{xy}\end{bmatrix}=\begin{bmatrix}\partial\psi/\partial x\\ -\partial\phi/\partial y\\ \partial\psi/\partial y-\partial\phi/\partial x\end{bmatrix}z=[\kappa]z \tag{3.5-13}$$

and

$$[\gamma]=\begin{bmatrix}\gamma_{xz}\\ \gamma_{yz}\end{bmatrix}=\begin{bmatrix}\psi+\partial w/\partial x\\ -\phi+\partial w/\partial y\end{bmatrix} \tag{3.5-14}$$

respectively where

$$[\kappa]=\begin{bmatrix}\partial\psi/\partial x\\ -\partial\phi/\partial y\\ \partial\psi/\partial y-\partial\phi/\partial x\end{bmatrix} \tag{3.5-15}$$

is the curvature matrix. The transverse shear strains can be seen to be constant over the thickness of the plate.

In the same way, the virtual curvatures $[\tilde{\kappa}]$ and the virtual transverse shear strains $[\tilde{\gamma}]$ are obtained from the virtual displacements $[\tilde{\boldsymbol{u}}]$.

With the plane-stress stiffness matrix

$$[E_M]=\frac{E}{1-\nu^2}\begin{bmatrix}1 & \nu & 0\\ \nu & 1 & 0\\ 0 & 0 & \dfrac{1-\nu}{2}\end{bmatrix} \tag{3.5-16}$$

and the shear modulus G, the bending stresses and the transverse shear stresses are given by

$$[\sigma_B]=\begin{bmatrix}\sigma_x\\ \sigma_y\\ \tau_{xy}\end{bmatrix}=[E_M][\kappa]z \text{ and } [\tau_T]=\begin{bmatrix}\tau_{xz}\\ \tau_{yz}\end{bmatrix}=G[\gamma]\quad . \tag{3.5-17}$$

Now, the virtual strain energy can be computed from

$$\tilde{E}^F=\int_V[\tilde{\kappa}]^T[E_M][\kappa]z^2dV+\int_V[\tilde{\gamma}]^TG[\gamma]dV\quad . \tag{3.5-18}$$

The material properties are assumed not to depend on z. Then, integration over z yields

$$\widetilde{E}^F = \frac{h^3}{12}\int_A [\widetilde{\kappa}]^T [E_M][\kappa]\,dA + h\,k_S \int_A G[\widetilde{\gamma}]^T[\gamma]\,dA \tag{3.5-19}$$

where h is the thickness of the plate. The shear correction factor k_S has been introduced to account for the actual parabolic dependence of the transverse shear on z. Mefisto uses $k_S = 5/6$ which corresponds to the shear correction factor of a beam with rectangular cross section (see e.g. [Bathe, 1996]).

For thin plates the second integral is considerably larger than the first. It can be considered a penalty term which makes the transverse shear vanish as is assumed in the Kirchhoff plate theory. Thus, the Reissner-Mindlin plate theory converges to the Kirchhoff plate theory if the thickness of the plate becomes very small.

3.5.4 Stiffness Matrix

The membrane part of the stiffness matrix is taken from the corresponding 3-dimensional membrane element.

The bending part of the stiffness matrix is obtained from the Reissner-Mindlin theory. Equation (3.5-19) shows that it consists of two parts. The first part is due to the bending stresses and the second due to the transverse shear stresses.

Interpolation functions

A linear interpolation is used for both the vertical displacement w and the rotations ϕ and ψ. For the *quadrilateral element*, the interpolation reads

$$\begin{bmatrix} w(r,s) \\ \phi(r,s) \\ \psi(r,s) \end{bmatrix} = \sum_{n=1}^{4} N_n(r,s) \begin{bmatrix} w_n \\ \phi_n \\ \psi_n \end{bmatrix} \tag{3.5-20}$$

where

$$\begin{aligned} N_1(r,s) &= \frac{1}{4}(1-r)(1-s), \quad N_2(r,s) = \frac{1}{4}(1+r)(1-s) \\ N_3(r,s) &= \frac{1}{4}(1+r)(1+s), \quad N_4(r,s) = \frac{1}{4}(1-r)(1+s) \end{aligned} \tag{3.5-21}$$

are the standard interpolation functions of linear quadrilateral elements. The derivatives of the shape functions are computed from

$$\begin{bmatrix} \frac{\partial N_n}{\partial x} \\ \frac{\partial N_n}{\partial y} \end{bmatrix} = [J]^{-1} \begin{bmatrix} \frac{\partial N_n}{\partial r} \\ \frac{\partial N_n}{\partial s} \end{bmatrix} \tag{3.5-22}$$

where

$$[J] = \begin{bmatrix} \frac{\partial x}{\partial r} & \frac{\partial y}{\partial r} \\ \frac{\partial x}{\partial s} & \frac{\partial y}{\partial s} \end{bmatrix} = \begin{bmatrix} \frac{\partial N_1}{\partial r} & \frac{\partial N_2}{\partial r} & \frac{\partial N_3}{\partial r} & \frac{\partial N_4}{\partial r} \\ \frac{\partial N_1}{\partial s} & \frac{\partial N_2}{\partial s} & \frac{\partial N_3}{\partial s} & \frac{\partial N_4}{\partial s} \end{bmatrix} \begin{bmatrix} x_1 & y_1 \\ x_2 & y_2 \\ x_3 & y_3 \\ x_4 & y_4 \end{bmatrix} \tag{3.5-23}$$

is the Jacobi matrix. The derivatives of the interpolation functions with respect to r and s are

$$\begin{aligned} &\frac{\partial N_1}{\partial r} = -\frac{1}{4}(1-s), \quad \frac{\partial N_2}{\partial r} = \frac{1}{4}(1-s), \quad \frac{\partial N_3}{\partial r} = \frac{1}{4}(1+s), \quad \frac{\partial N_4}{\partial r} = -\frac{1}{4}(1+s) \\ &\frac{\partial N_1}{\partial s} = -\frac{1}{4}(1-r), \quad \frac{\partial N_2}{\partial s} = -\frac{1}{4}(1+r), \quad \frac{\partial N_3}{\partial s} = \frac{1}{4}(1+r), \quad \frac{\partial N_4}{\partial s} = \frac{1}{4}(1-r) \end{aligned} \tag{3.5-24}$$

For the *triangular element*, the interpolation reads

$$\begin{bmatrix} w(r,s) \\ \phi(r,s) \\ \psi(r,s) \end{bmatrix} = \sum_{n=1}^{3} N_n(r,s) \begin{bmatrix} w_n \\ \phi_n \\ \psi_n \end{bmatrix} \tag{3.5-25}$$

where

$$N_1(r,s) = 1-r-s, \quad N_2(r,s) = r, \quad N_3(r,s) = s \tag{3.5-26}$$

(cf. Figure 3.5-3) are the standard interpolation functions of linear triangular elements. The derivatives of the interpolation functions with respect to r and s are

$$\begin{aligned} &\frac{\partial N_1}{\partial r} = -1, \quad \frac{\partial N_2}{\partial r} = 1, \quad \frac{\partial N_3}{\partial r} = 0 \\ &\frac{\partial N_1}{\partial s} = -1, \quad \frac{\partial N_2}{\partial s} = 0, \quad \frac{\partial N_3}{\partial s} = 1 \end{aligned} \tag{3.5-27}$$

The Jacobi matrix reads

$$[J] = \begin{bmatrix} \frac{\partial x}{\partial r} & \frac{\partial y}{\partial r} \\ \frac{\partial x}{\partial s} & \frac{\partial y}{\partial s} \end{bmatrix} = \begin{bmatrix} x_2 - x_1 & y_2 - y_1 \\ x_3 - x_1 & y_3 - y_1 \end{bmatrix} \tag{3.5-28}$$

Its inverse is

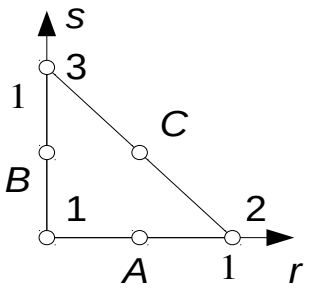


Figure 3.5-3: Parametric Coordinates of Triangle and Tying Points

where

$$A=\frac{1}{2}\det(J)=(y_3-y_1)(x_2-x_1)-(x_1-x_3)(y_1-y_2) \tag{3.5-30}$$

is the area of the triangle.

Bending stress part of the bending stiffness matrix

With the interpolations defined above, the curvature matrix reads

$$[\kappa]=\sum_{n=1}^{n_p}\begin{bmatrix}0 & 0 & \frac{\partial N_n}{\partial x}\\ 0 & -\frac{\partial N_n}{\partial y} & 0\\ 0 & -\frac{\partial N_n}{\partial x} & \frac{\partial N_n}{\partial y}\end{bmatrix}\begin{bmatrix}w_n\\ \phi_n\\ \psi_n\end{bmatrix}=\sum_{n=1}^{n_p}[B_{\kappa n}]\begin{bmatrix}w_n\\ \phi_n\\ \psi_n\end{bmatrix},\quad n_p=3,4 \tag{3.5-31}$$

where

$$[B_{\kappa n}]=\begin{bmatrix}0 & 0 & \frac{\partial N_n}{\partial x}\\ 0 & -\frac{\partial N_n}{\partial y} & 0\\ 0 & -\frac{\partial N_n}{\partial x} & \frac{\partial N_n}{\partial y}\end{bmatrix}. \tag{3.5-32}$$

Finally, with

$$[B_\kappa]=\begin{bmatrix}[B_{\kappa 1}] & \cdots & [B_{\kappa n_p}]\end{bmatrix} \tag{3.5-33}$$

and

$$[u_B]^T=\begin{bmatrix}w_1 & \phi_1 & \psi_1 & \cdots & w_{n_p} & \phi_{n_p} & \psi_{n_p}\end{bmatrix}, \tag{3.5-34}$$

the curvature matrix can be computed from

$$[\kappa(r,s)]=[B_\kappa(r,s)][u_B] \quad . \tag{3.5-35}$$

Now, the first integral in Equation (3.5-19) reads

$$\int_A [\tilde{\kappa}]^T[E_M][\kappa]dA=[\tilde{u}_B]^T\int_A [B_\kappa]^T[E_M][B_\kappa]dA[u_B] \quad . \tag{3.5-36}$$

Thus, the bending stress part of the stiffness matrix is

$$[K_b]=\frac{h^3}{12}\int_A [B_\kappa]^T[E_M][B_\kappa]dA \quad . \tag{3.5-37}$$

Transverse shear stress part of the bending matrix

With a linear interpolation for both the transverse displacement w and the rotations ϕ and ψ, the transverse shear strains cannot vanish identically. Thus, the element can not converge to the Kirchhoff theory if the thickness of the shell goes to zero. Instead, the element will suffer from shear locking.

One possibility to cure this problem is to use a reduced integration for the transverse shear part. However, this will lead to two spurious modes. Thus, a different method will be used that is based on an interpolation of the covariant shear strains from their values at the midpoints of the edges [Bathe, 1996].

The covariant base vectors of the element are

$$\boldsymbol{g}_r=\frac{\partial \boldsymbol{x}}{\partial r}, \quad \boldsymbol{g}_s=\frac{\partial \boldsymbol{x}}{\partial s}, \quad \boldsymbol{g}_z=\boldsymbol{b}_z \quad . \tag{3.5-38}$$

In the element coordinate system, these vectors read

$$\begin{aligned}\boldsymbol{g}_r&=\left(\sum_{n=1}^4 \frac{\partial N_n}{\partial r}x_n\right)\boldsymbol{b}_x+\left(\sum_{n=1}^4 \frac{\partial N_n}{\partial r}y_n\right)\boldsymbol{b}_y=g_{rx}\boldsymbol{b}_x+g_{ry}\boldsymbol{b}_y\\ \boldsymbol{g}_s&=\left(\sum_{n=1}^4 \frac{\partial N_n}{\partial s}x_n\right)\boldsymbol{b}_x+\left(\sum_{n=1}^4 \frac{\partial N_n}{\partial s}y_n\right)\boldsymbol{b}_y=g_{sx}\boldsymbol{b}_x+g_{sy}\boldsymbol{b}_y\end{aligned} \tag{3.5-39}$$

where

$$g_{rx}=\frac{\partial x}{\partial r}, \quad g_{ry}=\frac{\partial y}{\partial r}, \quad g_{sx}=\frac{\partial x}{\partial s}, \quad g_{sy}=\frac{\partial y}{\partial s} \quad . \tag{3.5-40}$$

Comparison with Equation (3.5-23) shows that

$$\begin{bmatrix} g_{rx} & g_{ry} \\ g_{sx} & g_{sy}\end{bmatrix}=[J] \quad . \tag{3.5-41}$$

The contravariant base vectors satisfy

$$\boldsymbol{g}_\alpha\cdot\boldsymbol{g}^\beta=\delta_\beta^\alpha, \quad \alpha,\beta=r,s \tag{3.5-42}$$

or

$$\begin{matrix} g_{rx}\,g_x^r+g_{ry}\,g_y^r=1, & g_{rx}\,g_x^s+g_{ry}\,g_y^s=0 \\ g_{sx}\,g_x^r\,g_{rx}+g_{sy}\,g_y^r=0, & g_{sx}\,g_x^s+g_{sy}\,g_y^s=1 \end{matrix} \quad , \tag{3.5-43}$$

i.e.

$$\begin{bmatrix} g_{rx} & g_{ry} \\ g_{sx} & g_{sy} \end{bmatrix} \begin{bmatrix} g_x^r & g_x^s \\ g_y^r & g_y^s \end{bmatrix} = \begin{bmatrix} 1 & 0 \\ 0 & 1 \end{bmatrix} \quad . \tag{3.5-44}$$

Thus, the components of the contravariant base vectors can be obtained from

$$\begin{bmatrix} g_x^r & g_x^s \\ g_y^r & g_y^s \end{bmatrix} = \begin{bmatrix} g_{rx} & g_{ry} \\ g_{sx} & g_{sy} \end{bmatrix}^{-1} = [J]^{-1} \quad . \tag{3.5-45}$$

The linearized Green-Lagrange strain tensor is

$$\epsilon_{ij} = \frac{1}{2}\left(\boldsymbol{g}_i \cdot \boldsymbol{u}_{,j} + \boldsymbol{g}_j \cdot \boldsymbol{u}_{,i}\right). \tag{3.5-46}$$

The covariant transverse shear strains are

$$\epsilon_{rz} = \frac{1}{2}\left(\boldsymbol{g}_r \cdot \boldsymbol{u}_{,z} + \boldsymbol{b}_z \cdot \boldsymbol{u}_{,r}\right), \quad \epsilon_{sz} = \frac{1}{2}\left(\boldsymbol{g}_s \cdot \boldsymbol{u}_{,z} + \boldsymbol{b}_z \cdot \boldsymbol{u}_{,s}\right). \tag{3.5-47}$$

With

$$\boldsymbol{u}(r,s,z) = \psi(r,s)\,z\,\boldsymbol{b}_x - \phi(r,s)\,z\,\boldsymbol{b}_y + w(r,s)\,\boldsymbol{b}_z \tag{3.5-48}$$

they read

$$\epsilon_{rz} = \frac{1}{2}\left(g_{rx}\psi - g_{ry}\phi + w_{,r}\right), \quad \epsilon_{sz} = \frac{1}{2}\left(g_{sx}\psi - g_{sy}\phi + w_{,s}\right). \tag{3.5-49}$$

For the *quadrilateral element*, g_{rs}, g_{ry} and $w_{,r}$ depend on s only. Thus, ε_{rz} is approximated by a function depending on s only. Likewise, ε_{sz} is approximated by a function depending on r only. ε_{rz} is obtained by interpolating its values at the tying points *A* and *C*, and ε_{sz} by interpolating its values at the tying points *B* and *D* (see Figure 3.5-1).

Point *A*: $r = 0$, $s = -1$

$$g_{rx}^A = -\frac{1}{2}x_1 + \frac{1}{2}x_2 = \frac{1}{2}(x_2 - x_1), \quad g_{ry}^A = \frac{1}{2}(y_2 - y_1), \quad w^A{}_{,r} = \frac{1}{2}(w_2 - w_1)$$

$$\phi^A = \frac{1}{2}\phi_1 + \frac{1}{2}\phi_2 = \frac{1}{2}(\phi_1 + \phi_2), \quad \psi^A = \frac{1}{2}(\psi_1 + \psi_2)$$

$$\epsilon_{rz}^A = \frac{1}{4}\left(w_2 - w_1 - \frac{1}{2}(y_2 - y_1)(\phi_1 + \phi_2) + \frac{1}{2}(x_2 - x_1)(\psi_1 + \psi_2)\right)$$

Point *B*: $r = 1$, $s = 0$

$$g_{sx}^B = -\frac{1}{2}x_2 + \frac{1}{2}x_3 = \frac{1}{2}(x_3 - x_2), \quad g_{sy}^B = \frac{1}{2}(y_3 - y_2), \quad w^B{}_{,s} = \frac{1}{2}(w_3 - w_2)$$

$$\phi^B=\frac{1}{2}\phi_2+\frac{1}{2}\phi_3=\frac{1}{2}(\phi_2+\phi_3),\quad \psi^B=\frac{1}{2}(\psi_2+\psi_3)$$

$$\epsilon_{sz}^B=\frac{1}{4}\left(w_3-w_2-\frac{1}{2}(y_3-y_2)(\phi_2+\phi_3)+\frac{1}{2}(x_3-x_2)(\psi_2+\psi_3)\right)$$

Point *C*: $r = 0$, $s = 1$

$$g_{rx}^C=\frac{1}{2}x_3-\frac{1}{2}x_4=\frac{1}{2}(x_3-x_4),\quad g_{ry}^C=\frac{1}{2}(y_3-y_4),\quad w^C{}_{,r}=\frac{1}{2}(w_3-w_4)$$

$$\phi^C=\frac{1}{2}\phi_3+\frac{1}{2}\phi_4=\frac{1}{2}(\phi_3+\phi_4),\quad \psi^C=\frac{1}{2}(\psi_3+\psi_4)$$

$$\epsilon_{rz}^C=\frac{1}{4}\left(w_3-w_4-\frac{1}{2}(y_3-y_4)(\phi_3+\phi_4)+\frac{1}{2}(x_3-x_4)(\psi_3+\psi_4)\right)$$

Point *D*: $r = -1$, $s = 0$

$$g_{sx}^D=-\frac{1}{2}x_1+\frac{1}{2}x_4=\frac{1}{2}(x_4-x_1),\quad g_{sy}^D=\frac{1}{2}(y_4-y_1),\quad w^D{}_{,s}=\frac{1}{2}(w_4-w_1)$$

$$\phi^D=\frac{1}{2}\phi_1+\frac{1}{2}\phi_4=\frac{1}{2}(\phi_1+\phi_4),\quad \psi^D=\frac{1}{2}(\psi_1+\psi_4)$$

$$\epsilon_{sz}^D=\frac{1}{4}\left(w_4-w_1-\frac{1}{2}(y_4-y_1)(\phi_1+\phi_4)+\frac{1}{2}(x_4-x_1)(\psi_1+\psi_4)\right)$$

In matrix notation, these equations read

$$\begin{bmatrix}\epsilon_{rz}^A\\ \epsilon_{sz}^B\\ \epsilon_{rz}^C\\ \epsilon_{sz}^D\end{bmatrix}=[\epsilon_E]=[B_{SE}][u_B]\quad . \tag{3.5-50}$$

The covariant shear strains at the integration points are obtained by linear interpolation:

$$\begin{aligned}\epsilon_{rz}(s)&=\frac{1}{2}(1-s)\epsilon_{rz}^A+\frac{1}{2}(1+s)\epsilon_{rz}^C\\ \epsilon_{sz}(r)&=\frac{1}{2}(1+r)\epsilon_{sz}^B+\frac{1}{2}(1-r)\epsilon_{sz}^D\end{aligned} \tag{3.5-51}$$

In matrix notation, Equation (3.5-51) reads

$$[\epsilon_S]=\begin{bmatrix}\epsilon_{rz}\\ \epsilon_{sz}\end{bmatrix}=\frac{1}{2}\begin{bmatrix}1-s & 0 & 1+s & 0\\ 0 & 1+r & 0 & 1-r\end{bmatrix}[\epsilon_E]=[B_S][\epsilon_E]\quad . \tag{3.5-52}$$

Finally, from

$$\epsilon_{\alpha\beta}\boldsymbol{g}^{\alpha}\otimes\boldsymbol{g}^{\beta}=\epsilon_{ij}\boldsymbol{b}_i\otimes\boldsymbol{b}_j \tag{3.5-53}$$

the Cartesian components of the engineering transverse shear strains are

$$\begin{aligned}\gamma_{xz}&=2\,\epsilon_{xz}=2\,\epsilon_{rz}\left(\boldsymbol{g}^r\cdot\boldsymbol{b}_x\right)\left(\boldsymbol{g}^z\cdot\boldsymbol{b}_z\right)+2\,\epsilon_{sz}\left(\boldsymbol{g}^s\cdot\boldsymbol{b}_x\right)\left(\boldsymbol{g}^z\cdot\boldsymbol{b}_z\right)\\ \gamma_{yz}&=2\,\epsilon_{yz}=2\,\epsilon_{rz}\left(\boldsymbol{g}^r\cdot\boldsymbol{b}_y\right)\left(\boldsymbol{g}^z\cdot\boldsymbol{b}_z\right)+2\,\epsilon_{sz}\left(\boldsymbol{g}^s\cdot\boldsymbol{b}_y\right)\left(\boldsymbol{g}^z\cdot\boldsymbol{b}_z\right)\end{aligned} \tag{3.5-54}$$

With

$$\boldsymbol{g}^r\cdot\boldsymbol{b}_x=g^r_x,\quad \boldsymbol{g}^s\cdot\boldsymbol{b}_x=g^s_x,\quad \boldsymbol{g}^r\cdot\boldsymbol{b}_y=g^r_y,\quad \boldsymbol{g}^s\cdot\boldsymbol{b}_y=g^s_y,\quad \boldsymbol{g}^z\cdot\boldsymbol{b}_z=1$$

and Equation (3.5-45), Equation (3.5-54) reads

$$[\gamma]=\begin{bmatrix}\gamma_{xz}\\ \gamma_{yz}\end{bmatrix}=2\begin{bmatrix}g^r_x & g^s_x\\ g^r_y & g^s_y\end{bmatrix}\begin{bmatrix}\epsilon_{rz}\\ \epsilon_{sz}\end{bmatrix}=2[J]^{-1}[\epsilon_S]\quad . \tag{3.5-55}$$

Combining results, the transverse shear strains at the integration points are related to the bending displacements by

$$[\gamma]=2[J]^{-1}[B_S][B_{SE}][u_B]=[B_\gamma][u_B] \tag{3.5-56}$$

where

$$[B_\gamma]=2[J]^{-1}[B_S][B_{SE}]\quad . \tag{3.5-57}$$

Thus, the transverse shear stress part of the stiffness matrix of the quadrilateral element is

$$[K_s]=h\,k_S G\int_A[B_\gamma]^T[B_\gamma]\,dA\quad . \tag{3.5-58}$$

A similar approach is used for the *triangular element* [Lee & Bathe, 2004, Lee, Noh & Bathe, 2007]. First, the covariant transverse shear strains at the tying points *A*, *B* and *C* (see Figure 3.5-3) are computed.

Point *A*: $r=0.5,\ s=0$

$g^A_{rx}=x_2-x_1,\quad g^A_{ry}=y_2-y_1,\quad w^A{}_{,r}=w_2-w_1$ (cf. Equations (3.5-27) and (3.5-28))

$$\phi^A=\frac{1}{2}(\phi_1+\phi_2),\quad \psi^A=\frac{1}{2}(\psi_1+\psi_2)$$

$$\epsilon^A_{rz}=\frac{1}{2}\left(w_2-w_1-\frac{1}{2}(y_2-y_1)(\phi_1+\phi_2)+\frac{1}{2}(x_2-x_1)(\psi_1+\psi_2)\right)$$

Point *B*: $r=0,\ s=0.5$

$g^B_{sx}=x_3-x_1,\quad g^B_{sy}=y_3-y_1,\quad w^B{}_{,s}=w_3-w_1$ (cf. Equations (3.5-27) and (3.5-28))

$$\phi^B=\frac{1}{2}(\phi_1+\phi_3),\quad \psi^B=\frac{1}{2}(\psi_1+\psi_3)$$

$$\epsilon_{sz}^{B}=\frac{1}{2}\left(w_3-w_1-\frac{1}{2}(y_3-y_1)(\phi_1+\phi_3)+\frac{1}{2}(x_3-x_1)(\psi_1+\psi_3)\right)$$

Point *C*: $r=0.5$, $s=0.5$

$$g_{rx}^{C}=x_2-x_1,\quad g_{ry}^{C}=y_2-y_1,\quad g_{sx}^{C}=x_3-x_1,\quad g_{sy}^{C}=y_3-y_1$$

$$w^{C},_r=w_2-w_1,\quad w^{C},_s=w_3-w_1$$

$$\phi^{C}=\frac{1}{2}(\phi_2+\phi_3),\quad \psi^{C}=\frac{1}{2}(\psi_2+\psi_3)$$

$$\epsilon_{rz}^{C}=\frac{1}{2}\left(w_2-w_1-\frac{1}{2}(y_2-y_1)(\phi_2+\phi_3)+\frac{1}{2}(x_2-x_1)(\psi_2+\psi_3)\right)$$

$$\epsilon_{sz}^{C}=\frac{1}{2}\left(w_3-w_1-\frac{1}{2}(y_3-y_1)(\phi_2+\phi_3)+\frac{1}{2}(x_3-x_1)(\psi_2+\psi_3)\right)$$

The interpolation of the covariant shear strains reads

$$\epsilon_{rz}(s)=a+c\,s,\quad \epsilon_{sz}(r)=b-c\,r \tag{3.5-59}$$

where

$$a=\epsilon_{rz}^{A},\quad b=\epsilon_{sz}^{B},\quad c=\epsilon_{sz}^{B}-\epsilon_{rz}^{A}-\epsilon_{sz}^{C}+\epsilon_{rz}^{C}\ . \tag{3.5-60}$$

In matrix notation, Equations (3.5-60) read

$$a=[A][u_B],\quad b=[B][u_B],\quad c=[C][u_B], \tag{3.5-61}$$

where

$$\begin{aligned}
[A]&=\left[-1\quad -\frac{y_2-y_1}{2}\quad \frac{x_2-x_1}{2}\quad 1\quad -\frac{y_2-y_1}{2}\quad \frac{x_2-x_1}{2}\quad 0\quad 0\quad 0\right],\\
[B]&=\left[-1\quad -\frac{y_3-y_1}{2}\quad \frac{x_3-x_1}{2}\quad 0\quad 0\quad 0\quad 1\quad -\frac{y_3-y_1}{2}\quad \frac{x_3-x_1}{2}\right],\\
[C]&=\frac{1}{2}[0\quad y_2-y_3\quad x_3-x_2\quad 0\quad y_3-y_1\quad x_1-x_3\quad 0\quad y_1-y_2\quad x_2-x_1]\ .
\end{aligned} \tag{3.5-62}$$

Thus, the covariant shear strains at any point within the element can be computed from

$$[\epsilon_S]=\begin{bmatrix}\epsilon_{rz}\\ \epsilon_{sz}\end{bmatrix}=\frac{1}{2}\begin{bmatrix}[A]+s[C]\\ [B]-r[C]\end{bmatrix}[u_B]\ . \tag{3.5-63}$$

Finally, as for the quadrilateral element, the Cartesian components of the engineering transverse shear strains are obtained from Equation 3.5-55. Thus, for the triangular element,

$$[B_\gamma]=[J]^{-1}\begin{bmatrix}[A]+s[C]\\ [B]-r[C]\end{bmatrix}\ . \tag{3.5-64}$$

A dimensional analysis shows that the ratio of the transverse shear part of the stiffness matrix to the bending stress part is

$$\frac{h\,k_S G \left\| \int\limits_{A_E} \left[B_\gamma\right]^T \left[B_\gamma\right] dA \right\|}{\frac{h^3}{12} \left\| \int\limits_{A_E} \left[B_\kappa\right]^T \left[E_M\right] \left[B_\kappa\right] dA \right\|} = C \left(\frac{L_E}{h} \right)^2 \tag{3.5-65}$$

where C is a problem dependent constant and L_E is a typical element length. Thus, to ensure convergence to the Kirchhoff theory when the element size is decreased, the shear stress part must be scaled. This is achieved by multiplying the shear modulus of the shear stress part by a factor

$$s = \frac{x^2}{1+x^2} + \frac{1}{x^2} \tag{3.5-66}$$

where

$$x = \frac{\lambda}{\lambda_0}, \quad \lambda = \frac{L_E}{h} \quad \text{and} \quad \lambda_0 = 10 \quad .$$

Stabilization of the drilling degrees of freedom

For the **s3** or **s4** element, there is no stiffness for the drilling degrees of freedom. To prevent singularities of the assembled stiffness matrix, fictitious beams are added to the edges of the elements which have a stiffness only for bending in the plane of the element [Parisch, 1985]. This defines a stiffness matrix

$$\left[K_d\right] = \begin{bmatrix} 2k_d & -k_d & 0 & -k_d \\ -k_d & 2k_d & -k_d & 0 \\ 0 & -k_d & 2k_d & -k_d \\ -k_d & 0 & -k_d & 2k_d \end{bmatrix} \tag{3.5-67}$$

for the drilling degrees of freedom where

$$k_d = \alpha\, k_{MB} \quad . \tag{3.5-68}$$

k_{MB} is the mean bending stiffness of the element, i.e. the mean value of those diagonal elements of the bending part of the stiffness matrix that are related to rotational degrees of freedom, and α is a factor with a default value of 1 %.

In any case, the element still has one spurious mode where the rotations about the element normal at all nodes of the element have the same value. To prevent this spurious mode it is sufficient to constrain the rotation at one single node. The spurious mode is also prevented if at least one element is connected to a beam element, or if not all elements are in the same plane.

3.5.5 Mass Matrix

Both the consistent and the lumped mass matrix are identical with that of the corresponding membrane element.

3.5.6 Stresses and Stress Resultants

The bending and transverse shear stresses are obtained from Equation (3.5-17). The bending stresses vary linearly with z. Thus, it is sufficient to compute them at the upper and lower side of the element.

With Equations (3.5-35) and (3.5-36), the bending stresses and the transverse shear stresses at the midpoint of the element can be computed from

$$[\sigma_B]=\pm\frac{h}{2}[E_M]\left[B_\kappa(r_m,s_m)\right][u_B],\quad [\tau_B]=k_S G\left[B_\gamma(r_m,s_m)\right][u_B]\ . \tag{3.5-69}$$

The membrane stresses have to be added to the bending stresses.

Normal forces N_x, N_y and N_{xy} are obtained from the membrane stresses by multiplying them with the shell thickness h.

The bending moments M_x, M_y and M_{xy} are obtained from

$$\begin{bmatrix}M_x\\M_y\\M_{xy}\end{bmatrix}=\int_{-h/2}^{h/2}[\sigma_B]\,z\,dz=\frac{h^3}{12}[E_M][B_\kappa][u_B]=\frac{h^2}{6}\left[\sigma_B(h/2)\right] \tag{3.5-70}$$

and the transverse shear forces are computed from

$$\begin{bmatrix}Q_x\\Q_y\end{bmatrix}=h[\tau_B]\ . \tag{3.5-71}$$

4 Aerodynamic Methods

4.1 The Discrete Vortex Method

The Discrete Vortex Method is a numerical method to solve the integral equations of thin airfoil theory. A detailed description of the steady thin airfoil theory can be found e.g. in [Karamcheti, 1980].

4.1.1 The Steady Discrete Vortex Method

In thin airfoil theory, the flow over an airfoil is approximated by a superposition of a uniform flow with the flow induced by a vortex distribution along the chord line, see Figure 4.1-1. For the flow to be tangential to the camber line, the vortex distribution $\gamma(x)$ has to satisfy the integral equation [Bisplinghoff, 1983, Moran, 1984]

$$\frac{1}{v_\infty}\int_0^c \frac{\gamma(\xi)\,d\xi}{\xi - x} = 2\pi\left(\frac{dz_S}{dx} - \alpha\right) \tag{4.1-1}$$

together with the Kutta condition

$$\gamma(c) = 0 \tag{4.1-2}$$

where v_∞ is the velocity of the undisturbed flow, α is the angle of attack and $z_S(x)$ describes the camber line.

When the vortex distribution is known, the pressure difference coefficient can be computed from [Bisplinghoff, 1983, Moran, 1984]

$$\Delta c_P(x) = \frac{p_L(x) - p_U(x)}{q_\infty} = 2\frac{\gamma(x)}{v_\infty} \tag{4.1-3}$$

where p_U is the pressure on the upper surface, p_L is the pressure on the lower surface and q_∞ is the dynamic pressure of the undisturbed flow. Equation (4.1-3) shows that the Kutta condition is equivalent to requiring the pressure difference to be zero at the trailing edge.

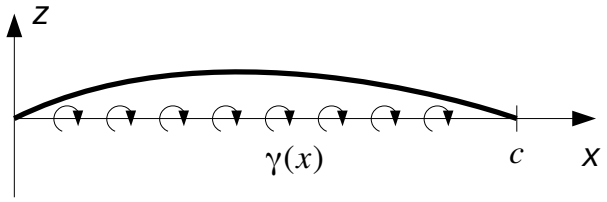


Figure 4.1-1: Camber Line and Vortex Distribution

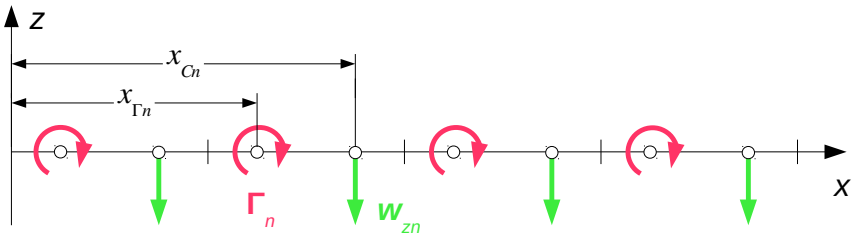


Figure 4.1-2: Discrete Vortices and Control Points

In the discrete vortex method, the chord is subdivided into N intervals. The continuous vortex distribution is approximated by N discrete vortices at the quarter points of the intervals. The N vortex strengths Γ_n are determined such that the boundary condition is satisfied at the control points located at the 3-quarter-points of the intervals. The resulting system of N linear equations for the vortex strengths reads:

$$\sum_{n=1}^{N} \frac{1}{x_{\Gamma n}-x_{CM}} \frac{\Gamma_n}{v_\infty} = 2\pi \left(\frac{dz_S}{dx}(x_{Cm}) - \alpha \right), \quad m=1,\ldots,N \tag{4.1-4}$$

Equation (4.1-4) can be solved for the vortex strengths Γ_n/v_∞. Subsequently, the coefficients of lift and moment can be computed from

$$c_L = \frac{2}{c} \sum_{n=1}^{N} \frac{\Gamma_n}{v_\infty}, \quad c_{M_0} = \frac{2}{c^2} \sum_{n=1}^{N} \left(\frac{c}{4} - x_{\Gamma n} \right) \frac{\Gamma_n}{v_\infty} \quad . \tag{4.1-5}$$

Finally, an approximation of the pressure coefficient is given by

$$\Delta c_P(x_{\Gamma n}) \approx \frac{2}{x_{n+1}-x_n} \frac{\Gamma_n}{v_\infty} \quad . \tag{4.1-6}$$

4.1.2 The Time-Harmonic Discrete Vortex Method

If the circulation around the airfoil varies with time, Kelvin's theorem requires vortices behind the airfoil. In a linear method, these vortices are arranged along the *x*-axis, see Figure 4.1-3.

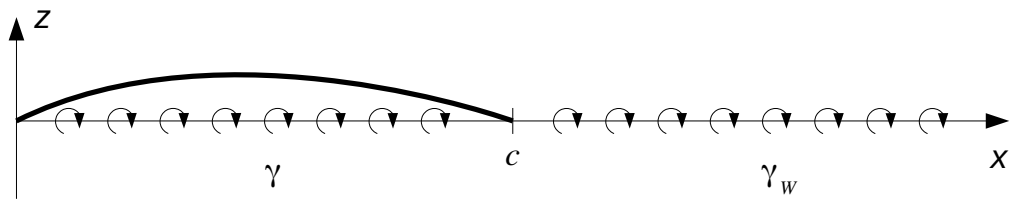


Figure 4.1-3: Wake Vortices

The boundary condition on the airfoil now reads

$$2\pi\left(\frac{\dot{z}_S}{v_\infty}+\frac{dz_s}{dx}\right)=\frac{1}{v_\infty}\left(\int_0^c \frac{\gamma(\xi,t)}{\xi-x}\,d\xi+\int_c^\infty \frac{\gamma_W(\xi,t)}{\xi-x}\,d\xi\right) \tag{4.1-7}$$

Kelvin's circulation theorem [Karamcheti, 1980], applied to a fluid curve in the wake, yields,

$$\gamma_W(x,t)=\gamma_W\left(c,t-\frac{x-c}{v_\infty}\right),\quad x\geq c \tag{4.1-8}$$

i.e. $\gamma_W(x,\ t)$ is completely determined by its value at the trailing edge (see [Wandinger, 2023], Chapter 6.2 for a detailed derivation).

Applying Kelvin's circulation theorem to a fluid curve surrounding the airfoil, we get

$$\gamma_w(c,t)=-\frac{1}{v_\infty}\frac{d\Gamma_0}{dt} \tag{4.1-9}$$

where

$$\Gamma_0(t)=\int_0^c \gamma(x,t)\,dx \tag{4.1-10}$$

is the circulation about the airfoil (see Chapter 6.2 of [Wandinger, 2023] for details).

It the motion is time-harmonic with circular frequency ω, then

$$z_S(x,t)=\Re\left(Z(x)e^{i\omega t}\right),\quad \dot{z}_S(x,t)=\Re\left(i\omega Z(x)e^{i\omega t}\right)$$
$$\gamma(x,t)=\Re\left(\hat{\gamma}(x)e^{i\omega t}\right),\quad \gamma_W(x,t)=\Re\left(\hat{\gamma}_W e^{i\omega t}\right)$$

where Z is the complex amplitude of the vertical motion and $\hat{\gamma}$ and $\hat{\gamma}_W$ are the complex amplitudes of the vortex distributions.

Now, from Equation (4.1-8), we get

$$\hat{\gamma}_W(x)e^{i\omega t}=\hat{\gamma}_W(c)e^{i\omega(t-(x-c)/v_\infty)}=\hat{\gamma}_W(c)e^{i\omega c/v_\infty}e^{-i\omega x/v_\infty}e^{i\omega t}\ .$$

With the *reduced frequency*

$$k=\frac{\omega c}{2v_\infty} \tag{4.1-11}$$

we obtain

$$\hat{\gamma}_w(x)=\hat{\gamma}_W(c)e^{2ik}e^{-2ikx/c} \tag{4.1-12}$$

Likewise, for a time-harmonic motion, Equation (4.1-9) reads

$$\hat{\gamma}_W(c)e^{i\omega t}=-\frac{i\omega}{v_\infty}\hat{\Gamma}_0 e^{i\omega t}$$

which, when written with the reduced frequency k, gives

$$\hat{\gamma}_W(c) = -2ik\frac{\hat{\Gamma}_0}{c} \tag{4.1-13}$$

Combining Equations (4.1-7) to (4.1-13), the integral equation to be solved for the vortex distribution reads [Bisplinghoff, 1983]

$$\begin{aligned} 2\pi\left(2ik\frac{Z}{c}+\frac{dZ}{dx}\right) &= \frac{1}{v_\infty}\left(\int_0^c \frac{\hat{\gamma}(\xi)\,d\xi}{\xi-x} - 2ik\,e^{2ik}\frac{\hat{\Gamma}_0}{c}\int_c^\infty \frac{e^{-2ik\xi/c}}{\xi-x}\,d\xi\right) \\ \hat{\Gamma}_0 &= \int_0^c \hat{\gamma}(\xi)\,d\xi \end{aligned} \tag{4.1-14}$$

The pressure difference coefficient is obtained from

$$\Delta\hat{c}_p(x) = \frac{2}{v_\infty}\left(\hat{\gamma}(x)+\frac{2ik}{c}\int_0^x \hat{\gamma}(\xi)\,d\xi\right) \quad . \tag{4.1-15}$$

The wake integral, i.e. the infinite integral on the right-hand side of Equation (4.1-14), can be written in a more convenient form. First,

$$I_w(x) = \int_c^\infty \frac{e^{-2ik\xi/c}}{\xi-x}\,d\xi = e^{-2ikx/c}\int_c^\infty \frac{e^{-2ik(\xi-x)/c}}{2ik(\xi-x)/c}\frac{2ik}{c}\,d\xi \quad .$$

Next, the substitution

$$t = \frac{2ik(\xi-x)}{c}, \quad dt = \frac{2ik\,d\xi}{c}, \quad t_0 = \frac{2ik(c-x)}{c}$$

yields

$$I_w(x) = e^{-2ikx/c}\int_{t_0}^\infty \frac{e^{-t}\,dt}{t} \quad .$$

Finally, with the exponential integral [Abramowitz & Stegun, 1972, Chapter 5.1, Formula 5.1.1]

$$E_1(z) = \int_z^\infty \frac{e^{-t}\,dt}{t} \tag{4.1-16}$$

the wake integral takes the form

$$I_w(x) = e^{-2ikx/c}E_1\left(\frac{2ik(c-x)}{c}\right) \quad . \tag{4.1-17}$$

As in the steady case, the continuous vortex distribution is approximated by discrete vortices located at the quarter points of the intervals, and the boundary condition is applied at the 3-quarter-points. Then, the system of equations to be solved for the discrete vortices Γ_n reads

$$\begin{bmatrix} \frac{1}{x_{\Gamma 1}-x_{C1}} & \cdots & \frac{1}{x_{\Gamma N}-x_{C1}} \\ \vdots & \ddots & \vdots \\ \frac{1}{x_{\Gamma 1}-x_{CN}} & \cdots & \frac{1}{x_{\Gamma 1}-x_{CN}} \end{bmatrix} \begin{bmatrix} \Gamma_1/v_\infty \\ \vdots \\ \Gamma_N/v_\infty \end{bmatrix} = 2\pi \begin{bmatrix} W_1 \\ \vdots \\ W_N \end{bmatrix} + \begin{bmatrix} F_1 \\ \vdots \\ F_N \end{bmatrix} \frac{\Gamma_0}{v_\infty}$$

$$\begin{bmatrix} 1 & \cdots & 1 \end{bmatrix} \begin{bmatrix} \Gamma_1/v_\infty \\ \vdots \\ \Gamma_N/v_\infty \end{bmatrix} = \frac{\Gamma_0}{v_\infty} \tag{4.1-18}$$

or

$$\begin{aligned} [C][\Gamma] &= 2\pi[W] + [F]\frac{\Gamma_0}{v_\infty} \\ [S][\Gamma] &= \frac{\Gamma_0}{v_\infty} \end{aligned} \tag{4.1-19}$$

where

$$F_m = \frac{2ik}{c} e^{2ik(c-x_{Cm})/c} E_1\left(\frac{2ik(c-x_{Cm})}{c}\right)$$

and

$$W_m = \frac{2ik}{c} Z(x_{Cm}) + \frac{dZ}{dx}(x_{Cm}) \quad .$$

Equations (4.2-19) can be rearranged to read

$$[C]\left([I]-[C]^{-1}[F][S]\right)[\Gamma] = 2\pi[W]$$

or

$$\left[C^u\right][\Gamma] = 2\pi[W] \tag{4.1-20}$$

where

$$\left[C^u\right] = [C]-[F][S] \tag{4.1-21}$$

is the unsteady matrix of aerodynamic influence coefficients. Only matrix $[F]$ depends on the reduced frequency.

By the Frobenius-Schur-Woodbury identity (see e.g. [Falk, 1984]), the inverse of $\left[C^u\right]$ is

$$\left[C^u\right]^{-1} = \left([I] + \frac{1}{r}[F_C][S]\right)[C]^{-1} \tag{4.1-22}$$

where $[F_C] = [C]^{-1}[F]$ and $r = 1-[S][F_C]$.

4.2 The Vortex Lattice Method

The Vortex Lattice Method (VLM) is an extension of the discrete vortex method to lifting surfaces. The discrete vortices are replaced by horseshoe vortices. The bound vortex of the horseshoe lies in the plane of the lifting surface, and the two free vortices are parallel to the *x*-axis.

To define the horseshoe vortices, the lifting surface is divided into vortex panels. Vortex panels are quadrangles with a trapezoidal shape, with two of the edges parallel to the *x*-axis. The bound vortex is along the quarter point line of the panel, and a control point *C* is at the three-quarter point, cf. Figure 4.2-1.

4.2.1 The Horseshoe Vortex

A horseshoe vortex consists of three parts:

1. a semi-infinite line ending at point *A*,
2. a finite line from point *A* to point *B* and
3. a semi-infinite line starting at point *B*.

Now, consider a horseshoe vortex with vortex strength $\Gamma = 1$. By the Biot-Savart law [Karamcheti, 1980], the velocity induced at point *P* by the finite line segment from *A* to *B*, is

$$\boldsymbol{v}_F(A,B,P) = -\frac{1}{4\pi}\int_A^B \frac{(\boldsymbol{r}_P - \boldsymbol{s}) \times d\,\boldsymbol{s}}{|\boldsymbol{r}_P - \boldsymbol{s}|^3} \tag{4.2-1}$$

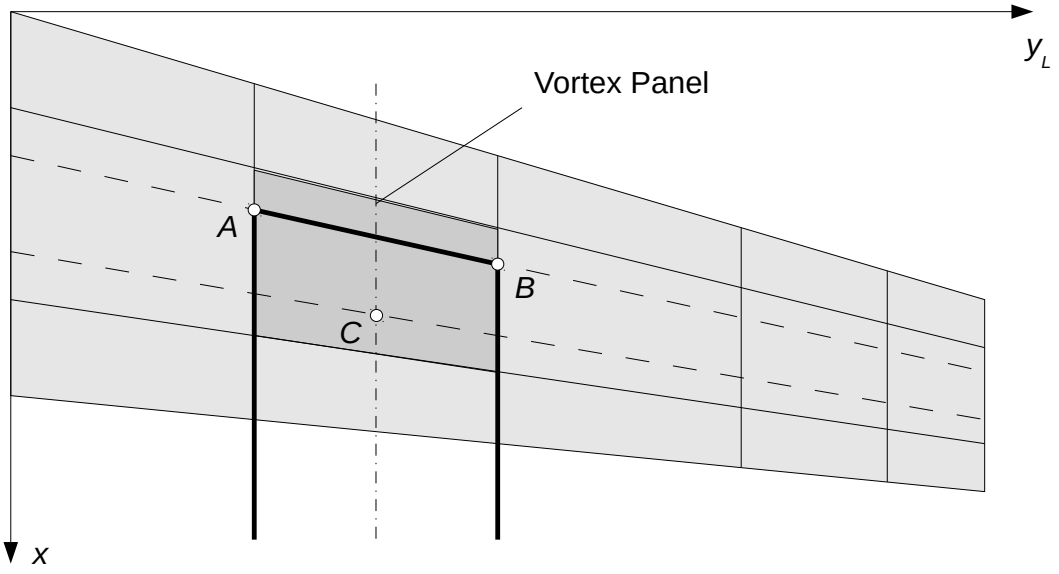


Figure 4.2-1: Geometry of Vortex Panel and Horsehoe

(see Figure 4.2-2). With

$$\boldsymbol{s}=\boldsymbol{r}_A+\lambda\,\boldsymbol{r}_{AB},\quad 0\le\lambda\le 1,\quad d\,\boldsymbol{s}=\boldsymbol{r}_{AB}\,d\lambda$$
$$\boldsymbol{r}_P-\boldsymbol{s}=\boldsymbol{r}_P-\boldsymbol{r}_A-\lambda\,\boldsymbol{r}_{AB}=\boldsymbol{r}_{AP}-\lambda\,\boldsymbol{r}_{AB}$$

and

$$a=\left|\boldsymbol{r}_{AB}\right|^2,\quad b=-2\,\boldsymbol{r}_{AB}\cdot\boldsymbol{r}_{AP},\quad c=\left|\boldsymbol{r}_{AP}\right|^2$$

the integral reads

$$\boldsymbol{v}_F(A,B,P)=\frac{1}{4\pi}\left(\boldsymbol{r}_{AB}\times\boldsymbol{r}_{AP}\right)\int_0^1\frac{d\lambda}{\left(a\lambda^2+b\lambda+c\right)^{3/2}} \tag{4.2-2}$$

Evaluation of the integral eventually leads to (see [Wandinger, 2023], chapter 4.2 for details)

$$\boldsymbol{v}_F(A,B,P)=\frac{1}{4\pi}\frac{\boldsymbol{r}_{AP}\times\boldsymbol{r}_{BP}}{\left|\boldsymbol{r}_{AP}\times\boldsymbol{r}_{BP}\right|^2}\left(\frac{\boldsymbol{r}_{AB}\cdot\boldsymbol{r}_{AP}}{\left|\boldsymbol{r}_{AP}\right|}-\frac{\boldsymbol{r}_{AB}\cdot\boldsymbol{r}_{BP}}{\left|\boldsymbol{r}_{BP}\right|}\right) \tag{4.2-3}$$

The contribution of the semi-infinite line starting at point *B* is obtained from Equation (4.2-2) by letting the upper bound of the integral go to infinity. With

$$\boldsymbol{r}_{AB}=\boldsymbol{e}_x$$

for a semi-infinite line parallel to the *x*-axis, the result is

$$\boldsymbol{v}_S(B,P)=\frac{1}{4\pi}\frac{\boldsymbol{e}_x\times\boldsymbol{r}_{BP}}{\left|\boldsymbol{e}_x\times\boldsymbol{r}_{BP}\right|^2}\left(1+\boldsymbol{e}_x\cdot\frac{\boldsymbol{r}_{BP}}{\left|\boldsymbol{r}_{BP}\right|}\right) \tag{4.2-4}$$

Thus, the velocity induced by a horseshoe vortex with vortex strength Γ is

$$\boldsymbol{v}(A,B,P)=\Gamma\left(\boldsymbol{v}_F(A,B,P)+\boldsymbol{v}_S(B,P)-\boldsymbol{v}_S(A,P)\right)\ . \tag{4.2-5}$$

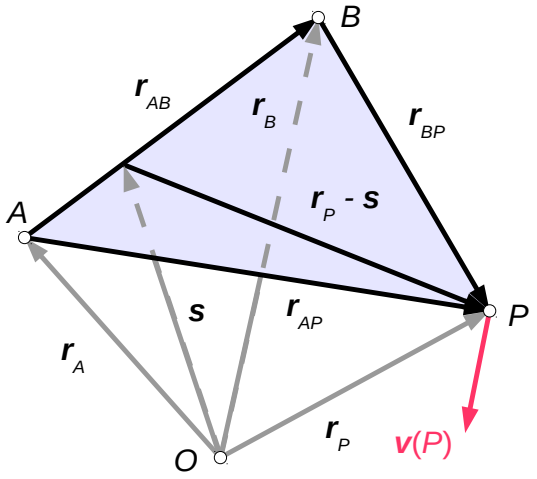


Figure 4.2-2: Velocity Induced by Finite Line Segment

4.2.2 The Steady Vortex Lattice Method

The boundary condition on the lifting surface reads

$$\frac{\boldsymbol{w}\cdot\boldsymbol{n}}{v_\infty}=\frac{d\zeta_s}{dx}-\alpha_i-\eta-\alpha\,\boldsymbol{e}_z\cdot\boldsymbol{n}-\beta\,\boldsymbol{e}_y\cdot\boldsymbol{n}+\alpha_r \tag{4.2-6}$$

where $\boldsymbol{w}$ is the velocity induced by all horseshoe vortices, $\boldsymbol{n}$ is the unit normal vector of the lifting surface, v_∞ is the velocity of the undisturbed flow, ζ_S is the camber of the airfoil, α_i is the rigging angle of incidence, η is the control surface angle, α is the angle of attack, β is the sideslip angle, and α_r contains the contribution of the pitch, yaw and roll rates q, r and p. It is computed from

$$\alpha_r=\left[\left(\boldsymbol{e}_x\frac{p}{v_\infty}+\boldsymbol{e}_y\frac{q}{v_\infty}+\boldsymbol{e}_z\frac{r}{v_\infty}\right)\times\boldsymbol{r}\right]\cdot\boldsymbol{n} \tag{4.2-7}$$

where $\boldsymbol{r}$ is the vector from the reference point to the point on the lifting surface. The left hand side of Equation (4.2-6) is known as normal wash.

The unknown vortex strengths Γ_n of the N horseshoe vortices are determined such that the boundary condition (4.2-6) is satisfied at the N control points. With

$$C_{mn}=\boldsymbol{n}_m\cdot\left(\boldsymbol{v}_F(A_n,B_n,C_m)+\boldsymbol{v}_S(B_n,C_m)-\boldsymbol{v}_S(A_n,C_m)\right) \tag{4.2-8}$$

the system of equations to be solved reads

$$\sum_{n=1}^{N}C_{mn}\frac{\Gamma_n}{v_\infty}=\frac{\boldsymbol{w}_m\cdot\boldsymbol{n}_m}{v_\infty},\quad m=1,\ldots,N \tag{4.2-9}$$

where $\boldsymbol{n}_m$ is the normal vector of the m-th panel.

Once the vortex strengths Γ_n have been determined, the pressure coefficient of the panel can be computed from

$$\Delta c_{pn}=\frac{2}{\Delta x_n}\frac{\Gamma_n}{v_\infty} \tag{4.2-10}$$

where Δx_n is the mean chord of the panel. The pressure on the panel is

$$\Delta p_n=q_\infty\Delta c_{pn}. \tag{4.2-11}$$

The lift perpendicular to the panel is given by

$$L_n=\Delta p_n A_n \tag{4.2-12}$$

where

$$A_n=\Delta x_n\Delta y_{Ln} \tag{4.2-13}$$

is the area of the panel. From equations (4.2-10) to (4.2-13) the following equation is obtained for the lift:

$$L_n = 2\,q_\infty\,\Delta\,y_{Ln}\,\frac{\Gamma_n}{v_\infty}. \tag{4.2-14}$$

In a static response analysis, the system of Equations (4.2-9) is solved to obtain the primary results, i.e. the vortex strengths of the horseshoe vortices. Panel results are computed from Equations (4.2-10) to (4.2-14).

4.2.3 The Time-Harmonic Vortex Lattice Method

The time-harmonic Vortex Lattice Method is obtained from the time-harmonic discrete vortex method by replacing the discrete vortices by horseshoe vortices, see Figure 4.2-3. The system of equations to be solved reads

$$\begin{gathered}\sum_n C_{mn}\frac{\hat\Gamma_n}{v_\infty} - 2\,i\,k\sum_l C^W_{ml}\frac{\hat\Gamma^W_l}{v_\infty} = \frac{\boldsymbol{W}_m\cdot\boldsymbol{n}_m}{v_\infty} \\ \sum_\mu \hat\Gamma_\mu - \hat\Gamma^W_l = 0\end{gathered} \tag{4.2-15}$$

where the index m ranges over the control points, the index n over the bound vortices on the wing, index l over the vortex strips and index μ over the bound vortices in the l-th vortex strip. $\boldsymbol{W}_m$ is the complex amplitude of the normal wash at the m-th control point.

The coefficients C_{mn} are identical with those of the steady Vortex Lattice Method. The coefficients C^W_{ml} describe the contribution of the wake of the l-th vortex strip to the m-th control point. They are obtained from

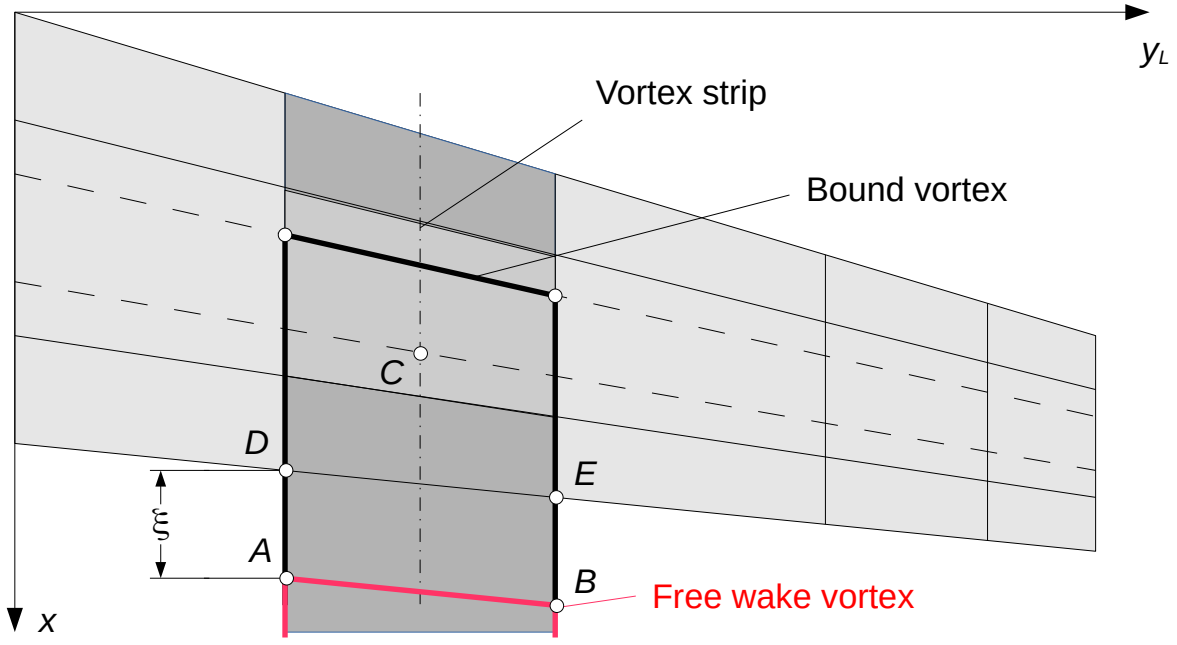


Figure 4.2-3: Bound and Free Vortices

$$C_{ml}^{W}=\int_0^\infty \boldsymbol{n}_m\cdot\boldsymbol{v}_{ml}(\xi)\,e^{-2ik\xi/c}\,d\xi \tag{4.2-16}$$

where $\boldsymbol{v}_{ml}(\xi)$ is the velocity induced at the m-th control point by a horseshoe vortex with unit vortex strength located at a distance ξ behind the trailing edge of the l-th vortex strip. c is the reference chord length. Please note that, in contrast to the discrete vortex method, variable ξ starts at the trailing edge, see Figure 4.2-3. Therefore, the factor e^{2ik} is missing in Equation (4.2-15).

With the dimensionless variable $s=\xi/c$ the position vectors of points *A* and *B* of a horseshoe in the wake read, see Figure 4.2-3,

$$\boldsymbol{r}_A=\boldsymbol{r}_D+c\,s\,\boldsymbol{e}_x,\quad \boldsymbol{r}_B=\boldsymbol{r}_E+c\,s\,\boldsymbol{e}_x \tag{4.2-17}$$

The vectors needed in Equations (4.2-3) and (4.2-4) to compute the velocity at an arbitrary control point *C* are

$$\begin{aligned}\boldsymbol{r}_{AC}&=\boldsymbol{r}_C-\boldsymbol{r}_A=\boldsymbol{r}_C-\boldsymbol{r}_D-c\,s\,\boldsymbol{e}_x=\boldsymbol{r}_{CP}-c\,s\,\boldsymbol{e}_x\\ \boldsymbol{r}_{BC}&=\boldsymbol{r}_{EC}-c\,s\,\boldsymbol{e}_x\\ \boldsymbol{r}_{AB}&=\boldsymbol{r}_B-\boldsymbol{r}_A=\boldsymbol{r}_E-\boldsymbol{r}_D=\boldsymbol{r}_{DE}\end{aligned} \tag{4.2-18}$$

With Equations (4.2-18), the dot products read

$$\begin{aligned}\boldsymbol{e}_x\cdot\boldsymbol{r}_{AC}&=\boldsymbol{e}_x\cdot\boldsymbol{r}_{DC}-c\,s\\ \boldsymbol{e}_x\cdot\boldsymbol{r}_{BC}&=\boldsymbol{e}_x\cdot\boldsymbol{r}_{EC}-c\,s\\ \boldsymbol{r}_{AB}\cdot\boldsymbol{r}_{AC}&=\boldsymbol{r}_{DE}\cdot\boldsymbol{r}_{DC}-\boldsymbol{r}_{DE}\cdot\boldsymbol{e}_x\,c\,s\\ \boldsymbol{r}_{AB}\cdot\boldsymbol{r}_{BC}&=\boldsymbol{r}_{DE}\cdot\boldsymbol{r}_{EC}-\boldsymbol{r}_{DE}\cdot\boldsymbol{e}_x\,c\,s\end{aligned} \tag{4.2-19}$$

In coordinates, Equations (4.2-19) read

$$\begin{aligned}\boldsymbol{e}_x\cdot\boldsymbol{r}_{AC}&=x_{DC}-c\,s\\ \boldsymbol{e}_x\cdot\boldsymbol{r}_{BC}&=x_{EC}-c\,s\\ \boldsymbol{r}_{AB}\cdot\boldsymbol{r}_{AC}&=x_{DE}\,x_{DC}+y_{DE}\,y_{DC}+z_{DE}\,z_{DC}-x_{DE}\,c\,s\\ \boldsymbol{r}_{AB}\cdot\boldsymbol{r}_{BC}&=x_{DE}\,x_{EC}+y_{DE}\,y_{EC}+z_{DE}\,z_{EC}-x_{DE}\,c\,s\end{aligned} \tag{4.2-20}$$

The cross products in Equations (4.2-3) and (4.2-4) are

$$\begin{aligned}\boldsymbol{e}_x\times\boldsymbol{r}_{AC}&=\boldsymbol{e}_x\times(\boldsymbol{r}_{DC}-c\,s\,\boldsymbol{e}_x)=\boldsymbol{e}_x\times\boldsymbol{r}_{DC}\\ \boldsymbol{e}_x\times\boldsymbol{r}_{BC}&=\boldsymbol{e}_x\times\boldsymbol{r}_{EC}\end{aligned} \tag{4.2-21}$$

and

$$\begin{aligned}\boldsymbol{r}_{AC}\times\boldsymbol{r}_{BC}&=(\boldsymbol{r}_{DC}-c\,s\,\boldsymbol{e}_x)\times(\boldsymbol{r}_{EC}-c\,s\,\boldsymbol{e}_x)\\ &=\boldsymbol{r}_{DC}\times\boldsymbol{r}_{EC}-c\,s(\boldsymbol{e}_x\times\boldsymbol{r}_{EP}+\boldsymbol{r}_{DP}\times\boldsymbol{e}_x)\\ &=\boldsymbol{r}_{DP}\times\boldsymbol{r}_{EC}-c\,s\,\boldsymbol{e}_x\times(\boldsymbol{r}_{EC}-\boldsymbol{r}_{DC})\\ &=\boldsymbol{r}_{DP}\times\boldsymbol{r}_{EC}+c\,s\,\boldsymbol{e}_x\times\boldsymbol{r}_{DE}\end{aligned} \tag{4.2-22}$$

In coordinates, the cross products read:

$$[\boldsymbol{e}_x \times \boldsymbol{r}_{QC}] = \begin{bmatrix}1\\0\\0\end{bmatrix} \times \begin{bmatrix}x_{QC}\\y_{QC}\\z_{QC}\end{bmatrix} = \begin{bmatrix}0\\-z_{QC}\\y_{QC}\end{bmatrix}, \quad Q = D, E \tag{4.2-23}$$

$$[\boldsymbol{r}_{DC} \times \boldsymbol{r}_{EC}] = \begin{bmatrix}x_{DC}\\y_{DC}\\z_{DC}\end{bmatrix} \times \begin{bmatrix}x_{EC}\\y_{EC}\\z_{EC}\end{bmatrix} = \begin{bmatrix}y_{DC}z_{EC} - z_{DC}y_{EC}\\z_{DC}x_{EC} - x_{DC}z_{EC}\\x_{DC}y_{EC} - y_{DC}x_{EC}\end{bmatrix} \tag{4.2-24}$$

$$[\boldsymbol{e}_x \times \boldsymbol{r}_{DE}] = \begin{bmatrix}1\\0\\0\end{bmatrix} \times \begin{bmatrix}x_{DE}\\y_{DE}\\z_{DE}\end{bmatrix} = \begin{bmatrix}0\\-z_{DE}\\y_{DE}\end{bmatrix} \tag{4.2-25}$$

Finally, the norms in Equations (4.2-3) and (4.2-4) are

$$\begin{aligned}
|\boldsymbol{r}_{AC}|^2 &= \boldsymbol{r}_{AC} \cdot \boldsymbol{r}_{AC} = (\boldsymbol{r}_{DC} - c\,s\,\boldsymbol{e}_x) \cdot (\boldsymbol{r}_{DC} - c\,s\,e_x) = |\boldsymbol{r}_{DC}|^2 - 2\,\boldsymbol{e}_x \boldsymbol{r}_{DC}\,c\,s + (c\,s)^2 \\
|\boldsymbol{r}_{BC}|^2 &= |\boldsymbol{r}_{EC}|^2 - 2\,\boldsymbol{e}_x \boldsymbol{r}_{EC}\,c\,s + (c\,s)^2 \\
|\boldsymbol{r}_{AC} \times \boldsymbol{r}_{BC}|^2 &= (\boldsymbol{r}_{DC} \times \boldsymbol{r}_{EC} + c\,s\,\boldsymbol{e}_x \times \boldsymbol{r}_{DE}) \cdot (\boldsymbol{r}_{DC} \times \boldsymbol{r}_{EC} + c\,s\,\boldsymbol{e}_x \times \boldsymbol{r}_{DE}) \\
&= |\boldsymbol{r}_{DC} \times \boldsymbol{r}_{EC}|^2 + 2\,c\,s\,(\boldsymbol{r}_{DC} \times \boldsymbol{r}_{EC}) \cdot (\boldsymbol{e}_x \times \boldsymbol{r}_{DE}) + (c\,s)^2 |\boldsymbol{e}_x \times \boldsymbol{r}_{DE}|^2 \\
&= \alpha_0 + \alpha_1\,c\,s + \alpha_2 (c\,s)^2 = \alpha(s)
\end{aligned} \tag{4.2-26}$$

or, in coordinates,

$$\begin{aligned}
|r_{AC}|^2 &= y_{DC}^2 + z_{DC}^2 + (x_{DC} - c\,s)^2 \\
|r_{BC}|^2 &= y_{EC}^2 + z_{EC}^2 + (x_{EC} - c\,s)^2
\end{aligned} \tag{4.2-27}$$

With these relations, the contribution of a semi-infinite wake vortex line starting at trailing edge point Q ($Q = D, E$) is (cf. Equation (4.2-4))

$$\boldsymbol{v}_S(Q, C) = \frac{1}{4\pi} \frac{\boldsymbol{e}_x \times \boldsymbol{r}_{QC}}{|\boldsymbol{e}_x \times \boldsymbol{r}_{QC}|^2} I_S(Q, C) \tag{4.2-28}$$

where

$$I_S(Q, C) = \int_0^\infty \left(1 + \frac{x_{QC} - c\,s}{\sqrt{y_{QC}^2 + z_{QC}^2 + (x_{QC} - c\,s)^2}} \right) e^{-2ik\,s}\, ds \tag{4.2-29}$$

From Equation (4.2-3), the contribution of the finite vortex lines behind trailing edge segment *DE* is obtained as

$$\boldsymbol{v}_F(D, E, C) = \frac{\boldsymbol{r}_{DC} \times \boldsymbol{r}_{EC}}{4\pi} I_{F1}(D, E, C) + \frac{\boldsymbol{e}_x \times \boldsymbol{r}_{DE}}{4\pi} I_{F2}(D, E, C) \tag{4.2-30}$$

where

$$I_{F1}(D,E,C)=\int_0^\infty \frac{\beta(s)}{\alpha(s)} e^{-2iks}\,ds \tag{4.2-31}$$

and

$$I_{F2}(D,E,C)=\int_0^\infty \frac{c\,s\,\beta(s)}{\alpha(s)} e^{-2iks}\,ds \tag{4.2-32}$$

with

$$\begin{aligned}\beta(s)&=\frac{\boldsymbol{r}_{AB}\cdot\boldsymbol{r}_{AC}}{|\boldsymbol{r}_{AC}|}-\frac{\boldsymbol{r}_{AB}\cdot\boldsymbol{r}_{BC}}{|\boldsymbol{r}_{BC}|}\\&=\frac{x_{DE}\,x_{DC}+y_{DE}\,y_{DC}+z_{DE}\,z_{DC}-x_{DE}\,c\,s}{\sqrt{y_{DC}^2+z_{DC}^2+(x_{DC}-c\,s)^2}}\\&\quad-\frac{x_{DE}\,x_{EC}+y_{DE}\,y_{EC}+z_{DE}\,z_{EC}-x_{DE}\,c\,s}{\sqrt{y_{EC}^2+z_{EC}^2+(x_{EC}-c\,s)^2}}\end{aligned} \tag{4.2-33}$$

Section 4.2.4 describes how the integrals in Equations (4.2-29), (4.2-31) and (4.2-32) can be evaluated numerically.

Equations (4.2-15) build a system of equations to determine the unknown vortex strengths $\hat{\Gamma}_{mn}$ and $\hat{\Gamma}_n^W$.

With the matrices

$$\hat{\Gamma}=\frac{1}{v_\infty}\begin{bmatrix}\hat{\Gamma}_1 & \cdots & \hat{\Gamma}_N\end{bmatrix}^T,\quad \hat{\Gamma}^W=\frac{1}{v_\infty}\begin{bmatrix}\hat{\Gamma}_1^W & \cdots & \hat{\Gamma}_{N_S}^W\end{bmatrix}^T \tag{4.2-34}$$

where N is the number of vortex panels and N_S the number of vortex strips, and

$$[W]=\frac{1}{v_\infty}\begin{bmatrix}\boldsymbol{W}_1\cdot\boldsymbol{n}_1 & \cdots & \boldsymbol{W}_N\cdot\boldsymbol{n}_N\end{bmatrix}^T \tag{4.2-35}$$

the first of Equations 4.2-15 becomes

$$[C][\hat{\Gamma}]-[F(k)][\hat{\Gamma}^W]=[W]\ . \tag{4.2-36}$$

Matrix $[C]$ is defined by the first sum on the left side of Equation (4.2-15) and matrix $[F(k)]$ by the second. Matrix $[C]$ is identical with the corresponding matrix of the steady Vortex Lattice Method.

In matrix notation, the second of Equations (4.2-15) reads

$$[\hat{\Gamma}^W]=[S][\hat{\Gamma}] \tag{4.2-37}$$

where $[S]$ is a summation matrix. The rows of matrix $[S]$ correspond to the vortex strips and the columns to the bound vortices. The n-th row contains 1 in the columns corresponding to bound vortices in the n-th vortex strip, and 0 in all other columns.

Inserting Equation (4.2-37) into Equation (4.2-36) results in

$$\left([C]-\left[F(k)\right][S]\right)[\hat{\Gamma}]=[W] \tag{4.2-38}$$

By the Frobenius-Schur-Woodbury identity (see e.g. [Falk, 1984]), the inverse of the unsteady matrix of aerodynamic influence coefficients

$$\left[C^u\right]=\left([C]-\left[F(k)\right][S]\right) \tag{4.2-39}$$

reads

$$\left[C^u\right]^{-1}=\left([I]+\left[F_C(k)\right]\left[R(k)\right]^{-1}[S]\right)[C]^{-1} \tag{4.2-40}$$

where $\left[F_C(k)\right)=[C]^{-1}\left[F(k)\right]$ and $\left[R(k)\right]=[I]-[S]\left[F_C(k)\right]$.

Once the vortex strengths are known, the pressure coefficient can be computed from

$$\Delta\hat{c}_{Pmn}=2\left(\frac{1}{x_{m+1}-x_m}\frac{\hat{\Gamma}_{mn}}{v_\infty}+\frac{2ik}{c_{ref}}\sum_{l=1}^{m-1}\frac{\hat{\Gamma}_{ln}}{v_\infty}\right),\quad 1\le m\le M_{Bn},\quad 1\le n\le S \tag{4.2-41}$$

where M_{Bn} is the number of bound vortices in the n-th vortex strip and S is the number of vortex strips. Equation (4.2-41) is obtained from the unsteady Bernoulli equation, also known as Kelvin's equation (see e.g. [Bisplinghoff, 1983]), by linearization and discretization.

Then, the aerodynamic forces perpendicular to the lifting surface are given by

$$L^A_{mn}=q_\infty\Delta\hat{c}_{Pmn}A_{mn} \tag{4.2-42}$$

where A_{mn} is the area of the m-th panel of the n-th vortex strip. In matrix notation, these equations read

$$\left[L^A_V\right]=q_\infty\left(\left[G^1\right]+ik\left[G^2\right]\right)[\hat{\Gamma}] \tag{4.2-43}$$

where matrix $[G^1]$ is defined by the first term of Equation (4.2-41) and matrix $[G^2]$ by the second.

4.2.4 Evaluation of the Wake Integrals

The integrals in Equations (4.2-29), (4.2-31) and (4.2-32) are of the form

$$I=\int_0^\infty f(s)e^{-2iks}\,ds\quad . \tag{4.2-44}$$

In [Filon, 1929] and [Tuck, 1967], quadrature formulas for integrals of this type are presented. The basic idea is to approximate $f(s)$ by piecewise polynomials that can be integrated analytically. The original paper of Filon uses a quadratic interpolation whereas Tuck uses a linear interpolation.

Mefisto currently uses a linear interpolation. As $f(s)$ strongly varies with s for

control points near the trailing edge, the formulas given by Tuck for a regular grid with equidistant points are extended to an arbitrary grid.

Let $[s_n, s_{n+1}]$ be an interval of the s-axis of size $h_n = s_{n+1} - s_n$. Within this interval, $f(s)$ is approximated by

$$f(s) \approx P_L(s) = L_{n1}^L(s)\, y_n + L_{n2}^L(s)\, y_{n+1} \tag{4.2-45}$$

where $y_n = f(s_n), y_{n+1} = f(s_{n+1})$ and

$$L_{n1}^L(s) = \frac{s_{n+1} - s}{h_n}, \quad L_{n2}^L(s) = \frac{s - s_n}{h_n} \tag{4.2-46}$$

Then,

$$I_n = \int_{s_n}^{s_{n+1}} f(s) e^{-2iks}\, ds \approx \int_{s_n}^{s_{n+1}} P_L(s) e^{-2iks}\, ds = l_{n1} y_n + l_{n2} y_2 \tag{4.2-47}$$

where

$$l_{n1} = \int_{s_n}^{s_{n+1}} L_{n1}^L(s) e^{-2iks}\, ds = \frac{1}{h_n} \int_{s_n}^{s_{n+1}} (s_{n+1} - s) e^{-2iks}\, ds \tag{4.2-48}$$

and

$$l_{n2} = \int_{s_n}^{s_{n+1}} L_{n2}^L(s) e^{-2iks}\, ds = \frac{1}{h_n} \int_{s_n}^{s_{n+1}} (s - s_n) e^{-2iks}\, ds \tag{4.2-49}$$

With

$$\int_{s_n}^{s_{n+1}} e^{-2iks}\, ds = \frac{-1}{2ik}\left(e^{-2iks_{n+1}} - e^{-2iks_n}\right) = \frac{i}{2k}\left(e^{-2iks_{n+1}} - e^{-2iks_n}\right)$$

and

$$\int_{s_n}^{s_{n+1}} s\, e^{-2iks}\, ds = \left[\frac{e^{-2iks}}{(-2ik)^2}(-2iks - 1)\right]_{s=s_n}^{s=s_{n+1}}$$
$$= \frac{1}{(2k)^2}\left((2iks_{n+1} + 1) e^{-2iks_{n+1}} - (2iks_n + 1) e^{-2iks_n}\right)$$

the coefficients l_{n1} and l_{n2} read

$$l_{n1} = \frac{is_{n+1}}{2kh_n}\left(e^{-2iks_{n+1}} - e^{-2iks_n}\right) - \frac{1}{(2k)^2 h_n}\left((2iks_{n+1} + 1) e^{-2iks_{n+1}} - (2iks_n + 1) e^{-2iks_n}\right)$$
$$= \frac{1}{(2k)^2 h_n}\left(e^{-2iks_n} - 2ik(s_{n+1} - s_n) e^{-2iks_n} - e^{-2iks_{n+1}}\right)$$

and

$$l_{n2}=\frac{1}{(2k)^2 h_n}\left((2iks_{n+1}+1)e^{-2iks_{n+1}}-(2iks_n+1)e^{-2iks_n}\right)-\frac{is_n}{2kh_n}\left(e^{-2iks_{n+1}}-e^{-2iks_n}\right)$$
$$=\frac{1}{(2k)^2 h_n}\left(2ik(s_{n+1}-s_n)e^{-2iks_{n+1}}+e^{-2iks_{n+1}}-e^{-2iks_n}\right)$$

With

$$e^{-2iks_{n+1}}=e^{-2iks_n}e^{-2ikh_n}$$

the following result is obtained for the coefficients:

$$l_{n1}=\frac{e^{-2iks_n}}{(2k)^2 h_n}\left(1-2ikh_n-e^{-2ikh_n}\right)$$
$$l_{n2}=\frac{e^{-2iks_{n+1}}}{(2k)^2 h_n}\left(1+2ikh_n-e^{2ikh_n}\right) \qquad (4.2\text{-}50)$$

Summing up the contributions of all N intervals, the integral is approximated by

$$I\approx\sum_{n=1}^{N} I_n=\sum_{n=1}^{N+1} y_n w_n e^{-2iks_n} \qquad (4.2\text{-}51)$$

where the weights are given by

$$w_1=\frac{1-2ikh_1-e^{-2ikh_1}}{4k^2 h_1}$$
$$w_n=\frac{1+2ikh_{n-1}-e^{2ikh_{n-1}}}{4k^2 h_{n-1}}+\frac{1-2ikh_n-e^{-2ikh_n}}{4k^2 h_n},\quad n=2,\ldots,N \qquad (4.2\text{-}52)$$
$$w_{N+1}=\frac{1+2ikh_N-e^{2ikh_N}}{4k^2 h_N}$$

In the special case that all intervals have the same size, i.e. $h_n = h$, the formulas agree with those derived in [Tuck, 1967].

In Mefisto, two different grids are used. In the regular grid, all intervals have the same size $h=1/n$ where n = **`opts.nx`**. For control points on the lifting surface attached to the trailing edge processed, a graded grid is used in the interval $0\le s\le 1$. This grid is defined as follows:

1) $h_1=x_{min}/(c\,m_1)$ where x_{min} is the smallest distance of a control point from the trailing edge and m_1 = **`opts.m1`**
2) $h_{n+1}=r\,h_n$, $h_N=r^{N-1}h_1=h$
3) $\sum_{n=1}^{N} h_n=h_1\sum_{n=1}^{N-1} r^n=h_1\frac{r^N-1}{r-1}=1$

From these conditions, N and r can be determined. First, the second condi-

tion yields

$$r^{N-1}=\frac{h}{h_1} \quad .$$

Then, the third condition can be written in the form

$$r-1=h_1\left(r\frac{h}{h_1}-1\right)=r\,h-h_1$$

leading to

$$r=\frac{1-h_1}{1-h} \quad .$$

Then, N is the smallest integer such that

$$N>1+\frac{\ln(h/h_1)}{\ln(r)}$$

4.3 Rigid Trim Analysis

The trim analysis determines the values of the trim parameters needed to fly a specific manoeuvre. In a rigid trim analysis, the aircraft is considered to be rigid.

The trim parameters include the configuration parameters

$$\left[u^K\right]=\left[\alpha \quad \beta \quad p/v_\infty \quad q/v_\infty \quad r/v_\infty \quad \eta_1 \quad \cdots \quad \eta_K\right]^T$$

and the rigid body accelerations

$$\left[a^R\right]=\left[a_x \quad a_y \quad a_z \quad \dot{p} \quad \dot{q} \quad \dot{r}\right]^T.$$

The trim parameter matrix $[t]$ contains both of these matrices:

$$[t]=\begin{bmatrix}[a^R]\\ [u^K]\end{bmatrix} \tag{4.3-1}$$

Let matrix $[l^0]$ contain those loads that do not depend on the aerodynamics, and matrix $[l^A]$ the aerodynamic loads. Then, the dynamic equilibrium reads

$$[R]^T\left(\left[l^0\right]+\left[l^A\right]\right)-\left[M_{RR}\right]\left[a^R\right]=[0] \tag{4.3-2}$$

where matrix $[R]$ describes the six rigid body motions. The first three columns contain the velocities due to unit translations in *x*-, *y*- and *z*-direction, and the remaining three columns the velocities due to unit rotations about the *x*-, *y*- and *z*-axis. Matrix $[M_{RR}]$ is the rigid body mass matrix of the rigid aircraft.

In a linear trim analysis, the aerodynamic loads are assumed to depend linearly on the configuration parameters, i.e.

$$[l^A] = q_\infty \left([q^0] + [Q^K][u^K] \right). \tag{4.3-3}$$

Matrix $[q^0]$ contains the aerodynamic loads due to the camber and the rigging angle of incidence. Matrix $[Q^K]$ describes the linear dependence of the aerodynamic loads from the configuration parameters. Both matrices can be computed by the Vortex Lattice Method, using the normal wash due to unit values of the configuration parameters.

With Equation (4.3-3), Equation (4.3-2) reads

$$[M_{RR}][a^R] - q_\infty [R]^T [Q^K][u^K] = [R^T] \left([l^0] + q_\infty [q^0] \right). \tag{4.3-4}$$

With the *trim matrix*

$$[T] = \left[[M_{RR}] \quad -q_\infty [R]^T [Q^K] \right] \tag{4.3-5}$$

Equation (4.3-4) can be written

$$[T][t] = [R]^T \left([l^0] + q_\infty [q^0] \right). \tag{4.3-6}$$

This is a system of six linear equations that can be solved for six unknown trim parameters. The values of the remaining trim parameters must be specified. They define the manoeuvre to be analysed.

The definition of some more sophisticated manoeuvres may include linear constraints

$$[C][t] = [r] \tag{4.3-7}$$

between the trim parameters. Then, the number of unknown trim parameters is increased by the number of linear constraints. The unknown trim parameters can be obtained by solving the combined system of linear equations

$$\begin{bmatrix} [T] \\ [C] \end{bmatrix} [t] = \begin{bmatrix} [R]^T \left([l^0] + q_\infty [q^0] \right) \\ [r] \end{bmatrix}. \tag{4.3-8}$$

5 Methods in Aeroelasticity

5.1 Splines

Splines transfer the displacements of the solid model to the aerodynamic model and the aerodynamic loads to the solid model. The torsion-bending spline assumes that the motion of a lifting surface mainly consists of a bending motion combined with torsion.

Splines are defined in the local coordinate system of the lifting surface. The x-axis of the lifting surface coincides with the global x-axis. The z_L-axis is perpendicular to the lifting surface and defines its upper side. The y_L-axis is in spanwise direction (see Figure 5.1-1).

The structural displacement $u_n = \boldsymbol{u}\cdot\boldsymbol{n}$ normal to the lifting surface is approximated by

$$u_n(x, y_L) = b(y_L) - x\,\theta(y_L). \tag{5.1-1}$$

Function $b(y_L)$ describes the bending and function $\theta(y_L)$ the torsion about the y_L-axis. These functions are cubic splines.

To define the cubic splines, the y_L-axis is divided into N intervals $[y_{Ln-1},\ y_{Ln}]$. The $N+1$ functions $B_n(y_L)$ are cubic splines that satisfy

$$B_n(y_{Ln}) = 1,\quad B_n(y_{Lm}) = 0 \text{ for } n \neq m,\quad n = 0, \ldots, N. \tag{5.1-2}$$

With the matrices

$$\begin{gathered}\left[B(y_L)\right] = \left[B_0(y_L) \quad \cdots \quad B_N(y_L)\right] \\ [b] = \left[b_0 \quad \cdots \quad b_N\right]^T,\quad [\theta] = \left[\theta_0 \quad \cdots \quad \theta_N\right]^T\end{gathered} \tag{5.1-3}$$

Equation (5.1-1) reads

$$u_n(x, y_L) = \left[B(y_L)\right]([b] - x[\theta]). \tag{5.1-4}$$

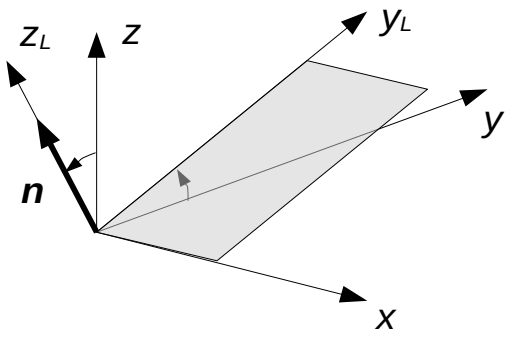


Figure 5.1-1: Lifting Surface Coordinate System

Matrices $[b]$ and $[\theta]$ are determined so that the structural displacements are best approximated in the sense of least squared errors.

Let $\boldsymbol{u_k}=\boldsymbol{u}(x_k, y_{Lk}, z_{Lk})$ be the displacements at K nodal points of the solid model. Then, matrices $[b]$ and $[\theta]$ are determined from

$$\sum_k \left(\boldsymbol{u_k}\cdot\boldsymbol{n}-u_n(x_k, y_{Lk})\right)^2=\text{Min}. \tag{5.1-5}$$

With the matrices

$$[u^S]_L=\begin{bmatrix}\boldsymbol{n}\cdot\boldsymbol{u_1}\\ \vdots\\ \boldsymbol{n}\cdot\boldsymbol{u_K}\end{bmatrix},\quad [H^S]=\begin{bmatrix}[B(y_{L1})] & -x_1[B(y_{L1})]\\ \vdots & \vdots\\ [B(y_{LK})] & -x_K[B(y_{LK})]\end{bmatrix},\quad [h]=\begin{bmatrix}[b]\\ [\theta]\end{bmatrix} \tag{5.1-6}$$

Equation (5.1-5) reads

$$\left([u^S]_L-[H^S][h]\right)^T\left([u^S]_L-[H^S][h]\right)=\text{Min}. \tag{5.1-7}$$

which is equivalent to

$$[H^S]^T[H^S][h]=[H^S]^T[u^S]_L. \tag{5.1-8}$$

With the QR-decomposition

$$[H^S]=[Q_H][R_H] \tag{5.1-9}$$

the solution of Equation (5.1-8) is

$$[h]=[R_H]^{-1}[Q_H]^T[u^S]_L. \tag{5.1-10}$$

Now, let $[a^S]$ be a Boolean matrix that extracts the displacements of those nodal points of the solid model that are involved in the spline from the matrix of all solid displacements, and

$$[P]=\begin{bmatrix}[\boldsymbol{n}]^T & \cdots & [0]\\ \vdots & \ddots & \vdots\\ [0] & \cdots & [\boldsymbol{n}]^T\end{bmatrix} \tag{5.1-11}$$

the projection matrix normal to the lifting surface. Then,

$$[u^S]_L=[P][a^S][u_G] \tag{5.1-12}$$

where matrix $[u_G]$ contains the displacements of all nodal points of the solid model. With the spline matrix

$$[S_{hG}]=[R_H]^{-1}[Q_H]^T[P][a^S] \tag{5.1-13}$$

the spline coefficients are related to the solid displacements by

$$[h]=[S_{hG}][u_G]. \tag{5.1-14}$$

According to Equation (4.2-6), the normal wash at control point m due to the

elastic deformation is

$$\frac{w_m^E}{v_\infty}=\frac{\partial\left(\boldsymbol{n}\cdot\boldsymbol{u}_{Cm}\right)}{\partial x}=\frac{\partial u_n}{\partial x}(x_{Cm},y_{LCm})=-\left[B(y_{LCm})\right][\theta]. \tag{5.1-15}$$

With the matrices

$$\left[w^E\right]_L=\frac{1}{v_\infty}\begin{bmatrix}w_1^E\\ \vdots\\ w_M^E\end{bmatrix},\quad \left[D_h^1\right]=\begin{bmatrix}[0] & -\left[B(y_{LC1})\right]\\ \vdots & \vdots\\ [0] & -\left[B(y_{LCM})\right]\end{bmatrix} \tag{5.1-16}$$

Equation (5.1-15) reads

$$\left[w^E\right]_L=\left[D_h^1\right][h]\ . \tag{5.1-17}$$

For unsteady problems, the complex normal wash is obtained from

$$\left[W^E\right]_L=\left(\left[D_h^1\right]+2\,i\,k\left[D_h^2\right]\right)[H] \tag{5.1-18}$$

where matrix [H] contains the complex spline coefficients, k is the reduced frequency and matrix

$$\left[D_h^2\right]=\frac{1}{c_{ref}}\begin{bmatrix}\left[B(y_{L1})\right] & -x_1\left[B(y_{L1})\right]\\ \vdots & \vdots\\ \left[B(y_{LN})\right] & -x_N\left[B(y_{LN})\right]\end{bmatrix} \tag{5.1-19}$$

relates the displacements at the control points normal to the lifting surface to the spline coefficients.

The virtual work of the aerodynamic loads on the aerodynamic model must be the same as the virtual work of the aerodynamic loads on the structural model:

$$\left[\widetilde{u}_V\right]_L^T\left[l_V^A\right]_L=\left[\widetilde{u}_G\right]^T\left[l_G^A\right] \tag{5.1-20}$$

Matrix $\left[\widetilde{u}_V\right]_L$ contains the virtual displacements of the vortex points, i.e. the mid points of the bound vortices of the horseshoe vortices, in the local coordinate system of the lifting surface, matrix $\left[\widetilde{u}_G\right]$ contains the virtual displacements of the nodal points of the solid model, matrix $\left[l_V^A\right]_L$ contains the aerodynamic loads at the vortex points with respect to the local coordinate system of the lifting surface, and matrix $\left[l_G^A\right]$ contains the aerodynamic loads at the nodal points of the solid model.

The virtual displacements of the vortex points are related to the virtual spline coefficients $\left[\widetilde{h}\right]$ by

$$[\tilde{u}_V]_L = [S_{Vh}][\tilde{h}] \tag{5.1-21}$$

where

$$[S_{Vh}] = [H^V] = \begin{bmatrix} [B(y_{LV1})] & -x_1[B(y_{LV1})] \\ \vdots & \vdots \\ [B(y_{LVM})] & -x_M[B(y_{LVM})] \end{bmatrix} \tag{5.1-22}$$

and

$$[\tilde{h}] = [S_{hG}][\tilde{u}_G]. \tag{5.1-23}$$

Inserting of Equations (5.1-21) and (5.1-23) into Equation (5.1-20) yields

$$[\tilde{u}_G]^T [S_{hG}]^T [S_{Vh}]^T [l_V^A]_L = [\tilde{u}_G]^T [l_G^A] \quad \forall [\tilde{u}_G]. \tag{5.1-24}$$

Thus, the aerodynamic loads on the solid model can be computed from

$$[l_G^A] = [S_{hG}]^T [S_{Vh}]^T [l_V^A]_L. \tag{5.1-25}$$

Mefisto computes and stores the matrices $[S_{hG}]$, $[S_{Vh}]$, $[D^1{}_h]$ and $[D^2{}_h]$ as well as matrix $[S_{nh}]$ which can be used to compute the displacements at the panel corner nodes. Because the number of spline coefficients is usually small, the size of these matrices is small.

5.2 Steady Aerodynamic Matrices

The aerodynamic loads depend on the camber and the rigging angle of incidence, on the configuration parameters and on the elastic deformation. For small perturbations, this dependence is linear and is expressed using the aerodynamic matrices:

$$[l_G^A] = q_\infty \left([q_G^0] + [Q_G^K][u^K] + [Q_{GG}][u_G] \right) \tag{5.2-1}$$

- Matrix $[q_G^0]$ contains the aerodynamic loads on the solid due to the camber and the rigging angle of incidence.
- Matrix $[Q_G^K]$ relates the configuration parameters $[u^K]$ to the aerodynamic loads on the solid.
- Matrix $[Q_{GG}]$ relates the elastic displacements of the solid to the aerodynamic loads on the solid.

The aerodynamic loads are computed from the normal wash using the equations of the Vortex Lattice Method. In the lifting surface coordinate system, the normal wash reads

$$[w]_L = [w_0]_L + [D_K^1][u^K] + [D_G^1][u_G] \tag{5.2-2}$$

where $[w_0]_L$ is the normal wash due to the camber and the rigging angle of incidence, matrix $[D_K^1]$ computes the contribution of the configuration parameters, and matrix $[D_G^1]$ computes the contribution of the elastic deformation to the normal wash.

Matrix $[w_0]_L$ reads (cf. Equation (4.2-6))

$$[w_0]_L = \begin{bmatrix} \frac{d\zeta_S}{dx}(x_{C1}, y_{LC1}) - \alpha_{i1} \\ \vdots \\ \frac{d\zeta_S}{dx}(x_{CN}, y_{LCN}) - \alpha_{iN} \end{bmatrix} \tag{5.2-3}$$

where $\zeta_S(x,\ y_L)$ describes the camber in the lifting surface coordinate system, N is the number of panels and α_{in} is the rigging angle of incidence of panel n.

The entries of matrix $[D_K^1]$ are defined as follows (cf. Equations (4.2-6) and (4.2-7)):

- Angle of attack α: $-\boldsymbol{e}_z \cdot \boldsymbol{n} = -n_z$
- Sideslip angle β: $-\boldsymbol{e}_y \cdot \boldsymbol{n} = -n_y$
- Roll rate p: $(y_C - y_R) n_z - (z_C - z_R) n_y$
- Pitch rate q: $(z_C - z_R) n_x - (x_C - x_R) n_z$
- Yaw rate r: $(x_C - x_R) n_y - (y_C - y_R) n_x$
- Control surfaces: $-f$

x_R, y_R and z_R are the coordinates of the reference point for the rigid body motion, and f is the control surface factor as defined in the input data.

Matrix $[D_G^1]$ is computed from the spline matrices:

$$[D_G^1] = [D_h^1][S_{hG}] \tag{5.2-4}$$

Matrix

$$[\Gamma] = \frac{1}{v_\infty}[\Gamma_1 \quad \cdots \quad \Gamma_N]^T \tag{5.2-5}$$

containing the vortex strengths is computed from the normal wash by solving the system of equations

$$[C][\Gamma] = [w]_L \tag{5.2-6}$$

where

$$[C]=\begin{bmatrix} \boldsymbol{v}_{11}\cdot\boldsymbol{n}_1 & \cdots & \boldsymbol{v}_{1N}\cdot\boldsymbol{n}_1 \\ \vdots & \ddots & \vdots \\ \boldsymbol{v}_{N1}\cdot\boldsymbol{n}_N & \cdots & \boldsymbol{v}_{NN}\cdot\boldsymbol{n}_N \end{bmatrix} \tag{5.2-7}$$

(cf. Equation (4.2-9)).

The aerodynamic force on one panel is obtained from

$$L_n=2\,q_\infty\left(y_{LBn}-y_{LAn}\right)\frac{\Gamma_n}{v_\infty} \tag{5.2-8}$$

(cf. Equation (4.2-14)).The aerodynamic force is perpendicular to the lifting surface, i.e. the other two components are zero. Thus, in the lifting surface coordinate system, the matrix of aerodynamic loads is given by

$$\left[l_V^A\right]_L=2\,q_\infty\begin{bmatrix} \left(y_{LB1}-y_{LA1}\right)\Gamma_1/v_\infty \\ \vdots \\ \left(y_{LBN}-y_{LAN}\right)\Gamma_N/v_\infty \end{bmatrix}=q_\infty[G][\Gamma] \tag{5.2-9}$$

with

$$[G]=2\begin{bmatrix} y_{LB1}-y_{LA1} & \cdots & 0 \\ \vdots & \ddots & \vdots \\ 0 & \cdots & y_{LBN}-y_{LBN} \end{bmatrix}. \tag{5.2-10}$$

By combining the equations, the following equations are obtained to compute the aerodynamic matrices:

$$\begin{aligned} \left[q_G^0\right]&=\left[S_{hG}\right]^T\left[S_{Vh}\right]^T[G][C]^{-1}\left[w_0\right]_L \\ \left[Q_G^K\right]&=\left[S_{hG}\right]^T\left[S_{Vh}\right]^T[G][C]^{-1}\left[D_K^1\right] \\ \left[Q_{GG}\right]&=\left[S_{hG}\right]^T\left[S_{Vh}\right]^T[G][C]^{-1}\left[D_G^1\right] \end{aligned} \tag{5.2-11}$$

The matrices are computed as follows:

(1) $\left[\left[q_h^0\right]\ \left[Q_h^K\right]\ \left[Q_{hh}\right]\right]=\left(\left[S_{vh}\right]^T[G]\right)[C]^{-1}\left[\left[w_0\right]_L\ \left[D_K^1\right]\ \left[D_h^1\right]\right]$

(2) $\left[\left[q_G^0\right]\ \left[Q_G^K\right]\right]=\left[S_{hG}\right]^T\left[\left[q_h^0\right]\ \left[Q_h^K\right]\right]$

(3) $\left[Q_{GG}\right]=\left[S_{hG}\right]^T\left[Q_{hh}\right]\left[S_{hG}\right]$

5.3 Static Response

In a static response analysis, all configuration parameters are specified by the user. The analysis determines the deformation of the solid and the vortex strengths. From these primary results, secondary results like stresses and aerodynamic pressure can be computed. The solid is assumed to be constrained so that rigid body motions are prevented.

The equation to be solved is

$$[K_{LL}][u_L]=[l_L^A]. \tag{5.3-1}$$

With

$$[l_L^A]=q_\infty\left([q_L^0]+[Q_L^K][u^K]+[Q_{LL}][u_L]\right) \tag{5.3-2}$$

Equation (5.3-1) reads

$$\left([K_{LL}]-q_\infty[Q_{LL}]\right)[u_L]=q_\infty\left([q_L^0]+[Q_L^K][u^K]\right) \tag{5.3-3}$$

or

$$\left([I_{LL}]-q_\infty[K_{LL}]^{-1}[Q_{LL}]\right)[u_L]=q_\infty[K_{LL}]^{-1}\left([q_L^0]+[Q_L^K][u^K]\right) \tag{5.3-4}$$

where $[I_{LL}]$ is the unit matrix.

With

$$[u_L^0]=q_\infty[K_{LL}]^{-1}\left([q_L^0]+[Q_L^K][u^K]\right) \tag{5.3-5}$$

and

$$[K_{LL}]^{-1}[Q_{LL}]=[K_{LL}]^{-1}[S_{hL}]^T[Q_{hh}][S_{hl}]=[Q_{Lh}][S_{hL}] \tag{5.3-6}$$

(cf. Section 5.2) where

$$[Q_{Lh}]=[K_{LL}]^{-1}[S_{hL}]^T[Q_{hh}] \tag{5.3-7}$$

Equation (5.3-4) reads

$$\left([I_{LL}]-q_\infty[Q_{Lh}][S_{hL}]\right)[u_L]=[u_L^0] \quad . \tag{5.3-8}$$

Equation (5.3-8) can be solved efficiently using the Frobenius-Schur-Woodbury identity (see e.g. [Falk, 1984])

$$\left([I_{LL}]-q_\infty[Q_{Lh}][S_{hL}]\right)^{-1}=[I_{LL}]+q_\infty[Q_{Lh}][R_{hh}]^{-1}[S_{hL}] \tag{5.3-9}$$

where

$$[R_{hh}]=[I_{hh}]-q_\infty[S_{hL}][Q_{Lh}] \quad . \tag{5.3-10}$$

The solution is

$$[u_L]=[u_L^0]+q_\infty[Q_{Lh}][R_{hh}]^{-1}[S_{hL}][u_L^0] \quad . \tag{5.3-11}$$

Alternatively, Equation (5.3-8) can be solved iteratively using a biconjugate gradient method (see e.g. [Saad, 2003]).

Once the displacements $[u_L]$ have been calculated, the vortices can be determined from

$$[C][\Gamma]=[w_0]_L+[D_K^1][u^K]+[D_L^1][u_L] \tag{5.3-12}$$

(cf. Equations (5.2-2) and (5.2-6)).

5.4 Static Divergence

If the matrix on the left hand side of Equation (5.3-3) is singular, there is no unique solution of this equation. This is equivalent to equation

$$\left([K_{LL}]-q_\infty[Q_{LL}]\right)[u_L]=[0] \tag{5.4-1}$$

having non-trivial solutions. Equation (5.4-1) is a non-symmetric linear eigenvalue problem. Its lowest positive real eigenvalue is the dynamic pressure at which static divergence occurs. Negative real eigenvalues and complex eigenvalues have no physical meaning.

5.5 Trim Analysis

The linear equation of motion of the flexible aircraft reads

$$[M_{GG}][\ddot{u}_G]+[D_{GG}][\dot{u}_G]+[K_{GG}][u_G]=\left[l_G^0\right]+\left[l_G^A\right]. \tag{5.5-1}$$

The first term on the left side of this equation describes the inertia loads, the second the damping loads and the third the elastic loads. The first term on the right side describes the loads that do not depend on the aerodynamics, and the second the aerodynamic loads.

The displacements can be subdivided into a rigid body motion $\left[u_G^R\right]$ and an elastic deformation $\left[u_G^E\right]$ relative to the rigid body motion:

$$[u_G]=\left[u_G^R\right]+\left[u_G^E\right] \tag{5.5-2}$$

In a trim analysis, the elastic loads as well as the aerodynamic loads are assumed to be constant in time. Consequently, the elastic deformation must be constant in time. Thus,

$$[\dot{u}_G]=\left[\dot{u}_G^R\right],\ \ [\ddot{u}_G]=\left[\ddot{u}_G^R\right]. \tag{5.5-3}$$

With

$$[D_{GG}]\left[\dot{u}_G^R\right]=[0],\ \ [K_{GG}]\left[u_G^R\right]=[0] \tag{5.5-4}$$

and

$$\left[\ddot{u}_G^R\right]=[R_G]\left[a^R\right] \tag{5.5-5}$$

(cf. Section 4.3) Equation (5.5-1) reads

$$\left([K_{GG}]-q_\infty[Q_{GG}]\right)\left[u_G^E\right]=\left[l_G^0\right]-[M_{GG}][R_G]\left[a^R\right]+q_\infty\left(\left[q_G^0\right]+\left[Q_G^K\right]\left[u^K\right]\right) \tag{5.5-6}$$

where Equation (5.2-1) has been used for the aerodynamic loads. The influence of the rigid body motion on the aerodynamic loads is included in the

configuration parameters, i.e. the angle of attack and the sideslip angle.

In Equation (5.5-6), apart from the elastic displacements, also six of the trim parameters are unknown.

An additional set of six equations is obtained by projecting Equation (5.5-6) onto the rigid body motion:

$$[M_{RR}][a^R]-q_\infty[R_G]^T\left([Q_G^K][u^K]+[Q_{GG}][u_G^E]\right)=[R_G]^T\left([l_G^0]+q_\infty[q_G^0]\right) \tag{5.5-7}$$

In contrast to the rigid trim equation (4.3-4), Equation (5.5-7) also contains the elastic displacements and hence can be solved only together with Equation (5.5-6).

5.5.1 Restrained Trim Analysis

The subdivision of the motion into a rigid body motion and an elastic deformation is not unique. The elastic deformation is the motion relative to a coordinate system that follows the rigid body motion.

In a restrained analysis, the elastic deformation is relative to a restrained coordinate system that is rigidly connected to the aircraft at six degrees of freedom. These degrees of freedom have to be selected such that they define statically determinate supports, preventing rigid body motions. The elastic deformation at these degrees of freedom is zero.

Let subscript *L* denote the remaining local degrees of freedom. Then, Equation (5.5-6) reads

$$\left([K_{LL}]-q_\infty[Q_{LL}]\right)[u_L^E]_R=[l_L^0]-[M_{LG}][R_G][a^R]+q_\infty\left([q_L^0]+[Q_L^K][u^K]\right) \tag{5.5-8}$$

The subscript *R* of matrix $[u_L^E]_R$ indicates that this matrix contains the components of the elastic deformation relative to a restrained coordinate system.

Unless in case of static divergence (cf. Section 5.4), the matrix on the left side is invertible. Thus, the elastic displacements can be computed from

$$[u_L^E]_R=\left([K_{LL}]-q_\infty[Q_{LL}]\right)^{-1}\left([l_L^0]-[M_{LG}][R_G][a^R]+q_\infty\left([q_L^0]+[Q_L^K][u^K]\right)\right). \tag{5.5-9}$$

With

$$[u_L^0]=\left([K_{LL}]-q_\infty[Q_{LL}]\right)^{-1}\left([l_L^0]+q_\infty[q_L^0]\right) \tag{5.5-10}$$

and

$$[U_{LT}]=\left([K_{LL}]-q_\infty[Q_{LL}]\right)^{-1}\left[[M_{LG}][R_G] \quad -q_\infty[Q_L^K]\right] \tag{5.5-11}$$

the elastic deformation can be written as

$$[u_L^E]_R=[u_L^0]-[U_{LT}][t] \tag{5.5-12}$$

where matrix $[t]$ contains the trim parameters (see Equation (4.3-1)).

Equations (5.5-10) and (5.5-11) can be evaluated efficiently using the Frobenius-Schur-Woodbury identity (see e.g. [Falk, 1984]). With

$$[Q_{Lh}]=[K_{LL}]^{-1}[S_{hL}]^T[Q_{hL}] \tag{5.5-13}$$

the inverse matrix reads

$$\left([K_{LL}]-q_\infty[Q_{LL}]\right)^{-1}=\left([I_{LL}]+q_\infty[Q_{Lh}][R_{hh}]^{-1}[S_{hL}]\right)[K_{LL}]^{-1} \tag{5.5-14}$$

where

$$[R_{hh}]=[I_{hh}]-q_\infty[S_{hL}][Q_{Lh}] \tag{5.5-15}$$

(cf. Section 5.3).

Inserting of Equation (5.5-12) into the trim equation (5.5-7) yields

$$\begin{aligned}[M_{RR}][a^R]-q_\infty[R_G]^T[Q_G^K][u^K]+q_\infty[R_G]^T[Q_{GL}][U_{LT}][t]\\ =[R_G]^T\left([l_G^0]+q_\infty\left([q_G^0]+[Q_{GL}][u_L^0]\right)\right).\end{aligned} \tag{5.5-16}$$

With the flexible trim matrix

$$[T^F]=\left[[M_{RR}] \quad -q_\infty[R_G]^T[Q_G^K]\right]+q_\infty[R_G]^T[Q_{GL}][U_{LT}] \tag{5.5-17}$$

Equation (5.1-13) reads

$$[T^F][t]=[R_G]^T\left([l_G^0]+q_\infty\left([q_G^0]+[Q_{GL}][u_L^0]\right)\right). \tag{5.5-18}$$

This system of six equations can be solved for six of the trim parameters. As in case of a rigid trim analysis, the values of the remaining trim parameters must be specified. They define the manoeuvre to be analysed.

5.5.2 Unrestrained Trim Analysis

In an unrestrained trim analysis, the elastic deformation is relative to the mean axis system. The mean axis system has its origin at the centre of mass of the deformed aircraft and rotates with the principal axes of inertia. This is equivalent to the constraint

$$[R_G]^T[M_{GG}][u_G^E]_M=[0]. \tag{5.5-19}$$

The subscript *M* of matrix $[u_G^E]_M$ indicates that this matrix contains the components of the elastic deformation relative to the mean axis system.

The elastic deformation relative to the mean axis system differs from that relative to a restrained coordinate system by a rigid body motion only. Thus,

$$[u_G^E]_M=[u_G^E]_R+[R_G][q_R] \tag{5.5-20}$$

where matrix $[q_R]$ contains the six rigid body coordinates. The rigid body coordinates can be obtained from Equation (5.5-19):

$$[q_R] = -[M_{RR}]^{-1}[R_G]^T[M_{GL}]\left[u_L^E\right]_R \tag{5.5-21}$$

Inserting of

$$\left[u_G^E\right]_M = \begin{bmatrix}\left[u_L^E\right]_R \\ [0]\end{bmatrix} - [R_G][M_{RR}][R_G]^T[M_{GL}]\left[u_L^E\right]_R \tag{5.5-22}$$

into the trim equation (5.5-7) yields

$$[M_{RR}]\left[a^R\right] - q_\infty[R_G]^T\left[Q_G^K\right][u^K] = [R_G]^T\left(\left[l_G^0\right] + q_\infty\left(\left[q_G^0\right] + [Q_{GG}]\left[u_G^E\right]_M\right)\right). \tag{5.5-23}$$

With the trim matrix

$$[T] = \left[[M_{RR}] \quad -q_\infty[R_G]^T\left[Q_G^K\right]\right] \tag{5.5-24}$$

the trim equation reads

$$[T][t] = [R_G]^T\left(\left[l_G^0\right] + q_\infty\left(\left[q_G^0\right] + [Q_{GG}]\left[u_G^E\right]_M\right)\right) \tag{5.5-25}$$

which can be solved for six of the trim parameters.

The elastic deformation, the angle of attack and the sideslip angle depend on the coordinate system used. All other results are independent of the coordinate system.

5.6 Unsteady Aerodynamic Matrices

In the following, it is assumed that the time dependence is harmonic and described in complex notation.

The complex normal wash is

$$[W]_L = \left(\left[D_h^1\right] + 2\,i\,k\left[D_h^2\right]\right)[S_{hG}][U_G] + \left(\left[D_K^1\right] + 2\,i\,k\left[D_K^2\right]\right)\left[U^K\right] \quad . \tag{5.6-1}$$

The reduced frequency k is defined in Section 4.1.2. Matrices $\left[D_h^1\right]$, $\left[D_h^2\right]$ and $\left[S_{hG}\right]$ are defined in Section 5.1. Matrix $\left[D_K^1\right]$ is defined in Section 5.2. Matrix $\left[D_K^2\right]$ computes the vertical displacements normal to the lifting surface, scaled by the reference length c_{ref}, at the control points. Matrix $\left[U_G\right]$ contains the complex displacements and matrix $\left[U^K\right]$ the complex configuration parameters.

With the vortex strengths

$$[\hat{\Gamma}] = \left[C^u(k)\right]^{-1}[W]_L \tag{5.6-2}$$

(cf. Equations (4.2-38) and (4.2-39)) and the aerodynamic forces at the vortex

points

$$\left[L_V^A\right]_L = q_\infty \left(\left[G^1\right] + ik\left[G^2\right]\right)\left[\hat{\Gamma}\right] \tag{5.6-3}$$

(cf. Equation (4.2-43)), the aerodynamic loads on the solid model are given by

$$\begin{aligned}\left[L_G^A\right] = q_\infty \left[S_{hG}\right]^T \left[S_{Vh}\right]^T \left(\left[G^1\right] + ik\left[G^2\right]\right)\left[C(k)\right]^{-1} \\ \cdot \left(\left(\left[D_h^1\right] + 2ik\left[D_h^2\right]\right)\left[S_{hG}\right]\left[U_G\right] + \left(\left[D_K^1\right] + 2ik\left[D_K^2\right]\right)\left[U^K\right]\right) \quad .\end{aligned} \tag{5.6-4}$$

With the matrices

$$\begin{aligned}\left[Q_{GG}(k)\right] &= \left[S_{hG}\right]^T \left[S_{Vh}\right]^T \left(\left[G^1\right] + ik\left[G^2\right]\right)\left[C(k)\right]^{-1} \left(\left[D_h^1\right] + 2ik\left[D_h^2\right]\right)\left[S_{hG}\right] \\ \left[Q_G^K(k)\right] &= \left[S_{hG}\right]^T \left[S_{Vh}\right]^T \left(\left[G^1\right] + ik\left[G^2\right]\right)\left[C(k)\right]^{-1} \left(\left[D_K^1\right] + 2ik\left[D_K^2\right]\right)\end{aligned} \tag{5.6-5}$$

Equation (5.6-4) reads

$$\left[L_G^A\right] = q_\infty \left(\left[Q_{GG}(k)\right]\left[U_G\right] + \left[Q_G^K(k)\right]\left[U^K\right]\right) \quad . \tag{5.6-6}$$

5.7 Flutter Analysis

Flutter is a dynamic instability. A small perturbation of the equilibrium is increased by the aerodynamic loads. This increase may or may not be limited by nonlinear effects.

A linear flutter analysis can predict the velocity at which instability occurs, but it can not predict whether the increase is limited or not.

5.7.1 The Flutter Equation

If there is no external excitation and damping is neglected, Equation (5.5-1) reads

$$\left[M_{GG}\right]\left[\ddot{u}_G\right] + \left[D_{GG}\right]\left[\dot{u}_G\right] + \left[K_{GG}\right]\left[u_G\right] = \left[l_G^A\right]. \tag{5.7-1}$$

where matrix $\left[l_G^A\right]$ includes the aerodynamic loads due to the elastic deformation only. Matrix $\left[u_G\right]$ contains the displacements relative to the static equilibrium. With the ansatz

$$\left[u_G(t)\right] = \left[U_G\right] e^{\lambda t} \tag{5.7-2}$$

the dynamic equation of the aeroelastic system reads

$$\left(\lambda^2\left[M_{GG}\right] + \left[K_{GG}\right] - q_\infty\left[Q_{GG}(\lambda)\right]\right)\left[U_G\right] = \left[0\right] \quad . \tag{5.7-3}$$

This is a nonlinear eigenvalue problem the solution of which yields the complex eigenvalues λ_n at which Equation (5.7-3) has non-trivial solutions $[U_{Gn}]$. Eigenvalues with a positive real part indicate instability.

Like in modal frequency response analysis (cf. Section 2.4.2) the displacements $[U_G]$ are approximated by a linear combination of eigenvectors,

$$[U_G] \approx [X^p][U]_p \quad . \tag{5.7-4}$$

The modal reduction leads to

$$\left(\lambda^2[M]_p + [K]_p - q_\infty [Q(\lambda)]_p\right)[U]_p = [0] \tag{5.7-5}$$

with the modal matrices

$$\begin{gathered}[K]_p = [X^p]^T [K][X^p], \quad [M]_p = [X^p]^T [M][X^p] \\ [Q(\lambda)]_p = [X^p]^T [Q(\lambda)][X^p]\end{gathered} \tag{5.7-6}$$

Normal modes for which

$$[X^p]^T [Q(\lambda)][x_n] = [0] \tag{5.7-7}$$

are not included in the modal reduction. They are identified by inspecting the columns of matrix

$$[T] = [X^p]^T [S_{hG}]^T [S_{Vh}]^T \left([G^1] + i[G^2]\right)\left([D_h^1] + 2i[D_h^2]\right)[S_{hG}][X^p] \quad . \tag{5.7-8}$$

5.7.2 The k-Method

In the k-method, an additional term is added to Equation (5.7-5) such that the eigenvalues are purely imaginary. With $\lambda = i\omega$ the modified equation reads

$$\left(-\omega^2[M]_p - q_\infty [Q(i\omega)]_p + (1 + i\gamma)[K]_p\right)[U]_p = [0] \quad . \tag{5.7-9}$$

The factor γ can be interpreted as a structural loss factor. For $\gamma < 0$ energy is added to the system and for $\gamma > 0$ energy is extracted.

The factor γ is part of the solution. The system is stable for $\gamma < 0$ and unstable for $\gamma > 0$.

With $\omega = 2 v_\infty k / c_{ref}$ and $q_\infty = \rho v_\infty^2 / 2$, Equation (5.7-9) reads

$$\left([K]_p - \frac{v_\infty^2}{1 + i\gamma}\left(4\frac{k^2}{c_{ref}^2}[M]_p + \frac{\rho}{2}[Q(k)]_p\right)\right)[U]_p = [0] \quad . \tag{5.7-10}$$

For given values of k and ρ, this is a linear eigenvalue problem with eigenvalue

$$\mu = \frac{v_\infty^2}{1 + i\gamma} \quad . \tag{5.7-11}$$

The GNU Octave function **`eig`** is used to solve the eigenvalue problem (5.7-10). Subsequently, the velocity and the loss factor can be computed from

$$\gamma = -\frac{\Im(\mu)}{\Re(\mu)} \tag{5.7-12}$$

and

$$v_\infty = \sqrt{\frac{\Re^2(\mu)+\Im^2(\mu)}{\Re(\mu)}} \quad . \tag{5.7-13}$$

The structural loss factor can be plotted versus the reduced frequency k or versus the velocity v_∞ to find the zero crossings indicating the transition from stable to unstable or from unstable to stable.

For each reduced frequency, the solution of the eigenvalue problem yields p eigenvalues where p is the number of normal modes used in the modal reduction. To decide to which curve the different values belong, mode tracking is performed using the MAC values of the complex eigenvectors.

5.7.3 The pk-Method

In contrast to the k-method, the pk-method processes a list of velocities. The eigenvalue problem (5.7-5) is transformed into an eigenvalue problem with real matrices.

With

$$\left[Q^R(\lambda)\right]_p = \Re\left[Q(\lambda)\right]_p, \quad \left[Q^I(\lambda)\right]_p = \Im\left[Q(\lambda)\right]_p \tag{5.7-14}$$

the eigenvalue problem reads

$$\left(\lambda^2[M]_p - i\,q_\infty\left[Q^I(\lambda)\right]_p + [K]_p - q_\infty\left[Q^R(\lambda)\right]_p\right)[U]_p = [0] \quad . \tag{5.7-15}$$

The complex eigenvalues are

$$\lambda_n = a_n + i\,\omega_n \quad . \tag{5.7-16}$$

Positive values of the real part a_n indicate instability and negative values stability. When the real part is plotted versus the velocity, the zero crossings indicate transition from stability to instability or vice versa.

As the main interest is to find the zero crossings, the aerodynamic matrix is computed for $\lambda = i\,\omega$. With $i = \lambda/\omega$, which is true for $a_n = 0$, Equation (5.7-15) reads

$$\left(\lambda^2[M]_p - \lambda\,\frac{q_\infty}{\omega}\left[Q^I(i\,\omega)\right]_p + [K]_p - q_\infty\left[Q^R(i\,\omega)\right]_p\right)[U]_p = [0] \quad . \tag{5.7-17}$$

With

$$\omega = 2\,v_\infty\,k/c_{ref}$$

the following quadratic eigenvalue problem for λ is obtained:

$$\left(\lambda^2[M]_p-\lambda\frac{q_\infty c_{ref}}{2v_\infty}\frac{1}{k}\left[Q^I(k)\right]_p+[K]_p-q_\infty\left[Q^R(k)\right]_p\right)[U]_p=[0] \quad . \tag{5.7-18}$$

Finally, the substitution

$$[V]_p=-\lambda[M]_p[U]_p$$

leads to the linear eigenvalue problem

$$\begin{bmatrix}[0]_p & -[M]_p^{-1}\\ [K]_p-q_\infty\left[Q^R(k)\right]_p & \frac{q_\infty c_{ref}}{2v_\infty}\frac{1}{k}\left[Q^I(k)\right]_p[M]_p^{-1}\end{bmatrix}\begin{bmatrix}[U]_p\\ [V]_p\end{bmatrix}=\lambda\begin{bmatrix}[U]_p\\ [V]_p\end{bmatrix} \quad . \tag{5.7-19}$$

This eigenvalue problem is solved for given values of v_∞ and ρ (GNU Octave function **`eig`**). The $2p$ eigenvalues of this real unsymmetric eigenvalue problem are either real or complex conjugate pairs.

Initial guesses of the reduced frequencies are obtained from the circular eigenfrequencies of the solid structure:

$$k_m^{(0)}=\frac{\omega_m c_{ref}}{2v_\infty}$$

Subsequently, for each velocity (index n) and each flutter mode pair requested (index m), iterations are required to match the reduced frequencies k at which the aerodynamic matrix is computed with the reduced frequencies obtained from the eigenvalues.

The iteration steps are (iteration index l starts with $l=0$):

1) Compute $\left[Q\left(k_{mn}^{(l)}\right)\right]$ and solve the eigenvalue problem (5.7-19). Sort the eigenvalues according to ascending $\left|\Im\left(\lambda_{mn}^{(l)}\right)\right|$.

2) Compute reduced frequencies from eigenvalues: $k_{mn}^{(l+1)}=\dfrac{\Im\left(\lambda^{(l)}\right)c_{ref}}{2v_n}$

3) Check convergence: $\left|k_{mn}^{(l+1)}-k_{mn}^{(l)}\right|<k_{tol}$?

   a) If convergence has been achieved,

      1. store the results and set $k_{mn}=k_{mn}^{(l+1)}$.
      2. continue with the next pair of eigenvalues.

   b) If convergence has not been achieved,

      1. If $l>0$, obtain an improved guess of $k_{mn}^{(l+1)}$ from linear interpolation or extrapolation:

$$m_k=\frac{k_{mn}^{(l+1)}-k_{mn}^{(l)}}{k_{mn}^{(l)}-k_{mn}^{(l-1)}},\quad k_{mn}^{(l+1)}=\frac{k_{mn}^{(l)}-m_k k_{mn}^{(l-1)}}{1-m_k}$$

2. increment iteration index l and continue with step 1).

When the reduced frequencies of all flutter mode pairs requested at the current velocity have converged, initial guesses for the next velocity are obtained from

$$k_{mn+1}^{(0)} = k_{mn} \frac{v_n}{v_{n+1}} \ .$$

The value of the tolerance k_{tol} is defined in **`opts.tol`**. The default value is 10^{-3}.

The case $k = 0$ needs special consideration. With

$$\left[S^1\right]_p = \left[X^p\right]^T \left[S_{hG}\right]^T \left[S_{Vh}\right]^T \left[G^1\right], \ \left[S^2\right]_p = \left[X^p\right]^T \left[S_{hG}\right]^T \left[S_{Vh}\right]^T \left[G^2\right] \tag{5.7-20}$$

and

$$\left[D^1\right]_p = \left[D_h^1\right] \left[S_{hG}\right] \left[X^p\right], \ \left[D^2\right]_p = 2 \left[D_h^2\right] \left[S_{hG}\right] \left[X^p\right] \tag{5.7-21}$$

the modal aerodynamic matrix reads (cf. Equation (5.6-5))

$$\begin{aligned} \left[Q(k)\right]_p &= \left(\left[S^1\right]_p + i\,k \left[S^2\right]_p\right) \left[C(k)\right]^{-1} \left(\left[D^1\right]_p + i\,k \left[D^2\right]_p\right) \\ &= \left[S^1\right]_p \left[C(k)\right]^{-1} \left[D^1\right]_p - 2\,k^2 \left[S^2\right]_p \left[C(k)\right]^{-1} \left[D^2\right]_p \\ &\quad + i\,k \left(\left[S^1\right]_p \left[C(k)\right]^{-1} \left[D^2\right]_p + \left[S^2\right]_p \left[C(k)\right]^{-1} \left[D^1\right]_p\right) \ . \end{aligned}$$

Thus, because $[C(0)]$ is real,

$$\lim_{k \to 0} \frac{1}{k} \left[Q^I(k)\right]_p = \left[S^1\right]_p \left[C(0)\right]^{-1} \left[D^2\right]_p + \left[S^2\right]_p \left[C(0)\right]^{-1} \left[D^1\right]_p \ . \tag{5.7-22}$$

Equation (5.7-22) is used whenever $k <$ **`eps`** where **`eps`** is the machine precision returned by GNU Octave.

5.8 Frequency Response

The objective of a frequency response analysis is to determine the response to a time-harmonic excitation. The excitation may be an applied load, a gust or a prescribed motion of a control surface. Excitation by applied loads has not yet been implemented in Mefisto. The result of a frequency response analysis are frequency dependent transfer functions. Once these transfer functions are known, it is easy to compute the response to arbitrary transient gusts or control surface deflections as well as the response to atmospheric turbulence.

The complex deformation $\left[U_G\right]$ due to a time-harmonic excitation is obtained from

$$\left(-\Omega^2[M_{GG}]+i\,\Omega[D_{GG}]+[K_{GG}]-q_\infty\left[Q_{GG}(k)\right]\right)[U_G]=q_\infty\left[Q_G^K(k)\right]\left[U^K\right] \tag{5.8-1}$$

where Ω is the circular excitation frequency,

$$k=\frac{\Omega\, c_{ref}}{2\, v_\infty} \tag{5.8-2}$$

is the reduced frequency (cf. Equation (4.2-42)), and the aerodynamic matrices $\left[Q_{GG}(k)\right]$ and $\left[Q_G^K(k)\right]$ are defined by Equation (5.6-5).

In a direct frequency response analysis, Equation (5.8-1) is solved for each excitation frequency. In a modal frequency response analysis, the response is approximated by a superposition of normal modes. Both methods are implemented in function **`mfs_freqresp`**.

In a modal frequency response analysis, the displacements are approximated by

$$[U_G]\approx\left[U_G^p\right]=\sum_{n=1}^{p}[x_n]Q_n=\left[X^p\right][U]_p \tag{5.8-3}$$

where $[x_n]$ are the eigenvectors of the solid structure, the columns of matrix $\left[X^p\right]$ are the first p eigenvectors, and matrix $[U]_p$ contains the modal coordinates Q_n (cf. Section 2.4.2).

The modal transformation of Equation (5.8-1) using Equation (5.8-3) yields

$$\left(-\Omega^2[M]_p+i\,\Omega[D]_p+[K]_p-q_\infty\left[Q(k)\right]_p\right)[U]_p=q_\infty\left[Q^K(k)\right]_p\left[U^K\right] \tag{5.8-4}$$

where

$$\begin{aligned}&[M]_p=\left[X^p\right]^T[M_{GG}]\left[X^p\right],\ [D]_p=\left[X^p\right]^T[D_{GG}]\left[X^P\right],\\&[K]_p=\left[X^p\right]^T[K_{GG}]\left[X^p\right],\ \left[Q(k)\right]_p=\left[X^p\right]^T\left[Q_{GG}(k)\right]\left[X^p\right]\\&\text{and }\left[Q^K(k)\right]_p=\left[X^p\right]^T\left[Q_G^K(k)\right]\end{aligned} \tag{5.8-5}$$

are the modal matrices. The modal mass, damping and stiffness matrices are diagonal matrices but the modal aerodynamic stiffness matrix is not. Thus, the equations are always coupled.

The modal displacements $[U]_p$ can be obtained by solving Equation (5.8-4) for each excitation frequency. Subsequently, the approximate displacements $\left[U_G^p\right]$ can be computed from Equation (5.8-3).

In the *force summation method*, inertia, damping and aeroelastic loads are computed from the approximate displacements. Improved displacements are obtained by solving

$$[K_{GG}][U_G]=q_\infty\left(\left[Q_G^K(k)\right]\left[U^K\right]+\left[Q_{GG}(k)\right]\left[U_G^p\right]\right)+\left(\Omega^2[M_{GG}]-i\,\Omega[D_{GG}]\right)\left[U_G^p\right] \tag{5.8-6}$$

These displacements include the quasi-static response of the neglected modes and thus give better results for strains and all other responses computed from the strains.

Because the aircraft has rigid body modes, the solution of Equation (5.8-6) is not unique. A unique elastic deformation $\left[U_G^E\right]$ can be obtained by the additional constraint

$$\left[R_G\right]^T\left[M_{GG}\right]\left[U_G^E\right]=0 \tag{5.8-7}$$

where matrix $\left[R_G\right]$ contains the six basic rigid body motions. Because the elastic modes are mass orthogonal with respect to the rigid body modes, the elastic deformation is the superposition of the response of the elastic modes. The absolute deformation is obtained by adding the response of the rigid body modes. Stresses, strains and stress resultants depend on the elastic deformation only.

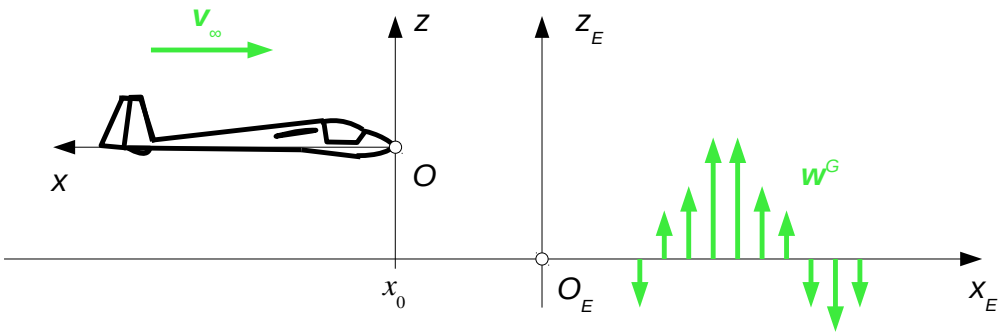
5.8.1 Gusts

In a coordinate system that is attached to the earth, a one-dimensional gust is described by a vertical velocity $w^G(x_E)$, see Figure 5.8-1. In a coordinate system that is attached to the aircraft,

$$x_E(x,t)=x_0+v_\infty t-x \tag{5.8-8}$$

where v_∞ is the velocity of the aircraft and $x_0=x_E(0)$ is the position of the origin *O* of the coordinate system attached to the aircraft at the time $t=0$. Thus, in the coordinate system attached to the aircraft, the gust velocity is

$$w^G(x,t)=w^G(x_0+v_\infty t-x)\ . \tag{5.8-9}$$



$O_E x_E z_E$: Coordinate system attached to the earth

Oxz : Coordinate system attached to the aircraft

Figure 5.8-1: Coordinate Systems to Describe Gusts

In the earth-fixed coordinate system, a harmonic gust is described by

$$w^G(x_E) = w_G \Re\left(e^{2\pi i\, x_E/\lambda}\right) \tag{5.8-10}$$

where w_G is the real amplitude of the gust and λ the wave length. Inserting of Equation (5.8-8) into Equation (5.8-10) leads to the following equation for the gust velocity in the aircraft-fixed coordinate system:

$$w^G(x,t) = w_G \Re\left(e^{2\pi i(x_0-x)/\lambda} e^{2\pi i v_\infty t/\lambda}\right) \tag{5.8-11}$$

With the circular frequency

$$\Omega = 2\pi \frac{v_\infty}{\lambda} \tag{5.8-12}$$

Equation (5.8-11) reads

$$w^G(x,t) = w_G \Re\left(e^{i\Omega(x_0-x)/v_\infty} e^{i\Omega t}\right) \quad . \tag{5.8-13}$$

The gust induces a change of the local angle of attack

$$\Delta\alpha(x,t) = \Re\left(\Delta\hat{\alpha}(x) e^{i\Omega t}\right) = \frac{w^G(x,t)}{v_\infty} = \frac{w_G}{v_\infty} \Re\left(e^{i\Omega(x_0-x)/v_\infty} e^{i\Omega t}\right) \quad , \tag{5.8-14}$$

i.e. the complex amplitude of the incremental angle of attack reads

$$\Delta\hat{\alpha}(x) = \frac{w_G}{v_\infty} e^{i\Omega(x_0-x)/v_\infty} \quad . \tag{5.8-15}$$

The normal wash at the control points is

$$\left[W^G\right]_L = -\begin{bmatrix} e^{i\Omega(x_0-x_1)/v_\infty} \boldsymbol{e}_z \cdot \boldsymbol{n}_1 \\ \vdots \\ e^{i\Omega(x_0-x_N)/v_\infty} \boldsymbol{e}_z \cdot \boldsymbol{n}_N \end{bmatrix} \frac{w_G}{v_\infty} \tag{5.8-16}$$

(cf. Section 5.2). A comparison with Equation (5.6-1) shows that for gusts,

$$\left[D_K^1\right] = -\begin{bmatrix} e^{i\Omega(x_0-x_1)/v_\infty} \boldsymbol{e}_z \cdot \boldsymbol{n}_1 \\ \vdots \\ e^{i\Omega(x_0-x_N)/v_\infty} \boldsymbol{e}_z \cdot \boldsymbol{n}_N \end{bmatrix}, \quad \left[D_K^2\right] = [0], \quad \left[U^K\right] = \begin{bmatrix} w_G \\ v_\infty \end{bmatrix} \quad . \tag{5.8-17}$$

With these relations, matrix $\left[Q_G^K\right]$ can be computed from Equation (5.6-5).

5.8.2 Manoeuvres

In the local coordinate system of a lifting surface, the change of the camber due to a flap motion reads (cf. Figure 5.8-2)

$$\Delta\zeta_S(x, y_L, t) = -\eta(t)(x - x_0), \quad x_0 \le x \le c \quad . \tag{5.8-18}$$

The normal wash is

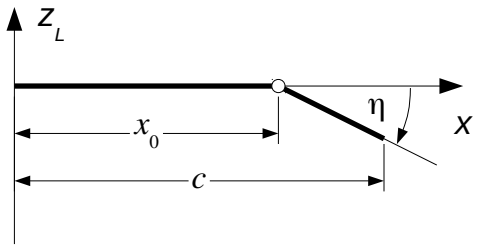


Figure 5.8-2: Geometry of Flap Motion

$$w=\Delta\dot{\zeta}_S+v_\infty\frac{\partial\Delta\zeta_S}{\partial x}=-\dot{\eta}(x-x_0)-v_\infty\eta,\quad x_0\le x\le c\quad . \tag{5.8-19}$$

If the flap motion is time-harmonic,

$$\eta(t)=\Re\left(\hat{\eta}e^{i\Omega t}\right)\quad , \tag{5.8-20}$$

the normal wash is time-harmonic, too,

$$W=-i\Omega\hat{\eta}(x-x_0)-v_\infty\hat{\eta}\quad , \tag{5.8-21}$$

where $\hat{\eta}$ is the complex amplitude of the flap angle, W is the complex amplitude of the normal wash and Ω is the circular frequency of the harmonic flap motion. With the reduced frequency k, the normal wash divided by the flight velocity reads

$$\frac{W}{v_\infty}=-\left(1+2ik\frac{x-x_0}{c_{ref}}\right)\hat{\eta} \tag{5.8-22}$$

With

$$\left[U^K\right]=\left[\hat{\eta}_1\quad\cdots\quad\hat{\eta}_K\right]^T \tag{5.8-23}$$

matrix $\left[D_K^1\right]$ reads

$$\left[D_K^1\right]=-\begin{bmatrix}0&\cdots&0&\cdots&0\\ \vdots&\ddots&\vdots&\ddots&\vdots\\ 0&\cdots&1&\cdots&0\\ \vdots&\ddots&\vdots&\ddots&\vdots\\ 0&\cdots&0&\cdots&0\end{bmatrix}\quad . \tag{5.8-24}$$

Each column corresponds to one control surface. All elements of a column are zero except those that correspond to control points on that control surface. These elements are one.

Likewise, matrix $\left[D_K^2\right]$ reads

$$\left[D_K^2\right] = -\frac{2}{c_{ref}} \begin{bmatrix} 0 & \cdots & 0 & \cdots & 0 \\ \vdots & \ddots & \vdots & \ddots & \vdots \\ 0 & \cdots & x_n - x_0 & \cdots & 0 \\ \vdots & \ddots & \vdots & \ddots & \vdots \\ 0 & \cdots & 0 & \cdots & 0 \end{bmatrix} \tag{5.8-25}$$

where x_n are the *x*-coordinates of the control points on the control surfaces.

References

Abramowitz, M. & I.A. Stegun (1972), *Handbook of Mathematical Functions*, National Bureau of Standards,

Bathe, K.J. (1996), *Finite Element Procedures*, Prentice Hall, New Jersey

Bisplinghoff, R.L., Ashley, H. & R.L. Halfman (1983), *Aeroelasticity*, Dover Publications, Inc., Mineola, New York

Filon, L.N.G. (1929), On a quadrature formula for trigonometric integrals, *Proc. Roy. Soc. Edinburgh* 49, pp. 38-47

Karamcheti, K. (1980), *Principles of Ideal-Fluid Aerodynamics*, Krieger Publishing Company, Malabar, Florida

Lee, P.S. & K.J. Bathe (2004), Development of MITC isotropic triangular shell finite elements, *Computers & Structures* Vol. 82, pp. 945-962

Lee, P.S., Noh, H.C. & K.J. Bathe (2007), Insight into 3-node triangular shell finite elements: the effects of element isotropy and mesh patterns, *Computers & Structures* Vol. 85, pp. 404-418

MacNeal, R.H. (1994), *Finite Elements: Their Design and Performance*, Marcel Dekker Inc., New York

Moran, J. (1984), *An Introduction to Theoretical and Computational Aerodynamics*, Dover Publications, Inc., Mineola, New York

Naganarayana, B.P. & G. Prathap (1989), Force and moment corrections for the warped four-node quadrilateral plane shell element, *Computers & Structures* Vol. 33, No. 4, pp. 1107-1115

Newmark, N.M. (1959), A Method of Computation for Structural Dynamics, *ASCE Journal of Engineering Mechanics Division* Vol. 85, pp. 67 - 94

Parisch, H. (1985), *The QUAD 4 Shell Elements in PERMAS*, INTES GmbH, Stuttgart

Saad, Y. (2003), *Iterative Methods for Sparse Linear Systems* , SIAM, Philadelphia

Tuck, E.O. (1967), A simple Filon-trapezoidal rule, *Math. Comp.* 21, pp. 239-241

Wandinger, J. (1990), *PERMAS-II Subspace Iteration*, INTES GmbH, Stuttgart

Wandinger, J. (2023), *Aeroelastik*, http://wandinger.userweb.mwn.de/Aeroelastik/index.html

Zurmühl, R. & S. Falk (1984), *Matrizen und ihre Anwendungen, Teil 1:*

Grundlagen, Springer, Berlin, Heidelberg, New York, Tokyo